

Collegio di Ingegneria Meccanica, Aerospaziale e dell'Autoveicolo Master of Science Course in Mechanical Engineering LM-33 2022/2023

# **Master of Science Thesis**

Characterization of Adhesives Modified with Thermally Expandable Microspheres for Reversible Structural Adhesive Bonding

# **Supervisors:**

Ing. Raffaele Ciardiello (DIMEAS)

Ing. Alessandro Benelli (DIMEAS)

Ing. Davide Salvatore Paolino (DIMEAS)

### **Candidate:**

Yüksel Altay Aksoy Student No: 312814 " Çalışmadan, yorulmadan ve üretmeden, rahat yaşamak isteyen toplumlar; evvela haysiyetlerini sonra hürriyetlerini daha sonra da istiklal ve istikballerini kaybetmeye mahkumdurlar."

Gazi Mustafa Kemal ATATÜRK

# **ACKNOWLEDGEMENTS**

I would like to express my heartfelt thanks to Ing. Raffaele Ciardiello, Ing. Alessandro Benelli, and Ing. Davide Salvatore Paolino for their supervision and guidance; to Mohammad Abbasi for his extensive support in the laboratory; to Dhaffer Youssef, Fairouz, and Haris Alexiou for filling my ears with their pure form of art; and to Fatih Altaylı for providing me with news from my fatherland every morning and showing a solid example of perseverance to all of us.

I would also like to thank Maria El Hadwe for her tender love and for showing unconditional support whenever I struggled to find my direction; to my comrades Melih Eren Genç and Birkan Kemal Ünlü for walking this gravel road shoulder to shoulder with me; to Daniele Assenza for cheering me up with his warm conversations on our balcony; and to Anna for all those enjoyable nights in our restful house.

I must express my deep gratitude to my supportive parents and to my lovely sister. If they had not been there for me all the time, I could not have achieved this. In simple words, if I exist today in this cruel and collapsing world, it is for them. Finally, Aslan Dede'm, you were always in my thoughts throughout this journey. I miss you a lot, and I know that the beautiful Kavak trees of our city are whispering my relief to your ears.

### **ABSTRACT**

The growing demand for sustainable bonding in structural applications has initiated the search for new adhesive bonding systems. The application of thermally expandable particles (TEPs) in adhesive systems is explored to enable debonding in structural adhesives. Thermally expandable particles, whose thermal expansion on heat stimulation is due to low-boiling-point hydrocarbons encapsulated within polymeric shells, were integrated into epoxy adhesive matrix to investigate their potential for providing controlled debonding of joints via thermal expansion. The current study involves comprehensive characterization of the modified adhesives by expansion behavior analysis, optical microscopy, and scanning electron microscopy (SEM) for examining the morphology changes provided by thermal activation. Mechanical properties of bonded joints were assessed by lap shear strength tests between TEP-modified and unmodified adhesives under the conditions of before and after heat treatment. The findings indicate that the introduction of TEPs significantly affects microstructure and mechanical properties of adhesive joints, and offers a potential path for sustainable bonding system development. This research offers key understanding for the creation of thermally responsive adhesive systems for use in applications where disassembly, recyclability, or repairability is desired, thereby facilitating the development of sustainable adhesive technologies.

**Key words:** Thermally Expandable Particles (TEPs), Adhesives, Debonding-on-command, Composites, Automotive

# **TABLE OF CONTENTS**

ACKNOWLEDGEMENTS	ii
ABSTRACT	iii
TABLE OF CONTENTS	iv
LIST OF FIGURES	vi
LIST OF TABLES	ix
l. Introduction	1
1.1 Background and Motivation	1
1.2 Objectives of the Thesis	3
1.3 State of the Art	3
1.3.1 Composite Materials and Their Applications	3
1.3.2 Adhesive Bonding in Composites	15
1.3.3 Challenges in Disassembly and Recycling of Adhesive Joints	24
1.3.4 Thermally Expandable Particles (TEPs)	29
2. Materials and Methods	40
2.1 Materials	40
2.1.1 Composite Materials	40
2.1.2 Adhesive Used	41
2.1.3 TEP Particles	44
2.2 Preparation of the Modified Adhesive	45
2.3 Volume Expansion Coefficient Testing	46
2.4 Preparation of the Adhesive Joint	48
2.5 Mechanical Testing	52
2.6 Heating Configuration	53
2.7 TGA Characterisation	54
2.8 FE-SEM Analysis	55
2.9 Optic Microscope Analysis	57
3. Results and Discussion	58
3.1 Characterisation of Materials	58

3.1.1 TGA Results of the Modified Adhesive	58
3.1.2 Microscope Analysis of Particles and Adhesive Morphology	60
3.1.3 Volume Expansion Coefficients	67
3.2 Mechanical Performance of Adhesive Joints	71
3.2.1 Lap Shear Strength of Joints with and without TEP	71
3.2.2 Failure Modes and Adhesive Distribution	82
4. Conclusions and Future Work	85
REFERENCES	86

# **LIST OF FIGURES**

Figure 1. Schematic of a Fiber Reinforced Composite Material	3
Figure 2. Boeing 787 Material Composition	6
Figure 3. Classification of Polymeric Composite Materials	7
Figure 4. Resin Transfer Molding Technology	
Figure 5. Reaction-injection Molding Technology	11
Figure 6. Vacuum-assisted Resin Infusion Technology	12
Figure 7. Compression Molding Technology	12
Figure 8. Prepreg Lay-up Technology in Autoclave	13
Figure 9. Filament Winding Technology	14
Figure 10. Pultrusion Technology	15
Figure 11. Typical Failure Modes of Single Lap Joints	19
Figure 12. Joint Configurations	20
Figure 13. Through Thickness Stresses in Single Lap Joint	21
Figure 14. Schematic Representations of (a) Bolted-bonded Joint, (b) Rivet-	
bonded Joint and (c) a Pin-bonded Joint	22
Figure 15. Clinch Bonding	23
Figure 16. Resistance Spot-welding with Adhesive Bonding	23
Figure 17. Fricrion Stir Welding with Adhesive Bonding	23
Figure 18. Debonding-on-command Techniques	25
Figure 19. ElectRelease Technology	26
Figure 20. Schematic of a Thermally Expandable Particle	30
Figure 21. SikaPower-1277 Epoxy Adhesive	42
Figure 22. ThinkyMixer ARE-250 Speed Mixer	45
Figure 23. TEP-modified Adhesive After Mixing	46
Figure 24. Cast-cured Specimens Inside the Hydrosoluble Molds	46
Figure 25. Thermocouple-attached Expansion Test Specimens	47
Figure 26. ECP Industrial OV301 Curing Oven	47
Figure 27. Prepreg Laminate Inside the Oven	48
Figure 28. WAZER Waterjet Cutting Equipment	49
Figure 29. Laminate Before Curing	50
Figure 30. Single Lap Joint Substrates with Geometrical Dimensions	50
Figure 31. SLJ Specimen Preparation Setup	51
Figure 32. Dimensions of the SLJ Specimen	52
Figure 33. ZwickRoell-050 Universal Testing Machine with SLJ Specimen Attach	ned
	53

Figure 34. Joule Heating Configuration For the Debonding Tests	54
Figure 35. Thermogravimetric Analysis Equipment	55
Figure 36. TESCAN MIRA3 Scanning Electron Microscopy (FESEM) Device	56
Figure 37. PRESI Mecatech 250 Polishing Device	57
Figure 38. Cold-mounted FESEM Specimen After Sputtering	57
Figure 39. Zeiss AxioVert A1 Microscope	58
Figure 40. Non-isothermal TGA analysis result for the GFRP	58
Figure 41. Non-isothermal TGA analysis result for the Sikapower-1277	59
Figure 42. Non-isothermal TGA analysis result for the Sikapower-1277 with Time	59
Figure 43. Isothermal TGA analysis result for the Sikapower-1277	60
Figure 44. Unexpanded TEPs under optical microscope (no adhesive matrix)	61
Figure 45. Expanded TEPs under optical microscope (no adhesive matrix)	62
Figure 46. Optic Microscope Methodology for Adhesive Morphology	64
Figure 47. Microscope Images of Unheated Specimens with Varying TEP-wt.%	65
Figure 48. Microscope Images of Reference, Heated, and Unheated Specimens	
with Varying TEP-wt.%	65
Figure 49. 2D-Porosity Analysis Results	66
Figure 50. TEPs-Induced Crack in Modified Adhesive Matrix	67
Figure 51. TEPs-Induced Crack Propagation in Modified Adhesive Matrix	67
Figure 52. Expansion Test Specimens Before and After Heating	68
Figure 53. Volumetric Expansion Coefficient Results with Varying TEPs wt.% (20	
Minutes of Heating)	68
Figure 54. Volumetric Expansion Coefficient Results with Varying TEPs wt.% (1 Ho	our
of Heating)	69
Figure 55. Volumetric Expansion Coefficient Results of 20 minutes and 1 Hour of	
Heating	70
Figure 56. Baseline Adhesive - Single Lap Shear Test Results	71
Figure 57. Unheated 5 wt.% TEP-modified Epoxy Adhesive - Single Lap Shear Te	st
Results	72
Figure 58. Heated 5 wt.% TEP-modified Epoxy Adhesive - Single Lap Shear Test	
Results	73
Figure 59. The Lap Shear Strength Plots of 5 wt.% TEP-Modified Specimens	74
Figure 60. Unheated 10 wt.% TEP-modified Epoxy Adhesive - Single Lap Shear Te	est
Results	74
Figure 61. Heated 10 wt.% TEP-modified Epoxy Adhesive - Single Lap Shear Test	
Results	75

Figure 62. The Lap Shear Strength Plots of 10 wt.% TEP-Modified Specimens	76
Figure 63. Unheated 15 wt.% TEP-modified Epoxy Adhesive - Single Lap Shear Te	st
Results	76
Figure 64. Heated 15 wt.% TEP-modified Epoxy Adhesive - Single Lap Shear Test	
Results	77
Figure 65. The Lap Shear Strength Plots of 15 wt.% TEP-Modified Specimens	78
Figure 66. The Lap Shear Strength Plots of Unheated Specimens	78
Figure 67. The Lap Shear Strength Plots of Heated Specimens	79
Figure 68. The Force-Displacement Master Graph	79
Figure 69. The Stress-Displacement Master Graph	80
Figure 70. The residual lap shear stress values for varying TEP wt.%	8
Figure 71. Failure Mode Analysis of Unheated Specimens with Varying TEP wt.%	83
Figure 72. Failure Mode Analysis of Heated Specimens with Varying TEP wt.%	84

# **LIST OF TABLES**

Table 1. Characteristics of Adhesive Types	17
Table 2. Adhesive Debonding Stimulus Methods	29
Table 3. Comparison for Different Adhesive Debonding Techniques	32
Table 4. Literature Search About TEP-Modified Adhesive Systems	38
Table 5. GFRP Specifications	40
Table 6. CFRP Specifications	41
Table 7. SikaPower-1277 Technical Properties	43
Table 8. TEPs - Technical Properties by Nouryon	44
Table 9. Particle Diameter Calculation Results	63
Table 10. Volumetric Expansion Coefficients and Volumetric Expansion Rates of	
TEPs	63
Table 11. Average Porosity Values for Unheated and Heated Specimens with	
Varying TEP wt.%	66
Table 12. Volumetric Expansion Coefficient Test Results and Test Information	70
Table 13. The Deconding Effectiveness Results for Varying TEP wt.%	81
Table 14. Comparison of Shear Strength, Stiffness, and Rupture Displacement wi	ith
Varvina TEP wt.%	82

# 1. Introduction

# 1.1 Background and Motivation

In the middle of the threats posed by climate change and the urgent call for a more sustainable global economic order, recent legislation by governments and environmental organizations is driving radical transformation in numerous industries. Lightweighting structural components, shifting to fewer but larger components, introducing disassembly-friendly designs, facilitating end-of-life, and moving towards a circular economy are all examples of these fundamental changes in the majority of manufacturing industries. [1].

Fiber-reinforced polymers are gaining greater popularity due to their superior specific properties, resistance to environmental factors, and ability to produce intricate and large parts, thereby minimizing the number of pieces and assembly requirements [2]. The (EU) 2019/631 legislation, introduced in 2009, setting the limit to 95 grams of CO2 emissions per kilometer in automotive transportation, has had a profound impact on the European automotive industry. In addition, complementary directives (2000/53/E.C. and 2005/64/E.C.) emphasize the need for using less hazardous materials during production, as well as the recoverability, reusability, and recyclability of these materials at the end-of-life (EoL) of the vehicle. Airbus A350 and Boeing 787 airframes, with more than 50% CFRP content, led the way in adopting FRP products in the aeronautical sector [3]. Around 2000 EoL civil airplanes with an average weight of 106 tonnes were projected, and another 250 are estimated to reach EoL annually for 20 years. With current blade lengths of up to 107 m with the potential to generate 12 MW of power, the wind energy industry is expected to generate the largest volume of EoL FRP waste [4]. The lightweighting concept, by its nature, encourages replacing metallic materials with FRP, eliminating mechanical fastening methods, and utilizing bonded joints through the application of irreversible cross-linked polymer adhesives. Unfortunately, the challenge in separating the parts joined by such adhesive joints weakens the design for the end-of-life concept.

First, there are logistical issues with the production and installation of the big, irregular pieces, particularly for offshore wind farms. Second, the connection of FRP elements is a common practice across many industries. The highly localized loads produced by conventional fasteners and the introduction of flaws, such as holes, to

aid in assembly, may not be suitable for FRP materials due to their brittle nature and threatining the structural integrity of the part by damaging the fibers. Inappropriate usage of conventional fasteners can drastically weaken the component, causing it to break too soon and require replacement. Lastly, there are additional difficulties in breaking down and reassembling the components into useful items for the circular economy when the high-value commodity part becomes outdated or irreparable.

Depending on the material under consideration, there are three primary methods for combining components: material joining through welding, soldering, and bonding; positively joining (by fitting parts into each other) through bending substrates together, and non positively joining (by holding parts together with force or friction) through pressing or clamping. Although materially joining techniques like brazing and welding are efficient, they can only be used with materials that have similar properties or affinities. Similarly, only materials that can tolerate significant plastic deformation can be used for positively joining techniques like crimping [5]. FRPs can be fastened with conventional mechanical fasteners, such as rivets, screws, and bolts. However, because of their intrinsic brittleness and anisotropy, which makes it difficult to sustain the formation of holes or any other consequent stress concentrators, caution must be exercised considering the load route and stress concentration.

There are many advantages to adhesively joining two materials, particularly when maintaining lightweighting and in situations where smooth profiles are crucial, such as aerodynamic surfaces. Moreover, adhesive bonding makes it possible to put together big, intricate parts. Currently, there is no preferred joining technique for the dismantling and recycling of FRPs in terms of EoL design. Regardless of whether a feedstock is being reduced or repurposed, it is crucial to preserve as much value as possible during the processing. Research and industry are interested in creating an adhesive system that can "debond-on-command" which could facilitate recycling and repair of adhesive bonds formed by dissimilar materials. Strong, superior adhesive qualities, quick activation of debonding within realistic timeframes (preferably seconds to minutes), minimal or no toxicity, and no negative impact on the bonded or de-bonded substrates are all essential components of a sustainable adhesive bonding. The price should ideally be on par with that of commercial adhesives already on the market, and it would be ideal if the feedstock was sustainable [2].

# 1.2 Objectives of the Thesis

This study aims to develop robust assessment methods to evaluate the integration of 043DU80 Expancel thermally expandable particles into SikaPower-1277 epoxy adhesive matrix. With the methodology used, it is aimed to assess the applicability of expandable particles in adhesive debonding without compromising the mechanical properties of the joint. This is achieved through analysing the TEP-modified adhesive's morphology by microscopy, investigating the expansion characteristics of both TEPs and TEP-modified epoxy adhesive, and conducting mechanical tests to calculate the lap shear strength of single lap joints bonded with modified adhesive.

#### 1.3 State of the Art

# 1.3.1 Composite Materials and Their Applications

A composite material combines two or more distinct materials, each with unique mechanical properties, resulting in a final material that exhibits superior characteristics compared to the constituent materials. These constituent materials are known as the fiber and the matrix, and unlike metal alloys, each component retains its unique chemical, physical, and mechanical properties after they are combined [6]. The schematic of fiber-reinforced composites can be seen in the Figure 1.

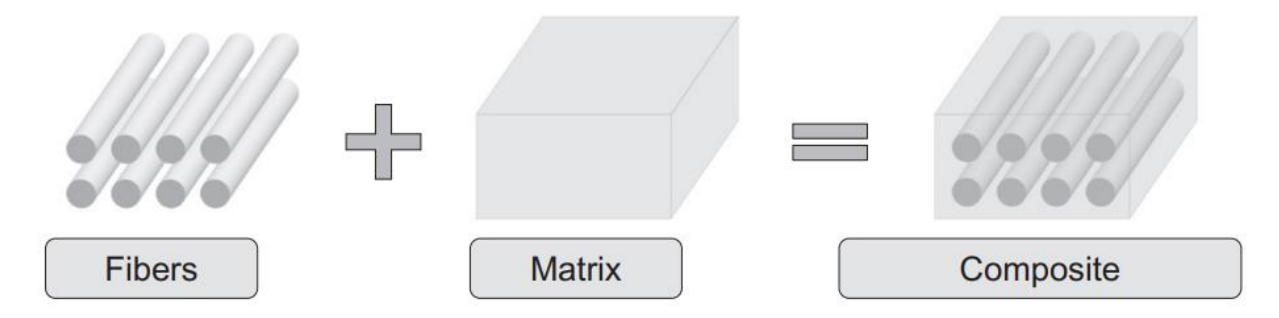


Figure 1. Schematic of a Fiber Reinforced Composite Material [6]

# 1.3.1.1 Automotive and Aerospace Sectors

In the automotive industry, composite materials are widely used due to their superior properties compared to conventional materials like steel and aluminum. Their advantages include a strong strength-to-weight ratio, durability, damage resistance, corrosion resistance, thermal conductivity, electrical non-conductivity, impact resistance, and design flexibility. Because of these benefits, numerous components, including chassis, hoods, leaf springs, bumpers, doors, sunroofs, engine cradles, brake pads, and fenders, are manufactured from composite

materials in both the automobile and aerospace industries, including fixed-wing and rotary-wing aircraft. [7].

#### Brake Pads

Brake pads are one of the most essential parts of the braking system of an automobile. In order to last long and function properly, they should exhibit good frictional and wear characteristics under various load, velocity, and temperature conditions. Phenolic resin-based composite materials are commonly used in brake pads due to their relatively higher coefficient of friction and reduced wear properties at a range of temperature circumstances [8]. Other than phenolic-based composites, coconut fibre reinforced aluminum and aramid fibers are considered as a promising alternative for both the brake pad and the brake disc [9, 10].

#### Hood

For the hood part of the automobiles, composite materials allow for lightweight and intricate designs thanks to their superior strength-to-weight and easily moulding characteristics. Furthermore, they have good impact strength. Natural flax fiber, glass fiber composite, and carbon fiber composite can replace the conventional materials, such as steel skin, by reducing the weight 30% and keeping the strength almost the same under bending and torsional stress loaded conditions [11, 12, 13].

#### Chassis

Composite materials are suitable to be use in the chassis of automobiles due to their lightweight nature for an efficient fuel economy, dampening characteristics to decrease the vibration transfer, and good fatigue resistance that allows for longer time cycles. Kevlar honeycomb core and syntactic foam are used for the sandwich structures [7].

# Leaf springs

Compared to leaf springs, which are manufactured by using conventional materials such as steel, glass fibre-reinforced epoxy polymer composites offer more than 5 times longer fatigue life and faster response to pressures created by the road shock [14].

#### Bumper

Carbon fiber reinforced polymers and glass fiber reinforced polymers are commonly used for the bumper part of the automobiles due to their superior impact absorption properties. In addition, bumpers are one of the extra-heavy parts of a car. For this reason, employing composite materials is essential in terms of reducing the vehicle weights [15].

#### Door

Automobile manufacturers are able to produce doors that are both light and strong and enable enhanced security and aesthetics by leveraging the advantages of composite materials [https://doi.org/10.1007/s00170-021-08569-z]. Carbon fibre reinforced polymer composites have more deformation energy than steel, with a weight reduction of 65% [16].

#### Sunroof

For certain sunroofs, composite materials are preferred to reduce the total weight without ruining the structural integrity. Continuous carbon fibers and laminated glass composites allow for impact-resistant components, which may support the automobile's safety features [17, 18].

## Engine cradle

Another deployment of composite materials in the automotive industry is for the engine cradle, which works as a component to carry and support the car's engine, transmission, and suspension, to reduce the vibration and shocks by the road [https://doi.org/10.1016/j.ijmecsci.2019.105115]. Composite materials can increase thermal management efficiency by limiting the heat transfer between the engine and the other parts of the car with their superior thermal insulation characteristics [19].

#### Fender

Fenders made of composites are used for sports cars to cut off the weight to improve the performance of the car. Thermoplastic matrix materials are preferred due to their recyclability and superior strength and toughness characteristics [20].

## Fixed-wing aircraft structures

Fiber-reinforced composites are widely used in the aerospace sector thanks to their lightweight, exceptional strength, durability, and resistance to corrosion and

fatigue. The composition of materials used in constructing the Boeing 787's airframe is illustrated in the Figure 2.

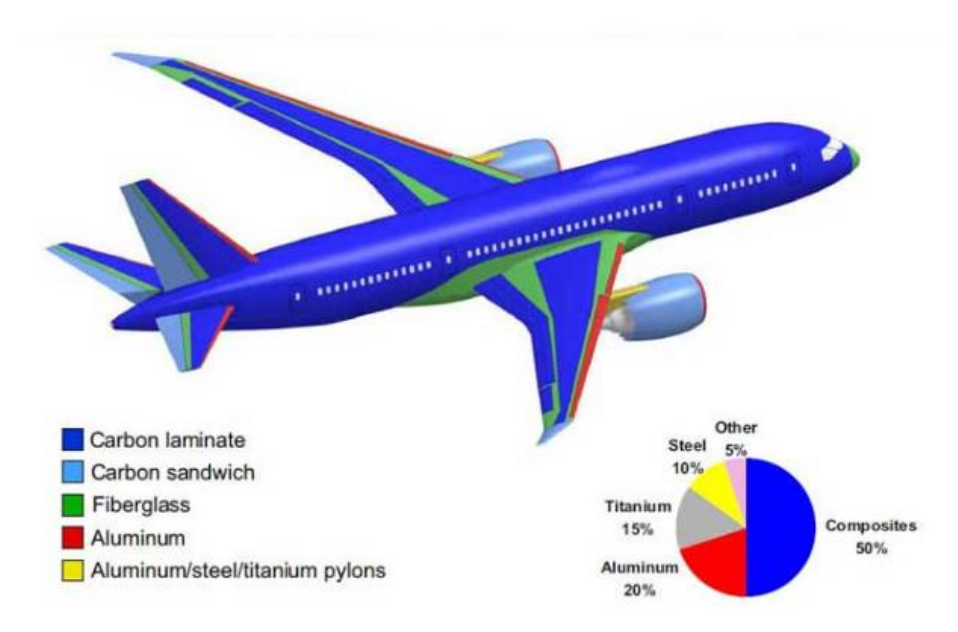


Figure 2. Boeing 787 Material Composition [21]

Another airplane, BOEING A320, incorporates composite materials in various components, including the fuselage belly skins, fin, fuselage fairings, wing's fixed leading and trailing edge bottom access panels, deflectors, trailing edge flaps, flap track fairings, spoilers, ailerons, nose wheel and main wheel doors, fairing doors for the main gear leg, nacelles, and carbon brakes [22].

### Rotary-wing aircraft structures

Helicopter structures, so-called rotary-wing aircraft, require high lifting powers to overcome the structure's weight. For this reason, a lighter and stronger fuselage is desired, which has an impact on reducing the costs. Use of composite rotor blades shows significant improvements in corrosion and damage resistance, fatigue strength, and life-cycle costs [23].

# 1.3.1.2 Common Composite Types (CFRP, GFRP)

As it is mentioned before, composite materials are defined as the combination of two or more different type materials. These materials, as the constituents, are called the fiber and the matrix. Glass, aramid, and carbon are typically used as fiber materials. The fibers can be unidirectional, woven, or filament wound in a continuous fiber form. For the discontinuous form of fibers, chopped fibers and mat can be given as examples. On the other hand, ceramic, carbon, and polymers are widely used as the matrix material [24].

Composites can be classified into 3 different types, which are fiber-reinforced composites, particulate reinforced composites, and sandwich panel composites. The classification can be seen in Figure 3.

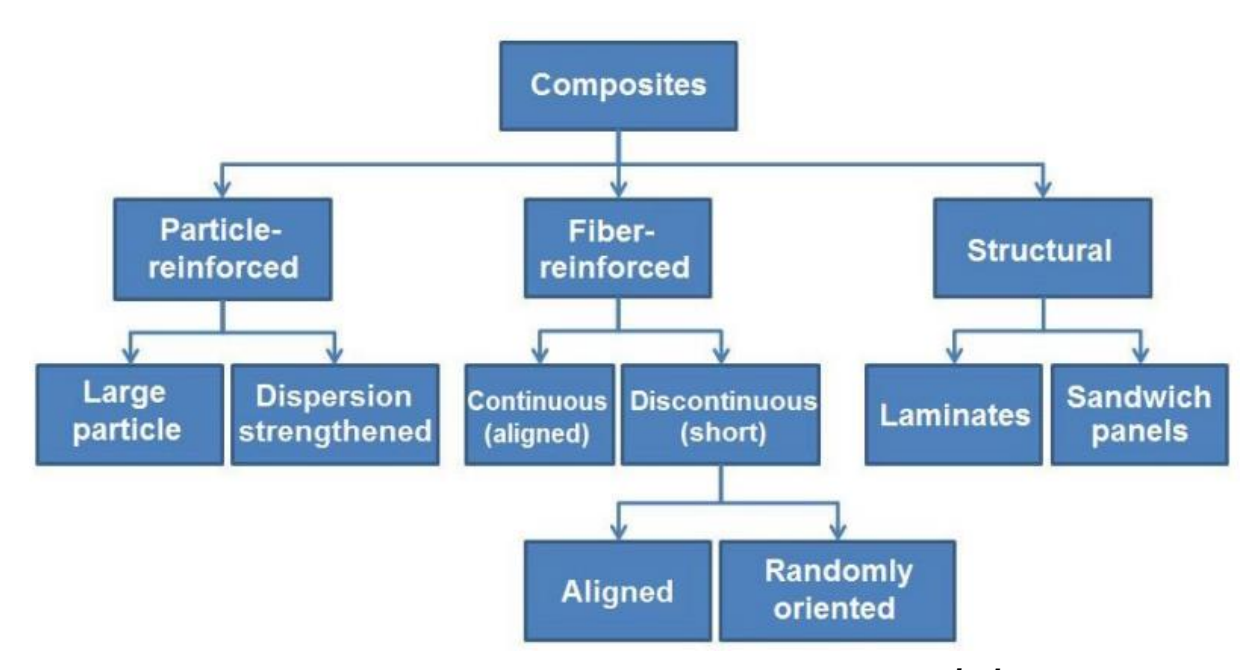


Figure 3. Classification of Polymeric Composite Materials [25].

However, in the last decades, fiber-reinforced composites have been getting the most attention due to their outstanding performance, superior mechanical properties, durability, and corrosion resistance. Among fiber-reinforced composites, Carbon Fiber-Reinforced Polymer (CFRP), Glass Fiber-Reinforced Polymer (GFRP), and Aramid Fiber-Reinforced Polymer (AFRP) are the most commonly used composite material types in the automotive and aerospace industries [26].

# Carbon fiber-reinforced composites

Carbon fiber-reinforced polymers (CFRPs) are a group of lightweight materials with high strength up to 4500 MPa [27], high modulus, and excellent resistance to temperature changes, which make them suitable for various structural and functional uses. These properties are due to the high carbon content (typically between 80% and 95%) of the fibers, combined with the strong interfacial interactions that are created between the fibers and the matrix after suitable surface treatments. Despite their good mechanical profile, CFRPs tend to have poor interfacial bonding because of the inert and smooth nature of carbon fibers, requiring treatments like oxidation, plasma treatment, and chemical grafting to

enhance wettability and adhesion between fibers and matrix. The CFRP components are produced via several manufacturing processes like hand lay-up, resin transfer molding (RTM), filament winding, and pultrusion. These processes influence the fiber orientation, matrix impregnation, and final part geometry. Thanks to their high specific strength and stiffness, CFRPs are employed in numerous sectors such as aerospace (e.g., fuselage structures, stealth components), automotive (e.g., suspension and gearbox parts in Formula 1 vehicles), renewable energy systems (e.g., wind turbines), defense applications, and high-end civilian products such as sports equipment and prosthetic devices [27].

## Glass fiber-reinforced composites

Glass fiber-reinforced polymer (GFRP) composites are widely used because they exhibit high tensile strength, good stiffness, low thermal conductivity, chemical resistance, and good electrical insulation properties. The mechanical behavior of GFRPs is different based on the type of glass fiber utilized, like E-glass, S-glass, or AR-glass. For example, E-glass fibers—those most widely applied in GFRP composites—have tensile strengths as high as 3450 MPa and Young's modulus of approximately 72.4 GPa, whereas S-glass fibers offer still better performance with tensile strengths as high as 4890 MPa and moduli over 85 GPa [28]. The drawback of GFRPs in comparison to carbon fiber composites is that they have a moderately lower modulus and higher density [28].

GFRP components are manufactured by various technologies, including injection molding, compression molding, resin transfer molding, and silicone rubber molding, which all have varying costs, production rates, and dimensional precision advantages. These processes determine the ultimate mechanical response, surface finish, and fiber dispersion within the products. Because of their useful properties and simplicity in production, GFRPs are utilized in different fields like the automotive sector (e.g., bodywork, tire reinforcement), marine sector (e.g., boat building), aerospace sector, construction, and electrical insulation. They find application in consumer goods, printed circuit boards, and other specialized products that require corrosion protection and heat insulation [28].

### Aramid fiber-reinforced composites

Aramid fiber reinforced polymer (AFRP) composites are advanced materials with high specific strength, stiffness, and thermal resistance. Para-aramid fibers, including Kevlar, Twaron, and Technora, have tensile strengths from 2.7 up to 4.5

GPa and Young's moduli from 60 up to 145 GPa, making them ideal for applications where superior mechanical properties are needed [29]. These fibers possess good flame resistance, as shown by their limiting oxygen index (LOI) values above 30, rendering them self-extinguishing materials. Para-aramid fibers are less dense, which renders them higher in specific strength relative to glass and carbon fibers [29].

AFRP composites are generally manufactured with thermoset matrices like epoxy and polyester resins by hand lay-up, spray-up, and autoclave curing. Developments in prepreg materials, where the fibers are impregnated with partially cured resin before processing, enable better control of fiber volume fractions, frequently close to 60%, a standard often encountered on most structural applications. These types of composites are employed extensively in aerospace hardware, sporting goods, and ballistic armor, where their blend of lighter weight, extremely high strength, and thermal resistivity is extremely beneficial [29].

#### 1.3.1.3 Fabrication Processes

Although composite materials offer superior properties in automotive and aerospace applications, the development of manufacturing technologies remains challenging in terms of cost-effectiveness and the speed of the process. To confront these difficulties, many types of manufacturing technologies have been introduced, such as resin transfer molding (RTM), reaction injection molding (RIM), vacuum-assisted resin infusion (VARI), compression molding, prepreg lay-up, filament winding, and pultrusion.

# Resin transfer molding (RTM)

Resin transfer molding is one of the most common and convenient manufacturing methods of composite materials that allows for mass production in the automotive industry. The RTM process consists of a rigid mold with the shape of the final product, dry preform fibers, and a resin injection mechanism. First, the stacked preform is placed on the mold, and then it is compressed. After the compression to the desired thickness, the liquid resin is injected, and the fibers get impregnated. Following the curing time, the final product is obtained after removal from the mold. The resin transfer molding process can be seen in Figure 4 below.

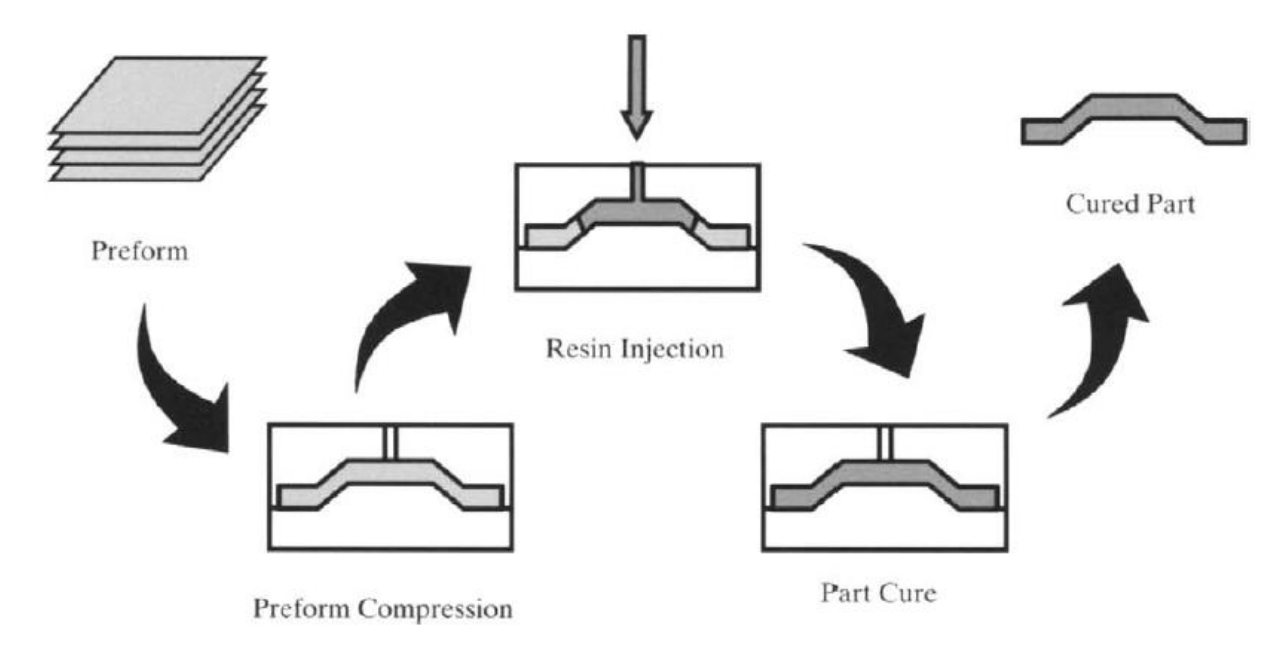


Figure 4. Resin Transfer Molding Technology [24]

RTM offers numerous advantages, such as low capital and operational costs. In addition, no treatment is required to obtain the desired dimensions as the fiber preform takes the shape of the mold during the process. Furthermore, the final product has a good surface finish, and a high fiber volume fraction percentage can be reached [30].

# Reaction-injection molding (RIM)

Reaction-injecting molding is a low-pressure composite manufacturing process in which two reactive liquids are injected into the mold cavity through a mixing chamber with stoichiometric proportions to be cured to form the polymer matrix [31]. Similar to the RTM process, the preform is placed in the mold and the resin is injected after mixing in the mixing chamber, as can be seen in Figure 5.

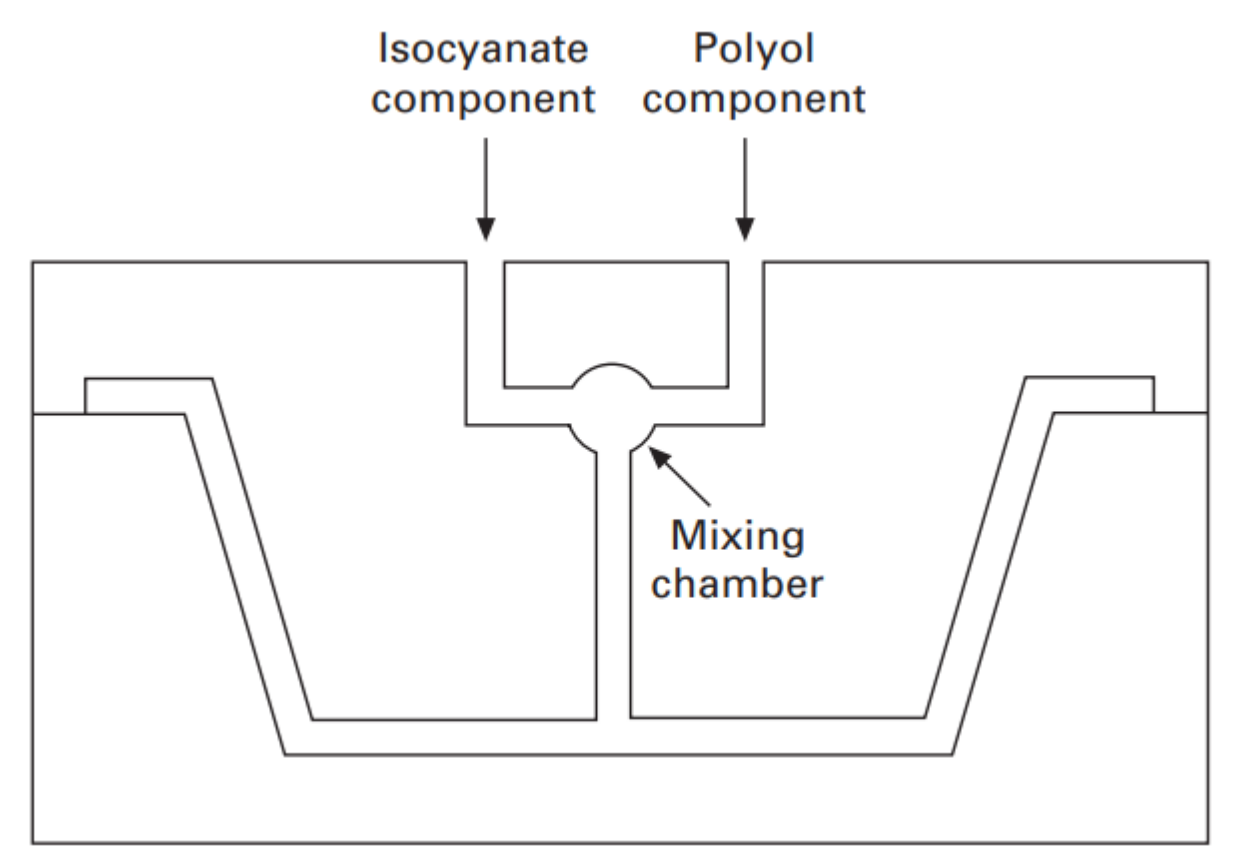


Figure 5. Reaction-injection Molding Technology [31]

There are two types of RIM processes, which are Structural RIM and reinforced RIM. In the structural RIM process, the resin is injected into the cavity where the preform is already placed, similar to the RTM. On the other hand, for the reinforced RIM, the short fibers are added to one of the components of the matrix material and then injected into the cavity together [32]. RIM is widely used in the automotive and marine industries to manufacture fiber-reinforced thermoset polyurethane matrix components. The reason for selecting thermoset polyurethane as the matrix material is due to its faster curing time than thermoset polyester, vinyl ester resin, and epoxies [33].

### Vacuum-assisted resin infusion (VARI)

The vacuum-assisted resin infusion method is one of the most common composite manufacturing methods used for small to large-sized components. Similar to the RTM process in principle, with the difference that the upper mold is replaced with a plastic vacuum bag, which makes the VARI method more economical than RTM in terms of reducing the tooling costs [34].

In the VARI technology, the dry fabric layers are placed into a mold and covered with a flexible plastic vacuum bag. However, this technology is prone to leakage

problems due to the unrigid nature of the vacuum bag. To address this issue, sealing tapes are used. After this, the polymer resin is infused by vacuuming. To allow a persistent and sufficient resin flow, a layer of highly permeable medium is placed on top of the fabric stack [35]. The schematic of the VARI technology can be seen in Figure 6.

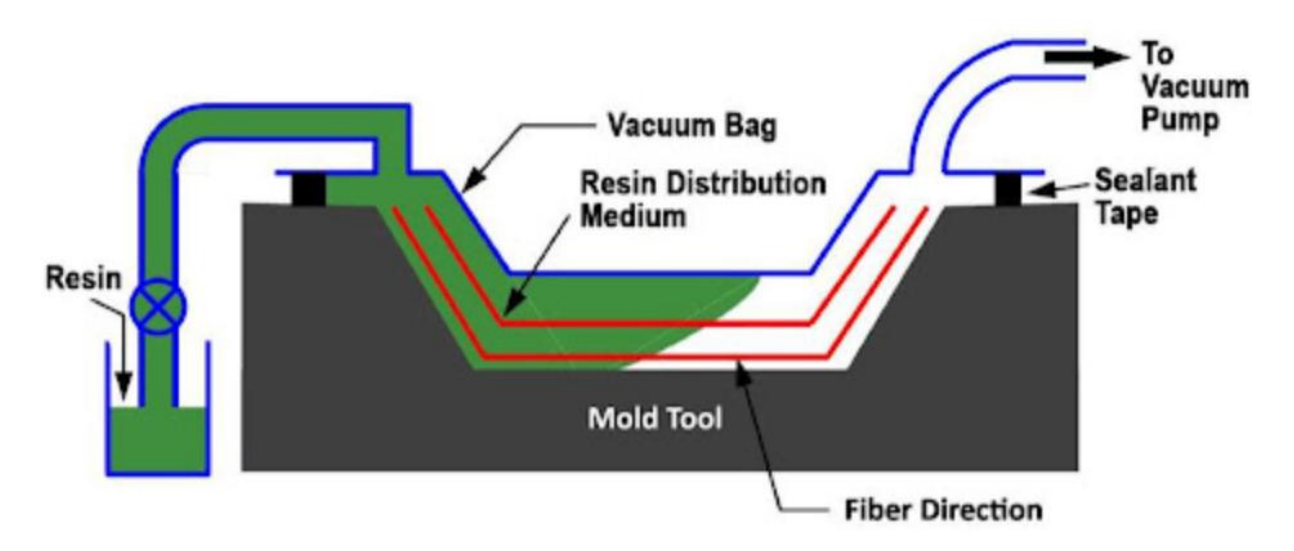


Figure 6. Vacuum-assisted Resin Infusion Technology [36]

# Compression molding

Compression molding is one of the most common technologies of composite component manufacturing in the automotive industry. It involves compression of a material charge, which is a mixture of resin and fibers, into the desired component shape under pressure and heat by using metal molds [37]. The schematic of the compression molding technology can be seen in Figure 7.

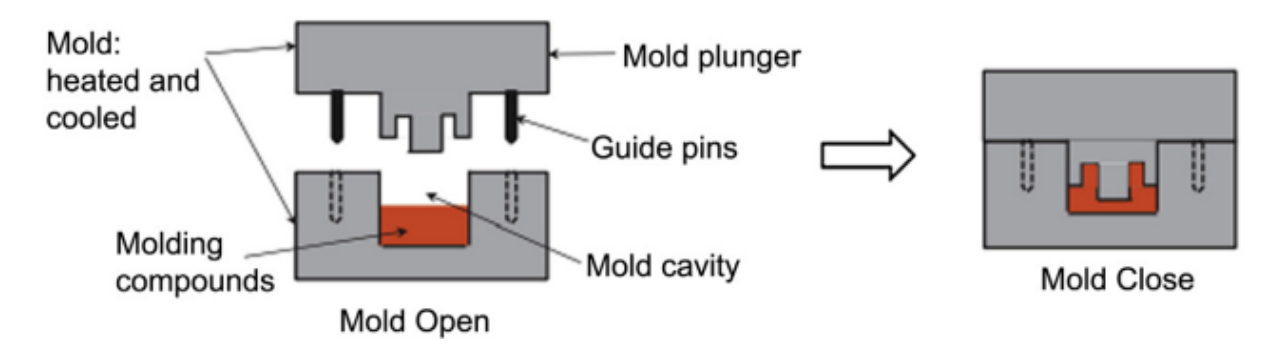


Figure 7. Compression Molding Technology [38]

The common material charges are reinforced glass fiber mat thermoplastic, sheet molding compounds, and bulk molding compounds. Compression molding is a widely preferred manufacturing method due to its relatively simple manufacturing process, fast cycle time, and capability to produce complex components. However,

the mechanical properties of the final product are worse than RTM and RIM technologies but comparable to VARI [39].

## Prepreg lay-up

Prepreg lay-up is a composite manufacturing technology that consists of pre-impregnated fibers stacked on a mold. The prepregs are covered with a plastic vacuum bag to remove the air between the plies. Then, cured by either placing the bagged part in an oven or in an autoclave under pre-determined temperature and pressure. An autoclave is a pressure vessel used to provide the desired gas pressure, and it has the advantage of reaching higher fiber-volume fractions and less porosity with better compaction. The application of prepregs with autoclave curing is mostly preferred in the aerospace industry [40]. The schematic of prepreg lay-up with autoclave can be seen in Figure 8.

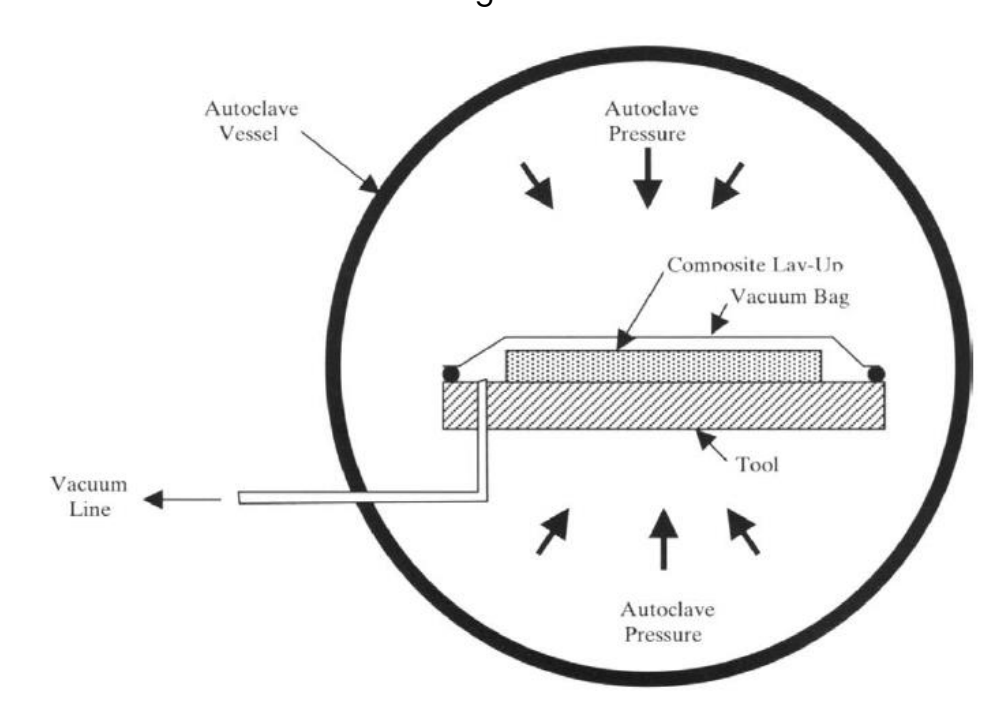


Figure 8. Prepreg Lay-up Technology in Autoclave [40]

# Filament winding

The filament winding technology is one of the most common and oldest composite manufacturing techniques used for the fabrication of hollow, circular, and prismatic shapes, such as pressure vessels, by utilizing the turning lathe principle. It is performed by winding the fiber bands onto a rotating mandrel after passing them through a resin bath by using special winding equipment [41]. The schematic of the filament winding process can be seen in Figure 9.

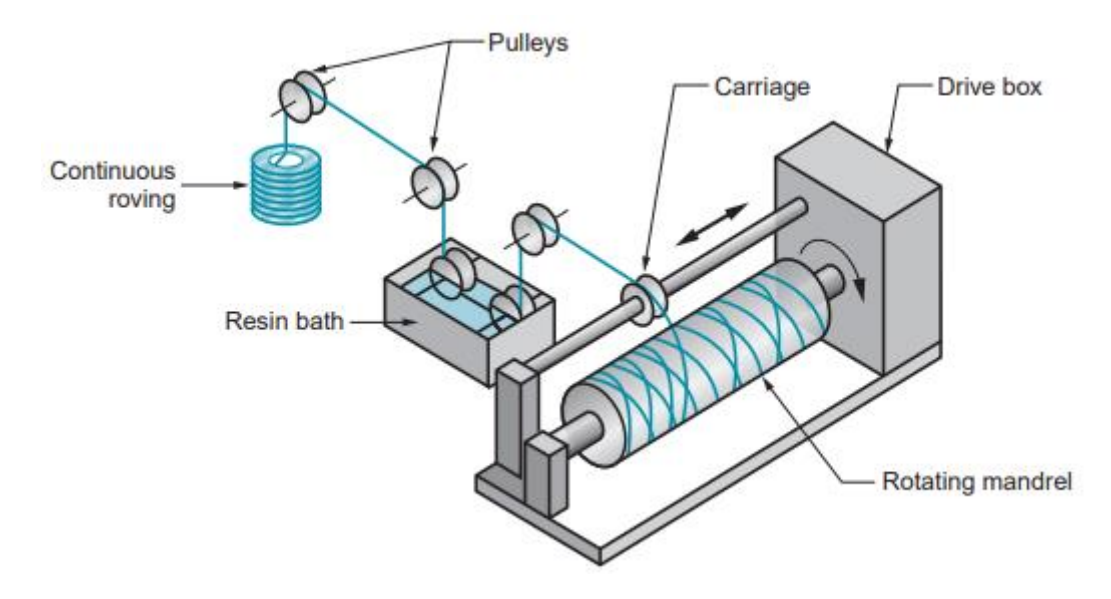


Figure 9. Filament Winding Technology [42]

Components manufactured by filament winding technology are commonly used in the aerospace, consumer product, and energy industries. Epoxy resins are by far the most common material for the matrix, and for the reinforcement, carbon, glass, kevlar, and boron are widely used.

#### **Pultrusion**

Pultrusion technology is a specialized composite manufacturing technique that is used for the production of long, constant-thickness composite parts. It is done by firstly pulling the fiber rovings through a resin bath and then giving the desired shape by the pre-die former before entering the heated die. Inside the die, the curing starts with the high temperature, and the component is pulled by a roller to the desired length and cut by a saw. The schematic of the pultrusion method can be seen in Figure 10.

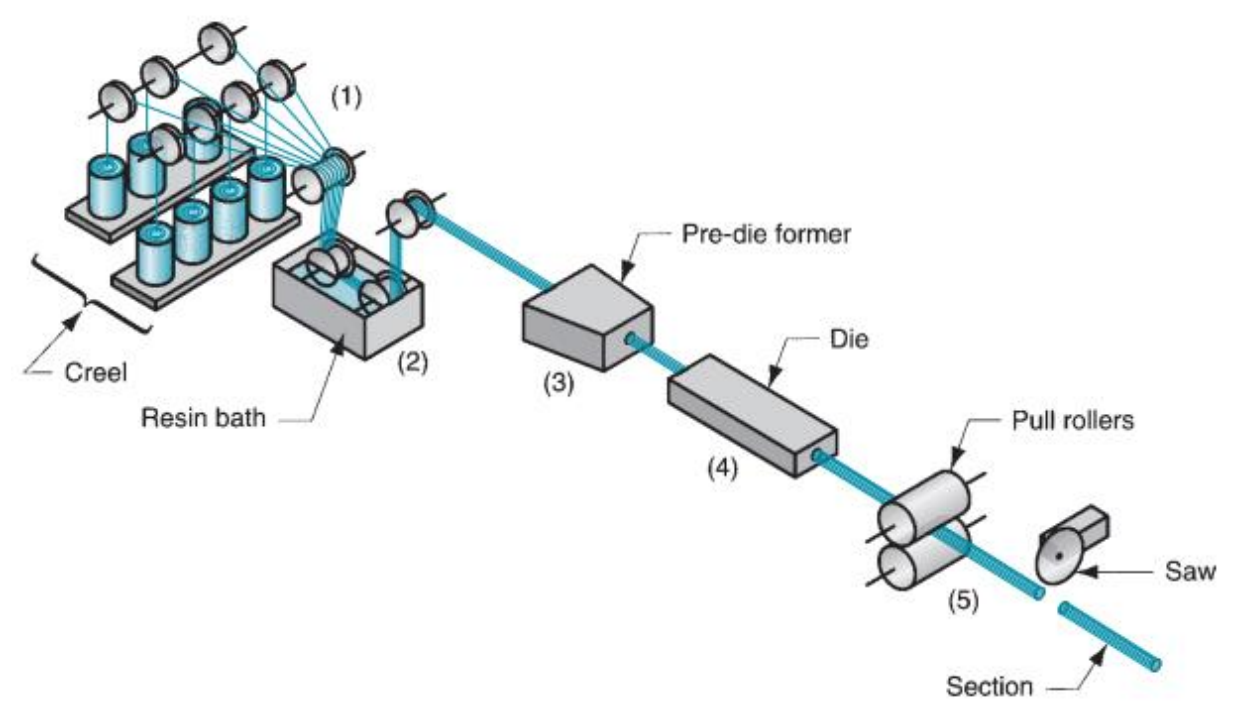


Figure 10. Pultrusion Technology [42]

In pultrusion, E-glass fibers are the most widely used reinforcement material. For the resins, all thermosetting polymers can be used, even if processing of the epoxy polymers can be challenging due to the sticking on the die surface.

# 1.3.2 Adhesive Bonding in Composites

Adhesive bonding is a material joining process in which the adhesive is spread between the surfaces of the adherents to create an adhesive bond. Traditional fasteners generally damage the fibres by cutting, resulting in stress concentration, both of which threaten the structural integrity. On the other hand, adhesive bonded joints, which are more continuous than the mechanically bonded joints, have a better strength-to-weight ratio, easier fabrication, and design freedom [43]. Compared to conventional joining techniques, such as mechanical fasteners (rivets or screws) or resistance spot welding, adhesive bonding presents a promising alternative with several advantages. These advantages include allowing the bonding of dissimilar materials, producing bonds at lower temperatures, offering electrical and thermal insulation, reducing overall structural weight, lowering manufacturing costs, delivering a smoother surface, and providing vibration and sound dampening and resistance to fatigue.

Although adhesive bonding offers many benefits, it requires more labor due to the additional surface preparation and longer curing times. Other limitations include

the operational temperature limit, peel strength, and restricted service conditions [44].

# 1.3.2.1 Adhesive Types

To create a strong adhesive bond, it is essential to begin the process with great care in selecting an appropriate adhesive. Yet this work frequently becomes complicated due to the fact that there is no adhesive to use in all cases, in addition to the enormous variety of products on the market. There are a few considerations in the selection of an adhesive: the type and nature of the substrates, the method of application and curing of the adhesive, the mechanical stresses and conditions the joint will be exposed to in service, and occasionally the cost of the adhesive, especially in production applications. Before an adhesive is selected for a particular application, preliminary screening tests must be conducted to compare and assess adhesion performance. This is particularly critical for structural adhesives, since failure during service can have catastrophic consequences. Since the properties of adhesives can be very dissimilar, thorough characterization, especially of stress–strain behavior and modulus, needs to be ensured to certify that the adhesive is compatible with the intended joint design and application [43].

Epoxy, polyurethane, acrylic, cyanoacrylate, anaerobic, and high-temperature adhesives (HTAs) such as polyimides, bis maleimides, and phenolics are the most frequently utilized adhesives for structural applications. Table 1 provides information about the characteristics of these adhesives.

Table 1. Characteristics of Adhesive Types [43]

	Comments	Service Temperature [°C]	Cure
Ероху	High strength and temperature resistance, easy to use, low cost	-40 to +100	One-part epoxies cure with temperature. Two- part epoxies cure at room temperature (cure can be accelerated with temperature)
Polyurethane	Good flexibility at low temperatures and resistant to fatigue, impact resistance, and durability	-200 to +80	Room temperature
Acrylic	Versatile adhesives with capabilities of fast curing and tolerate contaminated surfaces	-40 to +120	Cure through a free radical mechanism
Cyanoacrylate	Fast bonding capability to plastic and rubber but poor resistance to moisture and temperature	-30 to +80	Fast cure (seconds or minutes) upon exposure to moisture at room temperature
Silicones	Excellent sealant for low stress applications, high degree of flexibility and very high temperature resistance, capability to seal or bond materials of various natures, long cure times, and low strength	-60 to +300	Room temperature
Anaerobic	Designed for fastening and sealing applications in which a tight seal must be formed without light, heat or oxygen, suitable for bonding	-55 to +150	Cure in the absence of air or oxygen at room temperature
Polyimides	Thermal stability, dependent on a number of factors, difficult processability	-40 to 250	Cure with temperature and high pressure
Bismaleimides	Very rigid, low peel properties	-50 to +200	Cure with temperature and high pressure
Phenolics	Good strength retention for short periods of time, limited resistance to thermal shocks	-40 to +175	Cure with temperature and high pressure

# 1.3.2.2 Bonding Techniques and Joint Configurations

Unlike metals, ceramics, and wood, polymers and composites possess inherent physical properties that make them unsuitable for traditional joining methods such as fastening and clinching because these techniques create a high amount of stress. Composite production processes are also largely incompatible with conventional joining techniques. In fiber-reinforced plastic (FRP) structures, the process of hole drilling for bolts causes damage in the form of fiber cutting, ply peeling around the hole, resin degradation along the hole walls, and delamination of the remaining layers of the laminate. These damages can initiate fatigue cracks and therefore significantly reduce the fatigue strength of the mechanically fastened joints. Also, mechanical fasteners are a source of increased overall weight of the structure. In heavy structures like ships and aircraft, minimizing the number of fasteners is an effective weight-reduction measure. Adhesive bonding, therefore, becomes the optimum joining method for both similar (composite-composite) and (composite-metal) materials, particularly when dissimilar subsequent disassembly for maintenance or inspection is not required [45]. However, some parameters affect the quality of an adhesive bond. These are surface preparation and the joint configuration.

The surface quality of the adherents plays a significant role in the overall quality of the adhesive bonding process. It can be said that this is one of the vital steps to achieving maximum mechanical strength, as the cohesion of the surface directly affects durability. One misleading piece of information about surface treatment is that merely cleaning the surface is sufficient to obtain a good adhesive bond without any additional treatment. This misconception might cause to adhesive failure. The adhesive failure mode is illustrated in Figure 11 with other failure modes seen in adhesive bonding such as cohesive failure, thin-layer cohesive

failure, fibre-tear failure, light-fibre-tear failure, stock-break failure, or mixed failure [43]. To prevent adhesive failure, proper surface treatments should be taken into consideration.

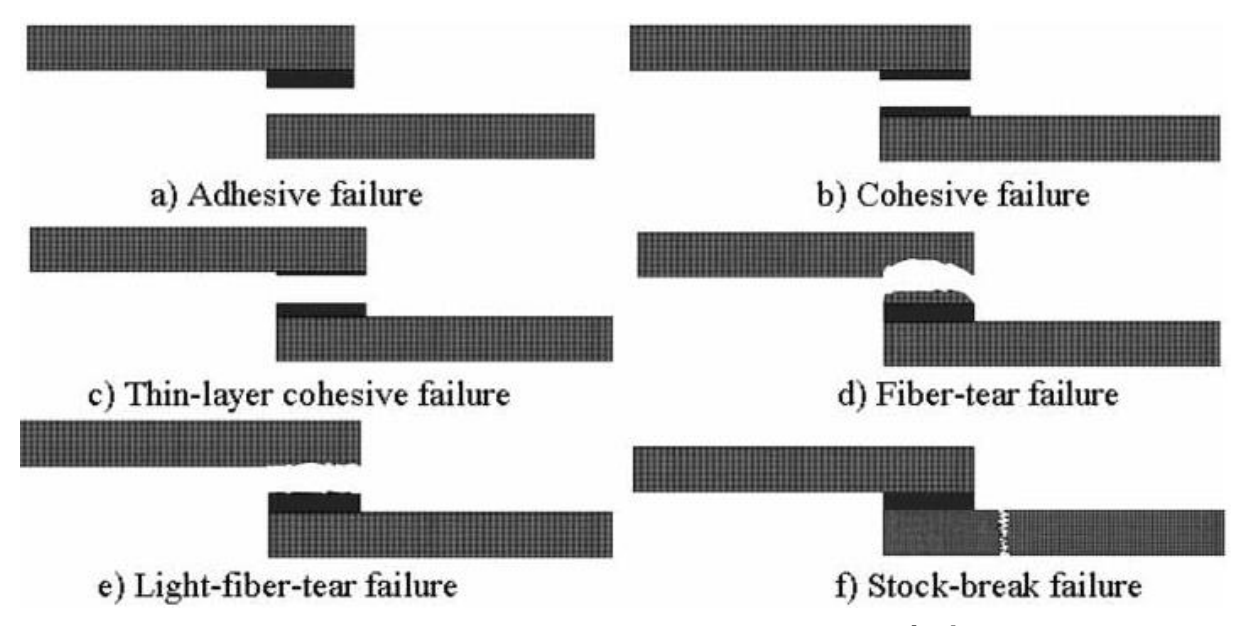


Figure 11. Typical Failure Modes of Single Lap Joints [43]

For thermoset composites, abrasion/solvent treatment is commonly preferred. Meanwhile, various surface treatments can be applied to adherends before bonding for thermoplastic composites to increase surface tension and roughness and to change surface chemistry. These surface treatment techniques include abrasion/solvent cleaning, grit blasting, peel-ply, tear-ply, acid etching, corona discharge, plasma, and laser treatment [43].

The effect of joint configuration is as significant as that of surface preparation. Joint design poses one of the biggest challenges in structural design due to its discontinuous nature. Because of this discontinuity, joints are susceptible to local stress concentrations. Various types of joint configurations are available for designers. Figure 12 illustrates these configurations. In the literature, single-lap joints, double-lap joints, scarf joints, and stepped-lap joints are commonly used to analyse the characteristics of adhesively bonded joints. Configurations such as strap joints, butt joints, stepped scarf joints, corner joints, T-shaped joints, L-shaped joints, tubular lap joints have been also examined.

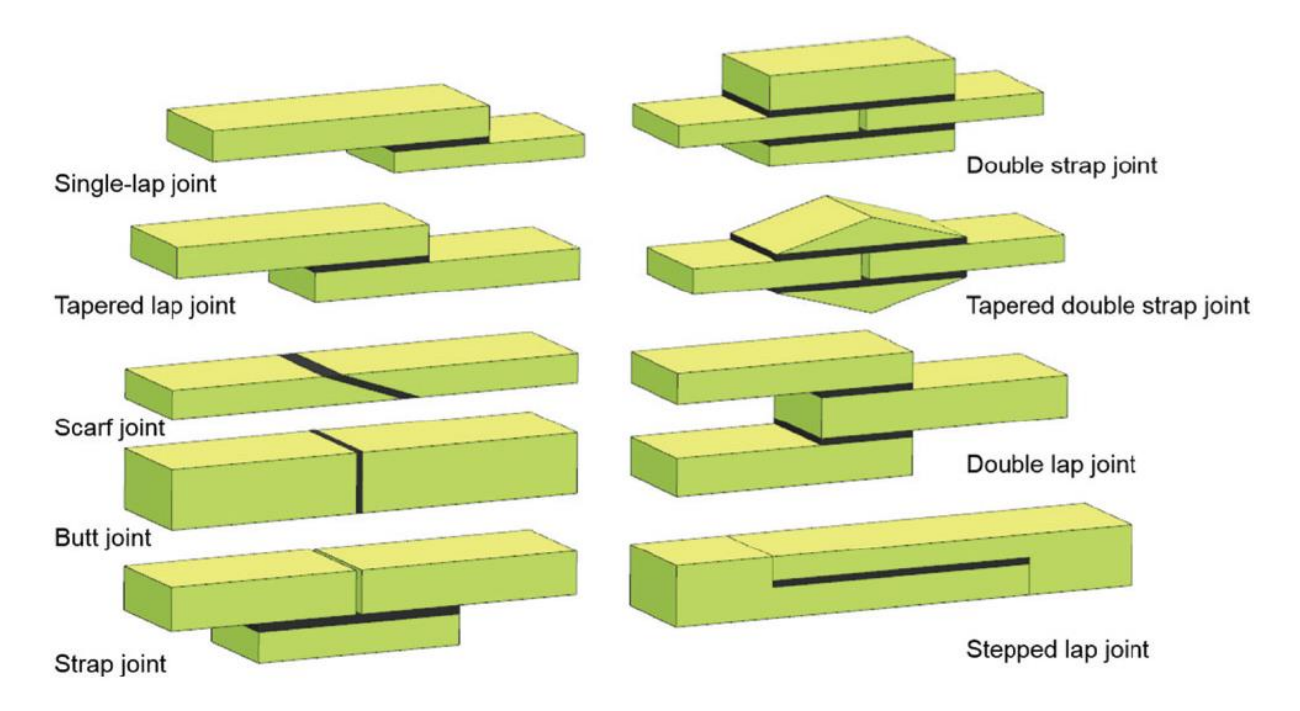


Figure 12. Joint Configurations [45]

The durability of an adhesively bonded joint depends on the stress distribution within the joint, which is influenced by the joint geometry and the mechanical properties of both the adhesive and the adherend. For instance, in the case of fiber-reinforced polymer composite adherents, some stresses, such as peel and cleavage, can lead to premature failures due to the higher through-thickness stresses at the overlap ends and the relatively lower through-thickness strength of the polymer composites. To overcome this issue, joints should be designed with the aim of minimizing the peel and cleavage stresses and maximizing shear and compressive stresses. For example, single-lap joints are susceptible to peel stresses; for this reason, double-lap, scarf, and stepped joints are preferred to overcome the high peel stress issue [43]. The stresses and the failure of a single-lap joint due to through-thickness stress can be seen in Figure 13.

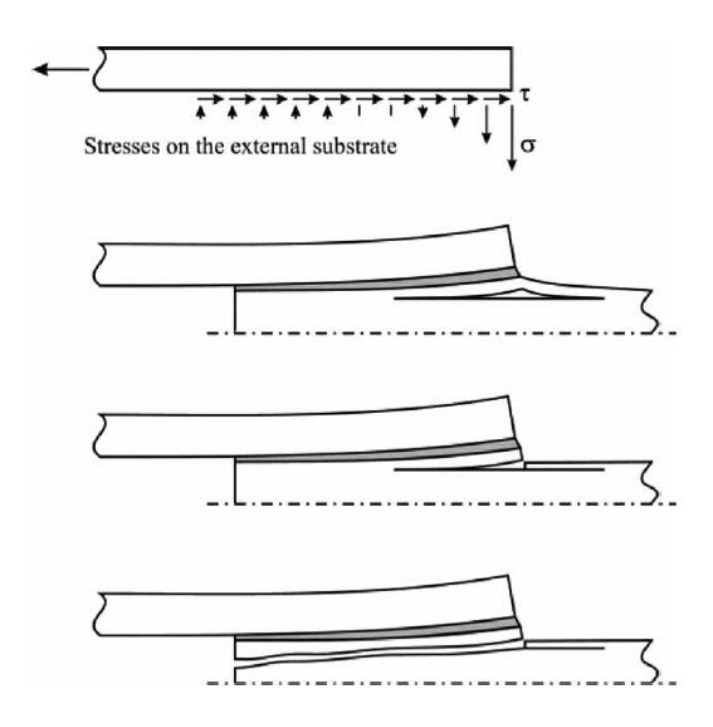


Figure 13. Through Thickness Stresses in Single Lap Joint [43]

Several techniques have been developed to improve the efficiency of the single-lap joints. These include changing the adherend, adhesive, and spew geometry (the spew is excess adhesive from the lap region during joint manufacture). Tapering the adherend and stepping are related to altering the adherend geometry in design guidelines and many studies [43] Lang and Mallick developed a new bonding method by removing some fractions of the adhesive layer (recession) [46]. Spew shape has been examined to provide a smoother transition in the joint area, which minimizes stress concentration [47]. One method utilizes different adhesive materials along the overlap with variable modulus to reduce stress concentrations at the overlap end region [48]. Another technique is varying the adherent material properties by modifying the braided fiber placement technology. Ganesh and [49] proved that grading the adherend elastic modulus can offer more uniformly distributed stresses in the adhesive layer.

Due to advancements in materials engineering, there is a greater emphasis on research and development activities focused on applying thin sheets and miniaturized structural elements. Furthermore, an emerging trend is observed in integrating conventional metals with polymeric composites. These composites enhance structural efficiency regarding the strength-to-weight ratio and are resistant to galvanic corrosion. On the other hand, metals exhibit higher damage tolerance and more predictable failure modes, along with solvent and high-temperature resistance that degrades polymers. To leverage the strengths of both

material types, there is an increasing focus on developing multi-material joints that combine metals and composites. Joining these structural components and polymer-metal hybrid structures requires the application of innovative methodologies. One of the most common techniques involves hybrid methods that integrate mechanical fastening, adhesive bonding, and welding principles.

Hybrid joining techniques can be listed as hybrid-bonded fastened joining, clinch bonding, and weld bonding. For the hybrid-bonded fastened joints, bolts, rivets and pins are utilized along with adhesive to prevent limitations of each joining method. The bolts/rivets help to withstand axial loads and the adhesive contributes to distribution of the remaning load more uniformly [50]. A schematic of the hybrid-bonded fastened joints can be seen in the Figure 14.

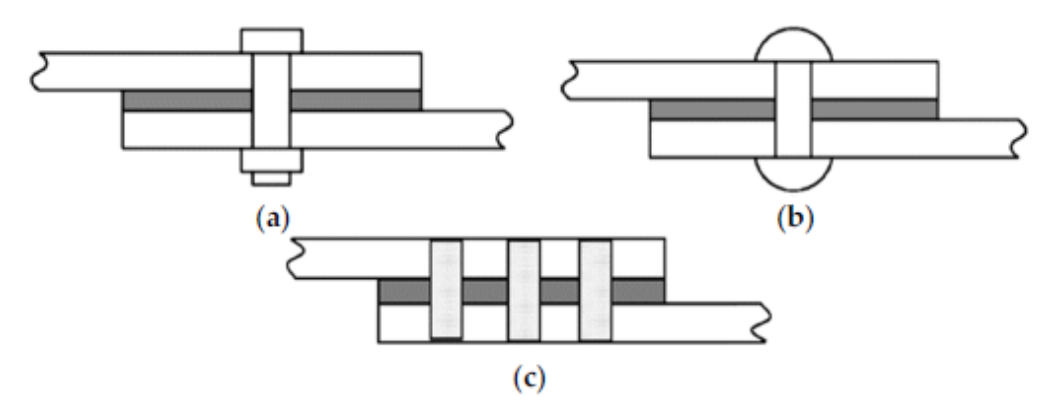


Figure 14. Schematic Representations of (a) Bolted-bonded Joint, (b) Rivet-bonded Joint and (c) a Pin-bonded Joint [50]

Clinching is used to join metal-to-metal joints and composite-metal dissimilar materials using the press-joining method [51]. On the other hand, clinch bonding merges clinching and adhesive bonding techniques. Compared to mere adhesive bonding, clinch bonding provides higher stiffness and load capacity, reduced vibration and noise, and corrosion resistance [52]. Figure 15 shows a schematic of clinch bonding.

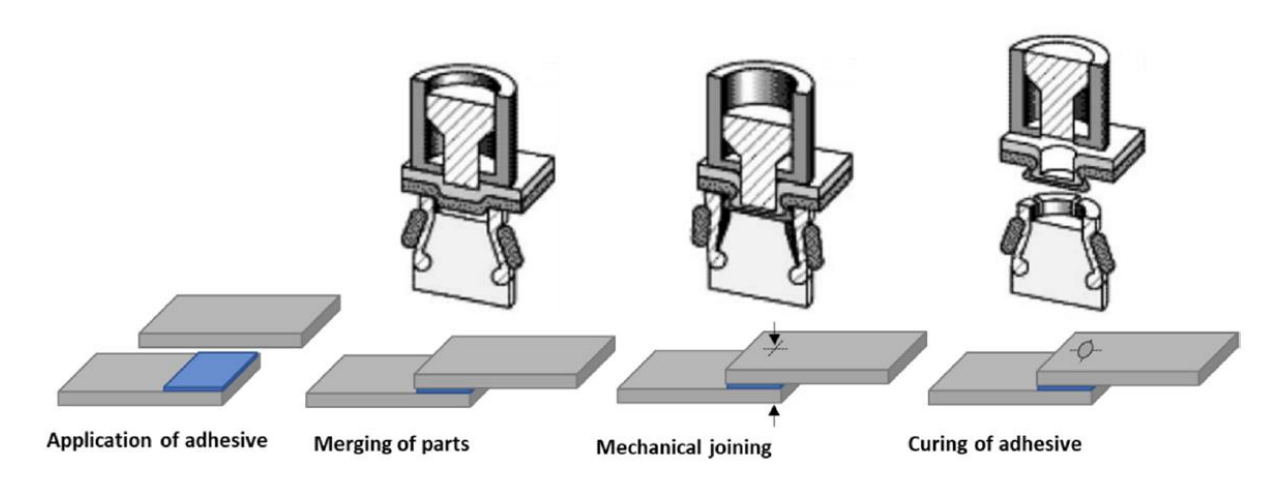


Figure 15. Clinch Bonding [50]

Hybrid techniques that integrate adhesive bonding and welding procedures can typically be classified into two general categories: weld bonding and other hybrid welding forms. Weld bonding is specifically referred to as the hybridization of resistance spot welding with adhesive bonding (RSW-AB). At the same time, other hybrid techniques involve techniques like Friction Stir Welding with adhesive bonding (FSW-AB), Friction Stir Spot Welding with adhesive bonding (FSSW-AB), Laser Weld Bonding (LBW), and Laser Spot Weld Bonding (LSWB) [50]. The schematics of resistance spot-welding with adhesive bonding and friction stir welding with adhesive bonding can be seen in Figures 16 and 17, respectively.



Figure 16. Resistance Spot-welding with Adhesive Bonding [50]

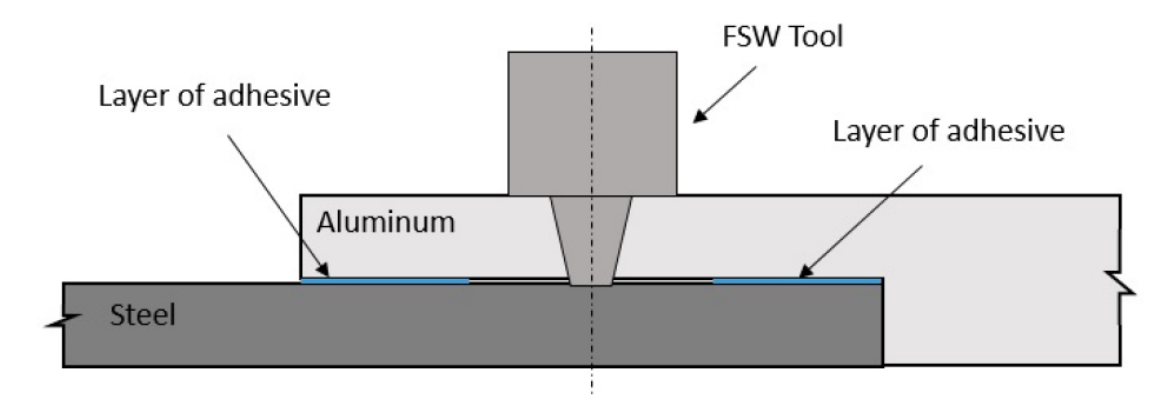


Figure 17. Fricrion Stir Welding with Adhesive Bonding [50]

# 1.3.3 Challenges in Disassembly and Recycling of Adhesive Joints

Some of the materials widely used in adhesive bonding, such as carbon fiberreinforced polymers (CFRPs) and ceramics, tend to be costly and pose environmental concerns by the time they reach the end of their useful life. In automotive applications, for instance, global concerns have arisen regarding the recycling, recovery, and reuse of end-of-life vehicles. In some countries, the production rate of vehicles has overwhelmed the capacity of recycling systems to dispose of them once they are retired from service. These vehicles are normally either dismantled for material recovery or just dumped, creating safety hazards in public areas and wasting resources. Due to these environmental and economic issues, the development of new technologies and methods that facilitate recycling and repair of bonded assemblies is increasingly becoming important across a range of industries. One of the greatest challenges for recycling adhesive joints is the separation of bonded parts without their damage, in order to reuse them. Several traditional methods are still applied to this purpose when unmodified adhesives are used. Mechanical separation is one of the oldest methods, which is typically ineffective and time-consuming due to the low quality of separation. One of the ways is to heat the adhesive beyond its glass transition temperature or beyond its flammability or auto-ignition temperature in order to degrade its structure. This, however, is not only costly but can also release toxic or irritating gases due to chemical decomposition. Another conventional technique is chemical immersion, where joints are subjected to acids or solvents. Common solvents used include isopropyl alcohol, methyl ethyl ketone, and acetone, all of which are good at degreasing and cleaning surfaces [2].

Due to the fact that mechanical separation is not an effective process in terms of applicability and is time-consuming, academics and companies are actively working on developing suitable adhesive systems to utilize debonding-on-command. These techniques have been classified based on external stimuli, such as UV light, thermal, chemical, magnetic, electrical, and ultrasound, as shown in Figure 18.

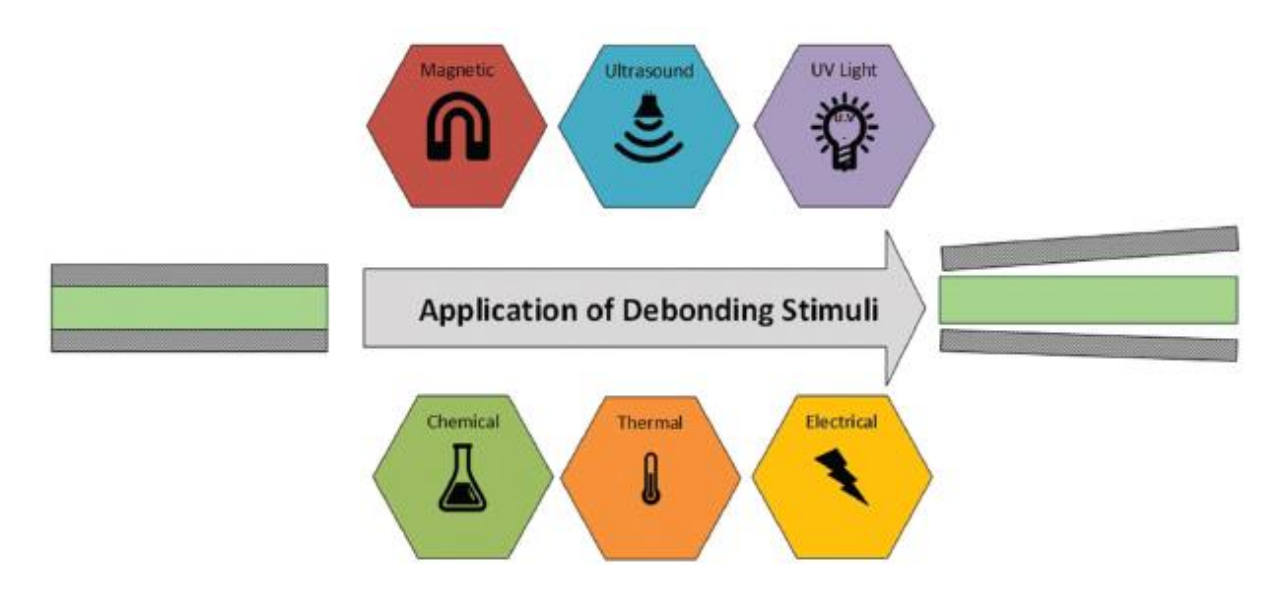


Figure 18. Debonding-on-command Techniques [53]

## **Light Debonding**

Whereas most modern debonding techniques are based on thermal applications to change physical properties of adhesives and thus lower their bonding capacity, light-assisted debonding is a more recent and less explored technique. The application of photoirradiation provides the following benefits compared to thermal techniques: precise, non-invasive, and remote stimulation with reliable control over the timing and location of stimulation. As an added benefit, parameters like wavelength, intensity of light, and exposure duration are simple to adjust. The technique also enables precise energy delivery to the adhesive alone, so substrates sensitive to heat are excluded or even eliminated from exposure. But an essential requirement is that one of the attached materials must be fairly transparent to light [54]

## Magnetic Debonding

Certain adhesive systems are incorporated with magnetic additives to trigger degradation upon exposure to an alternating magnetic field. For example, the incorporation of iron oxide ( $Fe_3O_4$ ) nanoparticles into commercial adhesives to enable magnetic-induced hysteresis heating, thereby producing localized heat. This can either directly melt the adhesive to facilitate separation or trigger secondary reactions like the degradation of cross-links or the activation of blowing agents. The time taken for the debonding process depends significantly on the concentration of  $Fe_3O_4$  nanoparticles and can be optimized further by incorporating other nanomaterials such as graphene that increase thermal conductivity and melting efficiency. R. Ciardiello et al. [55] reported that unlike many additives, which

weaken adhesive strength, these nanoparticles increase the adhesive strength and stiffness, enabling strong adhesion to various surfaces. Additional benefits of this approach are its cost-effectiveness, compatibility with existing adhesive systems, and extremely low potential for accidental activation due to the specificity of magnetic field exposure. Nevertheless, this technique is confined to adhesive bonding that uses non-ferromagnetic substrates, which may limit its applicability. Additionally, the magnetic fields involved are extremely high and require the use of specialized equipment. [53].

# Electrical Debonding

Electrical debonding, as presented in the framework of ElectRelease technology [56], is a new and controllable technique for the debonding of adhesives relying on electrochemical principles, which is illustrated in Figure 19.

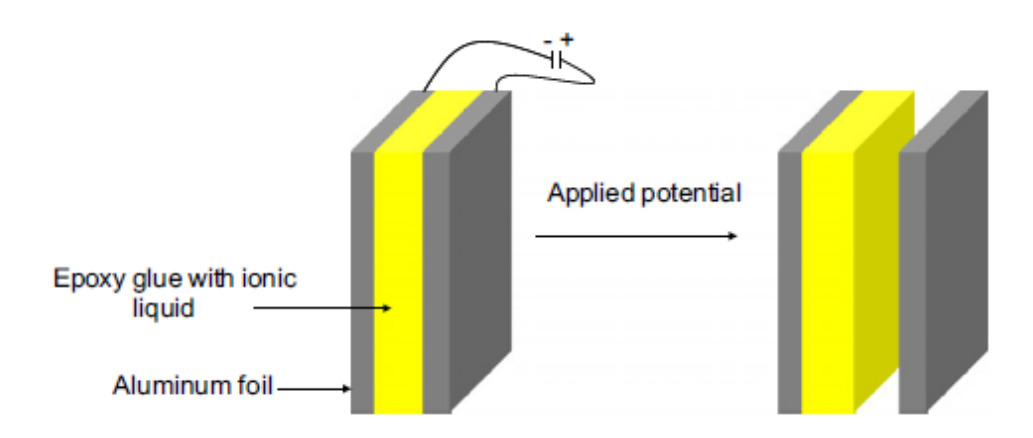


Figure 19. ElectRelease Technology [57]

Unlike conventional mechanical or thermal debonding techniques, this method is applied using a specially tailored adhesive with ionic conductive fillers. In the regular setup, two metal substrates, usually aluminum foils, are bonded together by an epoxy adhesive that simultaneously serves as an electrolyte, thus forming a kind of electrochemical cell. Upon application of an electric potential from outside the metal layers, a current passes through the adhesive layer and induces electrochemical reactions at one of the interfaces, i.e., either the anode or the cathode, depending on the composition of the adhesive. These reactions induce adhesion weakening and ultimately controlled delamination. This method has been successfully demonstrated in various metals like aluminum, steel, stainless steel, copper, and titanium. The key benefit of this technology is that it delivers debonding on demand, remotely and regardless of mechanical force. That said, there are certain limitations: the system needs conductive substrates, direct electrical

connections, and special adhesives, which may not be suitable for every application. Nonetheless, the ElectRelease approach creates new opportunities for reversible bonding in applications where maintenance, recycling, or replacement of parts is necessary [57].

### **Ultrasound Debonding**

Ultrasound has been extensively utilized as a non-destructive method for examining adhesive degradation. However, despite its widespread use, there is some potential for ultrasound to act as a trigger for adhesive debonding. Tachi et al. have developed an adhesive debonding system utilizing ultrasonic irradiation. They demonstrated that the peel strength of pressure-sensitive adhesives composed of acid-degradable polyurethanes and microcapsules containing thermal acid generators decreases with heating up to 80 °C and ultrasonic irradiation [58].

### Chemical Debonding

Chemical methods weaken the bondline by degrading the adhesive, thereby reducing the joint's strength. All techniques involve introducing an extra component and applying mechanical force to disassemble the joint.

Chemical forming agents (CFA) have been used to produce polymer foams, in the form of thermoplastic and thermoset, hence they are broadly available and suitable to modify adhesives. In old times, haloalkanes were widely used, but due to environmental concerns, they are now prohibited. Nowadays, organic and inorganic chemical foaming agents are widely used. These agents are easy to manipulate, and when they reach the decomposition temperature, they produce a high volume of gas, which weakens the adhesive and facilitates easier debonding. However, during decomposition of the chemical agents, a large amount of oxygen, nitrogen, carbon dioxide, or carbon monoxide is released, which might be considered an environmental threat [2]. R.H. McCurdy et al. [59] reported that chemical foaming agents can be utilized in automotive structural adhesives, as they effectively induce solid-state foaming that reduces the allowable stress that the adhesive can withstand and enables successful joint separation. However, it has been said that there is poor chemical compatibility between organic agents and epoxy or polyurethane due to the unpredictability of the reactive groups when mixed with each adhesive, which affects the bond strength.

Another approach for chemical debonding is breaking down the adhesive's chemical structure using aggressive chemicals and solvents. It is known that epoxies degrade when exposed to hydrochloric acid [60], and the chemical structure of polyurethanes can be broken down by glycolysis or hydrolysis. Recent studies [61] have demonstrated that solvolysis by using polyethylene/NaOH can break down epoxy resins under milder conditions. This process can either disrupt the chemical bonds within the cross-linked network or function as a plasticizer, penetrating the adhesive and weakening its overall structure. Factors such as pressure, temperature, catalysts, and solvent type affect the efficiency of the solvolysis process. Ideally, the process should degrade the polymer into lower molecular weight compounds or even into monomers. The issue is to develop a solvolysis method that operates under mild conditions using safe, non-toxic, and environmentally friendly materials. Although this method appears to be a good alternative for degrading and weakening epoxies and other structural adhesives, applying it to an adhesive joint presents significant practical challenges. Preventing damage to the bonded substrates might be challenging, making this approach more appropriate for post-disassembly recycling rather than debonding [2].

# Thermal Debonding

Thermal debonding of adhesive systems is another method that involves reaching elevated temperatures to thermally degrade the adhesive, resulting in joint failure. It requires a significant amount of energy, and the limitation is that localizing the heat to the adhesive bond line is not easy, which can result in damaging the substrates [2].

Heating the substrates to elevated temperatures can cause serious consequences. Microcracking might occur at the fibre-matrix interface due to the different thermal expansion coefficients of the FRP constituents. This leads to degradation of matrix-dominated mechanical properties, i.e., interlaminar shear strength, longitudinal compressive strength, and transverse tensile strength. These microcracks can act as initiators of more severe damage, such as transverse cracks, delamination, and longitudinal splitting, and also, moisture can enter the FRP [62]. Due to the thermal expansion mismatch between fiber and the matrix, a localized heater, such as a heat gun, must be used when thermal debonding is planned.

Shape memory additives (SMA) are another approach used for thermal debonding. It is based on the shape recovery principle of the SMA additives. During the preparation of the adhesive, they are embedded in the adhesive in the form of

polymer layers or randomly distributed fibers, and when the thermal stimulus is applied, SMA transforms its shape from flat to curved, which results in fracture in the adhesive matrix that allows for joint failure [53]. Hui-Yun Hwang [63] investigated the mechanical properties of adhesives modified with shape memory fibers (SMF). For the SMF, nickel-titanium alloys (Nitinol) are selected, and epoxy is chosen as the adhesive. It has been reported that the adhesion strength of the modified epoxy is higher than that of neat epoxy at room temperature. Additionally, the adhesion strength decreases by 30% as the shape recovery temperature (325 K) is reached and held for 30 min.

Table 2 lists potential uses, limitations, and notes for different debonding methods.

Table 2. Adhesive Debonding Stimulus Methods [53]

Stimulus	UV Light	Thermal	Electrical	Chemical	Magnetic	Ultrasound
Potential Uses	Thin transpare nt materials	Inorganic and metallic component s	Bonding metals and conductive substrates	Reactive composite adhesives with stable substrate	Biological / electronic applicatio ns	Better for weak adhesive bonds
Limitations	Opaque additives	Equipment operating at high temp  Non-thermally stable/conductive substrates	Non- conductive substrates must be bonded with an intermediate patch	Needs to not etch the substrate	Magnetic substrate s	Needs to be a wet recycling process
Notes	Harder with complex geometri es	Potentially applicable to most adhesives	Better for thin samples	Diffusion can be slow	Low cost, easy to develop	Surface wetting important

# 1.3.4 Thermally Expandable Particles (TEPs)

# 1.3.4.1 Principles and Mechanism of Expansion

Thermally expandable particles (TEPs) were first introduced in the early 1970s by Dow Chemical Co [64]. They are made of a co-polymer shell filled with liquid

hydrocarbon as the blowing agent. When heated, the blowing agent begins to gasify, pushing the softened co-polymer shell outward. As a consequence, the particle's size grows significantly. The volume of the particles can increase by a factor of 50 to 100. After removing the heat, the softened shell returns to its stiff form, and the particle retains its expanded form. The model of the TEPs can be seen in Figure 20.

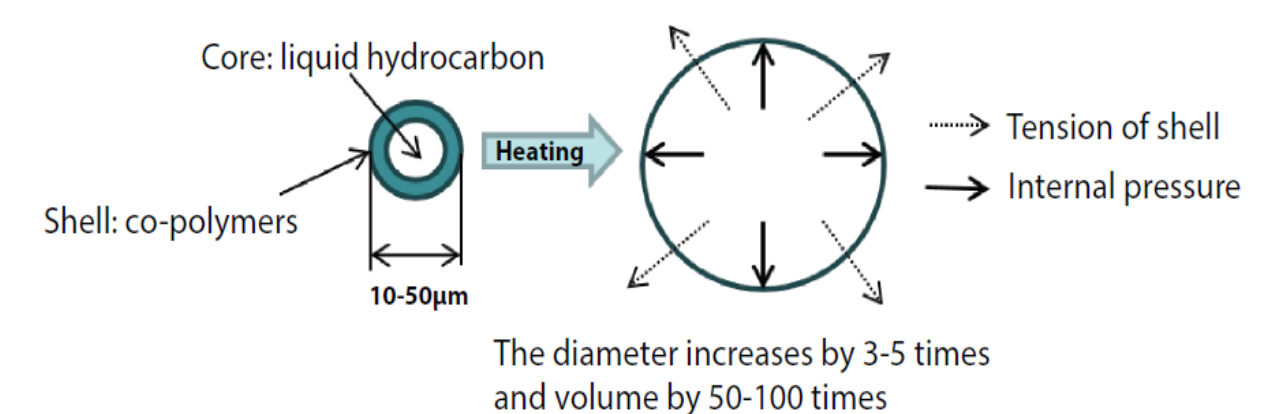


Figure 20. Schematic of a Thermally Expandable Particle [93]

TEPs are produced through suspension polymerization, where monomers are dispersed as droplets in a liquid phase to form spherical polymer particles by polymerization with the external stimulus of mechanical agitation [65]. TEPs are commercialized by Expancel Nobel Industries under the trademark of Expancel [66] and by Matsumoto Yushi Seiyaku, under the trademark of Micropearl. Thanks to their distinct properties, TEPs are utilized in a broad variety of applications by the industry. However, applying TEPs to structural adhesive systems started by Nishiyama et. al. to bond plywood boards [67].

### 1.3.4.2 Types, Morphology and Properties

Microspheres are composed of a shell made of thermoplastic polymer encapsulating a hydrocarbon fluid with a low boiling point. When they are heated, the shell material softens, and the hydrocarbon inside gets vaporized. The pressure applied by the vapor on the softened shell causes the microsphere to expand significantly. Thermally expandable microspheres have diameters from 5 to 50  $\mu$ m. The hydrocarbon that is encapsulated serves as a blowing agent. Microspheres are highly durable and can resist mechanical pressures as high as 300 kg/cm², and they agre resistant to a range of solvents. They should be stored indoors at temperatures below 40°C for optimum stability [68].

TEPs start expanding between approximately 35°C and 110°C, and will completely expand between 50°C and 150°C. Although different type of materials may be utilized to produce such particles, they typically possess a polymeric outer layer, such as polyacrylonitrile, and a hydrocarbon inner core. Additionally, microspheres are not biodegradable but they can be incorporated into biodegradable adhesive systems. Each microsphere type has a precise expansion onset temperature ( $T_{\rm start}$ ) and maximum expansion temperature ( $T_{\rm max}$ ).  $T_{\rm start}$  is the temperature at which they start to expand, and  $T_{\rm max}$  is the temperature at which most of the microspheres fully expand. Upon exposure to temperatures far above than  $T_{\rm max}$ , the microspheres can either collapse or rupture due to degradation of the co-polymer shell. The quantity of microspheres incorporated in a particular formulation is typically varied based on their maximum size [68].

# 1.3.4.3 Integration in Adhesives and Debonding Applications

Numerous researchers have investigated the integration of TEPS in adhesives and debonding applications due to the necessity of new joining technologies and efficient disassembly procedures. End-of-life legislations and concerns for recycling vehicles manufactured using different materials have highlighted the need for efficient solutions for debonding, and TEPs are regarded as a potential candidate to bring a solution to this issue by expanding in volume and causing the fracture of the adhesive bond line.

Table 3 provides a comprehensive comparison of different types of debonding techniques. Among several methods, the incorporation of functional additives such as thermally expandable particles and chemical foaming agents (CFA) has been regarded as the best potential candidate to achieve a successful debonding process. However, their compatibility with the adhesive matrix limits their application. This is because the CFAs act as a reactant inside the adhesive matrix, whereas the TEPs reduce the mechanical strength of the adhesive bond due to their low density.

Table 3. Comparison for Different Adhesive Debonding Techniques [69]

Techniques	Disbonding condition	Automotive applicability	Complexity	Capital cost	Disbonding efficiency	Overall rating*
Mechanical separation	N/A	Low	Low	Low	Low	*
Thermally reversible structure	Temperature (100–250°C)	Low	High	Medium	Medium	**
Thermally removable adhesive	Temperature (90 °C)	Low	High	Medium	Medium	**
Electrochemically reversible structure	Electric current (not specified)	High	High	High	N/A	**
Ionically conducting epoxy adhesive	Electric current (10- 50 V)	Medium	High	High	High	***
Oxidising agents	Temperature (300°C)	Low	Medium	Medium	Medium	**
Microcapsules	Temperature (175°C)	Low	High	High	Medium	**
Thermally expandable additives	Temperature (250–500°C)	Low	Medium	Medium	Medium	**
Chemical foaming agents (CFAs)	Temperature (130–250 °C)	Medium	Medium	High	High	***
Thermally expandable particles (TEPs)	Temperature (120–200°C)	Medium	Medium	Medium	High	****
Light-sensitive switchable adhesive	Exposure to light (20 s)	Low	High	High	High	**
Gecko-inspired nano-structured adhesive	N/A	Low	High	High	High	**

M. D. Banea et al. [70] have studied the behaviour of two different structural adhesives modified with Expancel 031DU40 particles. They have found that by

increasing the wt% TEPs content, the tensile strength at the yield point has decreased. The decrease was less for the less stiff adhesive, BetamateTM 2098, with Young's modulus of 0.93 GPa. The possible explanation is that TEPs are less constrained within the less rigid adhesive, as stiffer materials have lower free volume, higher cross-link density, and reduced molecular mobility. They stated that volume expansion increases with the weight percentage of the TEPs and the temperature, depending on the type of adhesive. FT-IR analysis indicated that the chemical interaction between the adhesive matrix and particles was absent.

Y. Nishiyama et al. [68] have investigated the volume expansion ratio of Bisphenol A type epoxy modified with 10% wt.. to 50% wt. Matsumoto F-30 particles with a diameter between 10 and 30  $\mu m$  under different temperature conditions, their bond strength with varying particle weight percentages, and dismantability. They concluded that the dismantability of the joints depends on both the weight fraction of the particles and the surface preparation technique of the adherends, such as gridpaper finishing and gridblast finishing. The lap shear strength increases with increasing weight fraction till 30% wt., and then it begins to decrease.

Y. Lu et al. [71] have modified the surface of 920DU120HEMA grade of TEPs, which contains 15 wt% 2-hydroxyethyl methacrylate on the thermoplastic shell material, by using atom transfer radical polymerisation and activators regenerated by electron transfer, a technique called ARGET ATRP. After surface modification, they achieved that the tensile lap shear strength and ultimate tensile strength have increased up to 15.8% and 24.0%, respectively, compared to the adhesive incorporating unmodified particles.

F. Wanghofer et al. [72] have investigated different types of filler particles, such as Nouryon 909DU80 TEPs, expandable graphite and nanoferrites for use in adhesive connections of photovoltaic modules. They calculated the volumetric expansion ratio of modified condensation-curing 2-component alkoxy-based silicone adhesive with varying particle content. The highest calculated expansion ratios for TEPs modified adhesive were 3, 11, and 21 for 10%, 30%, and 50% wt., respectively. Additionally, they incorporated 30% wt. nanoferrites and 30% wt. TEPs together to utilize inductive heating as the expansion triggering mechanism. They achieved thermal expansion within 5 minutes.

G. Piazza et al. [73] have investigated the reversibility performance of Expancel 031DU40 and Expancel 461DU20 TEPs modified two-part epoxy adhesive joints with varying weight concentrations in the range of 5% to 25%. They have used aluminum

and carbon fiber substrates and inductive heating for the expansion triggering mechanism. They have concluded that the fatigue strength of the adhesives decreased with the incorporation of TEPs. The reversibility was possible with weight concentrations of more than 5% and increasing the TEPs content helped to reduce the time and temperature required to debond the joints.

R.H. McCurdy et al. [59] have investigated the debonding characteristics of automotive manufacturer-approved structural adhesives (Betamate XD4600 epoxy and Betamate 2810MV polyurethane) modified with several TEPs and various weight concentrations. Their study showed that TEPs can enhance joint disbonding in structural adhesives through solid-state foaming. However, PFAs made minimal impact in moderate temperature-cured polyurethane adhesives compared to unfilled controls. For instance, in epoxy adhesives, performance was influenced by the expansion rate of PFAs and compatibility with the adhesive matrix. Low compatibility decreased joint performance and required higher PFA concentrations, which caused disbonding. In addition, elevated cure temperatures triggered premature activation of PFAs in liquid phase and resulted in weak, porous structures. While PFAs retained disbonding capability after environmental conditioning, they negatively impacted long-term bonded joints' durability.

Hasan Caglar et al. [74] have studied the debonding characteristics of glass fiber reinforced polymer joints with TEP-modified epoxy adhesive. They found that TEPs have no significant effect on the glass transition temperature of the epoxy. 10 wt.% TEPs-epoxy joints (both sandblasted and plasma-treated) exhibited the highest debonding effectiveness. In contrast, the 5 wt.%, 10 wt.%, and 15 wt.% TEPs-epoxy LSS samples demonstrated impressive debonding effectiveness rates of 86.4%, 89.6%, 89.5%, and 91.7% for plasma surface-treated joints at 145°C, respectively. They stated that the difference between the particles' maximum expansion temperature and the adhesive's glass transition temperature should be minimal to increase the debonding effectiveness.

M. D. Banea et al. [75] have conducted a preliminary study to be used for further examinations on the applicability of TEPs in adhesives. They conducted tensile bulk tests to compare tensile properties of unmodified and modified adhesives and Double Cantilever Beam test to investigate mode I crack propagation of Expancel 031DU40 TEPs-modified two-component structural polyurethane adhesive. They have concluded that toughness has increased without compromising stiffness or ductility with the increasing content of TEPs, which may be explained by crack

bridging or crack blunting provided by particles. Plus, adhesive strength has decreased drastically with increasing TEPs content. They also stated that the maximum expansion that the particles exhibit depends on the TEPs content, decreasing with increasing particle weight concentrations.

M. D. Banea et al. [76] developed a method for easy debonding using inductive heating of multi-material two-component epoxy adhesive joints modified by Expancel 03DU40 particles. Debonding was shown to apply to an automotive-grade adhesive, with TEP content and temperature being key influencing factors. Higher TEPs content reduced the required debonding temperature by up to 50%. Multi-material joints, such as Steel/CFRP and Aluminum/CFRP, required more induction heating power than Steel/Steel joints but had similar debonding temperatures. It was observed that the debonding time was mainly depended on the TEPs' expansion rate, which is influenced by factors like substrate thickness, thermal properties, and heating power. The method allowed for quick disassembly in 60 to 120 seconds without damaging the substrates.

Juana Abenojar et al. [77] have studied the effect of magnetization of TEPs on the thermal and debonding properties of joints. They examined the influence of magnetized TEPs on resin curing, bond strength, and durability by using the wedge test. They applied the low-pressure plasma (LPP) technique to the TEPs' surface to increase surface energy and therefore to enhance wettability in order to achieve better adhesion with the epoxy resin, plus to enhance the adsorption capability of magnetite onto the surface of TEPs. They concluded that magnetic TEPs reduced the required energy for disassembly at the cost of reduced shear strength. On the other hand, they increased the durability of the joints.

Amanda L. Higginbotham Duque et al. [78] have investigated the expansion of Expancel 930DU120 TEPs to develop a viable method to alter the microstructure of plastic-bonded explosive (PBX) – surrogates. After X-ray Computed Tomography analysis, they concluded that, for the cast-cured specimens of 10% wt. of TEPs within the silicone elastomer adhesive matrix, the average coid volume increases from 0.4% to 42% after expansion.

Yoshiaki Uratani et al. [79] have experimentally and numerically studied the expansion characteristics of TEPs under varying hydrostatic pressure and at high temperatures.. They utilized Matsumoto Microsphere F30D particles and transparent epoxy resin to observe the expansion visibly. They concluded that, under heat and pressure, the expansion pressure of the particles reached over 1.5

MPa at 90°C. In addition, adhesive joints modified with 50% wt. TEPs enabled successful debonding.

D. Kim et al. [80] have incorporated Matsumoto F-85 thermally expandable particles with polyurethane adhesive to investigate the volume expansion characteristics and dismantlable property by measuring peel strength of cross-linked rubber adherends. They concluded that a 25% weight concentration of TEPs within the adhesive matrix was the optimum content, showing superior adhesion strength and successful dismantlement of joints using 4 min of microwave treatment as the expansion triggering mechanism. They claimed that it was possible to shorten the duration of microwave treatment by adding zinc oxide inside the rubber adherends during preparation.

H. E. Cingil et al. [81] have studied the expansion onset time and total expansion time of TEPs coated with conducting polymers such as polypyrrole (PPy), polyaniline (PANi), and PEDOT, to enhance their heat-induced expansion by using infrared (IR) radiation. Coated TEPs were prepared at polymer weight concentrations ranging from 0.1% to 1.5%. It has been shown that IR heating led to rapid expansion, reducing mean onset times from 162 s (uncoated) to as little as 9–11 s for coated TEMs. It was noted that expansion was fastest and most efficient with PPy, which is cost-effective and less toxic than alternatives.

M. D. Banea et al. [82] have studied temperature-controlled debonding, and it has been proven that the required temperature levels to accomplish successful debonding are related to the TEPs content. They have studied two-component polyurethane and epoxy adhesives modified by varying weight concentrations of Expancel 031DU40 particles. They concluded that with increasing TEPs content, the debonding temperature for epoxy can be lowered by more than 50%, and for polyurethane by up to 40%, with an induction-triggered heating mechanism.

M. D. Banea et al. [83] have investigated the effect of moisture on the tensile properties of the Expancel 031DU40 TEP modified two-component epoxy adhesives. It has been noted that after drying the water-saturated specimens recovered the Young's modulus values. It was observed that the strength of the tensile muscles has reduced due to aging. On the other hand, the strain values at the tensile failure moment have increased, which is attributed to the extra ductility obtained by the moisture. The fatigue tests showed that with increasing amounts of TEPs inside the adhesive results a decrease in the fatigue limit compared to unmodified adhesive.

J. Bonaldo et al. [84] have studied the tensile and bending properties of joints with a selectively modified overlap, so-called functionally graded joints. They concluded that the tensile properties diminish even for a very small amount of particle content in the adhesive matrix. However, a small increase has been observed compared to homogenously prepared joints. Likewise, for the bending properties, a small increase has been observed for the graded joints compared to homogenously mixed modified adhesive joints. As a conclusion, selective distribution of TEPs on the overlap region did not significantly contribute to the joint strength.

Some of the studies on TEPs in the literature can be found in Table 4.

Some review articles on recent developments in debonding techniques and the employment of thermally expandable particles can be found in the literature [85, 68, 69].

Table 4. Literature Search About TEP-Modified Adhesive Systems

Expansion	SLJ	Debonding	Fracture Toughness	Tensile Bulk	Fatigue	Aging	Adhesive	Adherend	Particle	Authors
+	l	I	l	+	l	l	Epoxy, Polyurethane	I	Expancel 031DU40	M. D. Banea et al. [70]
+	I	+	I	I	I	I	Ероху	Aluminium alloy	Matsumoto F-30	Y. Nishiyama et al. [68]
ı	+	I	ı	+	I	l	Ероху	Aluminium	920DU120HE MA	Y. Lu et al. [71]
+	+	+	ı	I	I	+	Silicone	Aluminium	Nouryon 909DU80	F. Wanghofer et al. [72]
1	+	+	ı	I	+	+	Ероху	Aluminium/ CFRP	Expancel 031DU40 ,	G. Piazza et al. [73]
1	+	+	+	I	I	I	Epoxy, Polyurethane	Aluminium	Expancel551 DU40,	R.H. McCurdy et al.[59]
1	+	+	l	I	I	ı	Ероху	GFRP	Expancel 043DU80	Hasan Caglar et al. [74]
I	I	I	+	+	I	ı	Polyurethane	Steel	Expancel 031DU40	M. D. Banea et al. [75]

l	+	+	I	I	I	I	Ероху	Steel/CFRP, Aluminum/C	Expancel 03DU40	M. D. Banea et al. [76]
ı	+	+	+	I	I	I	Ероху	Aluminium	Not given	Juana Abenojar et al. [77]
+	I	I	I	I	I	I	Silicone	I	Expancel 930DU120	Amanda L Higginbotha m Duque et
+	I	I	I	I	I	I	Ероху	I	Matsumoto F30D	Yoshiaki Uratani et al. [79]
+	I	+	I	I	I	I	Polyurethane	Rubber	Matsumoto F85	D. Kim et al. [80]
+	I	I	I	I	I	I	I	I	Expancel 551DU40	H. E. Cingil et al. [81]
1	+	+	l	I	I	I	Epoxy, Polyurethane	Hard Steel	Expancel 031 DU40	M. D. Banea et al. [82]
ı	+	I	I	+	+	+	Ероху	Steel	Expancel 031 DU40	M. D. Banea et al. [83]
ı	+	I	+	+	I	l	Epoxy, Polyurethane	Steel	Expancel 031 DU40	J. Bonaldo et al. [84]

# 2. Materials and Methods

### 2.1 Materials

# 2.1.1 Composite Materials

For the substrates, XPREG® XC130 2x2 twill glass fiber reinforced polymer (GFRP) prepreg and XPREG® XC110 2x2 twill 6k carbon-fiber reinforced polymer (CFRP) prepreg materials have been used. Both of the prepregs were suitable for out-of-autoclave curing. The specification of the glass-fiber and carbon-fiber used are shown in Table 4 and Table 5, respectively.

Table 5. GFRP Specifications [91]

Property	Value			
Weave	2 x 2 Twill			
Resin Matrix	Ероху			
Areal Weight	280 g/m²			
Fibre Orientation	0, 90			
Resin Weight	38%			
T <sub>g</sub> Onset (DMA)	140 °C			
T <sub>g</sub> Peak (DMA)	148 °C			
Consolidated Thickness	0.3 mm			
Min Cure Temp	80 °C (16h)			
Max Cure Temp	120 °C (2h)			

Table 6. CFRP Specifications [92]

Property	Value			
Weave	2 x 2 Twill			
Resin Matrix	Ероху			
Areal Weight	416 g/m²			
Fibre Orientation	0, 90			
Resin Weight	38%			
Consolidated Thickness	0.45 mm			
Min Cure Temp	85 °C (16h)			
Max Cure Temp	120 °C (2h)			
Typical Lamin	ate Properties			
T <sub>g</sub> Onset (DMA)	121 °C			
T <sub>g</sub> Peak (DMA)	135 °C			
Compressive Strength	483 MPa			
Tensile Strength	521 MPa			
Tensile Modulus	55.1 GPa			
Flexural Strength	777 MPa			
Flexural Modulus	46.7 GPa			
Interlaminar Shear Strength	64.7 MPa			

### 2.1.2 Adhesive Used

In this study, SikaPower- 1277 [86] two-component epoxy adhesive has been used as the adhesive matrix. SikaPower- 1277 has been designed for applications where high strength and impact resistance properties are required, such as transportation and general industry. Its flexibility allows it to be utilized for repair applications. It contains agents to prevent corrosion and glass beads with a diameter of 0.3 mm to obtain ideal bonding thickness. The image of the SikaPower-1277 adhesive product can be seen in Figure 21.



Figure 21. SikaPower-1277 Epoxy Adhesive

SikaPower—1277 can be cured at different temperature levels regarding the available curing time, with a compromise of the bond strength. The datasheet states that the lap-shear strength value reaches 20 MPa if cured at 23  $^{\circ}$ C for 24 hours, 10 MPa if cured at 60  $^{\circ}$ C for 60 minutes, and 15 MPa if cured at 80  $^{\circ}$ C for 30 minutes.

The properties of the SikaPower – 1277 is given in Table 7.

Table 7. SikaPower-1277 Technical Properties [86]

Properties	SikaPower®-1277 (A)	SikaPower®-1277 (B)		
Chemical base	Ероху	Amine		
Colour (CQP001-1)	Red	White		
Mixed		Ligh	t red	
Density		1.08 g/cm³ 1.06 g/cm³		
Mixed (calculated)		1.07 g	J/cm³	
Mixing ratio	A:B by volume	2	::1	
	A:B by weight	2	:1	
Viscosity (CQP029-4) at 10 s <sup>-1</sup>		430 Pa·s <sup>A</sup>	100 Pa·s <sup>A</sup>	
Consistency		Thixotro	oic paste	
Application temperature		15 –	<b>35</b> ° <sup>℃</sup>	
Open time (CQP046-11 / ISO 4587)	(As contact adhesive)	1 hour <sup>B, C, D</sup>		
Handling time (CQP046-11 / ISO 4	587)	11 hours <sup>c, p</sup>		
Curing time (CQP046-9, ISO 4587)	(Time to reach 20 MPa)	24 hours <sup>c, d</sup>		
Shore D hardness (CQP023-1 / ISO	O 48-4)	75 <sup>C, E</sup>		
Tensile strength (CQP543-1 / ISO	527)	30 MPa <sup>c, E</sup>		
E-Modulus (CQP543-1 / ISO 527)		2 000 MPa <sup>c, E</sup>		
Elongation at break (CQP543-1/	ISO 527)	4 % <sup>C, E</sup>		
Tensile lap-shear strength (CQPC	)46-9 / ISO 4587)	28 MPa <sup>C, D, E</sup>		
Impact peel strength (CQP505-1	/ ISO 11343)	30 N/mm <sup>C, D, E, F</sup>		
Glass transition temperature (CC	0P509-1 / ISO 6721)	67 °C <sup>€</sup>		
Shelf life (CQP016-1) cartridges p	ails	24 months <sup>o</sup>		
	12 months <sup>G</sup>			
CQP = Corporate Quality Procedure A) tested at 20 °C B) applied on both bonding surfaces C) 23 °C / 50 % r. h.	k 10 x 0.3 mm / on stee t 23 °C s o and 30 °C	l		

### 2.1.3 TEP Particles

In this study, Expancel\* 043DU80 grade thermally expandable particles, provided by Nouryon, have been selected to be incorporated into the adhesive matrix. As the designation code points out, DU- dry unexpanded, these particles are delivered in unexpanded dry powder form. It has been seen by thermomechanical analysis, performed by a thermo-mechanical analyzer, that this grade of TEPs starts to expand in the temperature range of 95 – 115 °C ( $T_{start}$ ), and the maximum expansion occurs between 147 – 167 °C ( $T_{max}$ ). The unexpanded particle diameter varies between 16 and 24 µm, measured by laser diffraction. D(0.5) refers to the average particle size. Solvent resistance values are obtained by immersing the particles in a chemical liquid for several days at room temperature, and then performing thermo-mechanical analysis to see the after-effects. When expanded, the diameter of these particles can reach up to 80 µm, depending on which matrix they have integrated. Material properties of these particles and other types of particles provided by Nouryon can be found in Table 8.

Table 8. TEPs - Technical Properties by Nouryon [66]

Expancel®	T <sub>max</sub> [°C]	T <sub>start</sub>	Density [kg/m³]	Particle size D(0.5) [µm]	Solvent resistance
031 DU 40	120-135	80-95	≤ 12	10-16	3
053 DU 40	138-146	96-103	≤ 20	10-16	3
051 DU 40	144-153	106-111	≤ 25	9-15	4
043 DU 80	147–167	95-115	≤ 10	16-24	5
920 DU 20	155-175	120-145	≤ 25	5-9	5
920 DU 40	168-178	123-133	≤ 17	10-16	5
909 DU 80	175-190	120-130	≤ 10	18-24	5
920 DU 80	180-195	123-133	≤ 14	18-24	5
950 DU 80	188-200	138-148	≤ 12	18-24	5
093 DU 120	189-204	120-130	≤ 6.5	28-38	5
951 DU 120	190-205	133-143	≤ 9	28-38	5
930 DU 120	192-207	122-132	≤ 6.5	28-38	5
920 DU 120	194-206	122-132	≤ 14	28-38	5

# 2.2 Preparation of the Modified Adhesive

Dispersing the particles in the adhesive matrix is essential, as inhomogeneous particle distribution can affect the final results. For this reason, the modified adhesive was prepared using a ThinkyMixer ARE-250 speed mixer. This speed mixer with a degassing option allows for the successful dispersion of TEPs in high-viscosity structural adhesives in a short amount of time. The image of the speed mixer used can be seen in Figure 22.



Figure 22. ThinkyMixer ARE-250 Speed Mixer [87]

Initially, the modified adhesive has been prepared for 5%, 10%, and 15% weight concentrations of thermally expandable particles without the hardener in a speed-mixer container by measuring the weights using an electronic scale. Then, two steps were taken to mix the adhesive with the speed-mixer. The particles and the epoxy adhesive were first mixed for 2 minutes at 2000 rpm. As a second step, 30 seconds of degassing was applied to eliminate air bubbles that could have been trapped during the first step to obtain a visibly bubble-free modified adhesive. The image of the TEP-modified epoxy adhesive inside the speed-mixer container after mixing is shown in Figure 23.



Figure 23. TEP-modified Adhesive After Mixing

After the speed-mixer procedure, the containers were stored in the fridge to be mixed later with the hardener component of the SikaPower-1277. Whenever the modified adhesive is needed, the hardener is mixed with the modified epoxy by hand with a wooden stick until the adhesive's two components are visibly mixed, approximately 3–5 minutes. The weights were measured using an electronic scale.

# 2.3 Volume Expansion Coefficient Testing

Volume expansion coefficient tests have been performed to understand the expansion characteristics of the epoxy adhesive modified with a 5%, 10%, and 15% weight concentration of TEPs. Specimen preparation for this test involves casting the modified adhesives into molds 3D-printed with FiberForce Ghostforce [88] hydrosoluble filaments. Then, it was cured at room temperature for 24 hours. After curing, the molds are put in plastic containers filled with tap water, and after 20 minutes, the water-soluble mold starts to dissolve. After that, the 10 mm cubic specimens are removed by hand with the help of sandpaper. Cast-cured specimens inside the hydrosoluble molds are shown in Figure 24.



Figure 24. Cast-cured Specimens Inside the Hydrosoluble Molds

For heating, an ECP Industrial OV301 composites bench-top curing oven has been used, as shown in Figure 26. The specimens have been placed on an aluminium plate with a thermocouple wire attached to monitor the true temperature value around them. The thermocouple-attached specimens are shown in Figure 25.

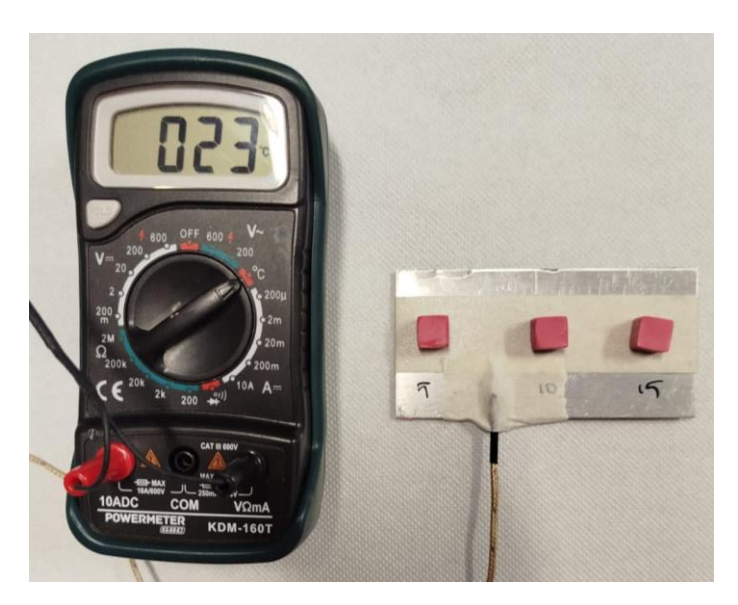


Figure 25. Thermocouple-attached Expansion Test Specimens

The oven is heated to 170 °C. Specimens are placed in the oven with a thermocouple attached to measure the actual temperature. They are kept either for 20 minutes or 1 hour after the thermocouple reads 160 °C. After this time, the oven is switched off, the oven's door is opened slightly, and specimens are kept inside for an extra 40 minutes to cool down to room temperature to prevent shrinkage due to the rapid cooling.



Figure 26. ECP Industrial OV301 Curing Oven

After cooling down, the cubes' width, length, and height were measured by an electronic calliper, which was used to calculate their expanded volumes. Each dimension was measured 3 times from different sections to eliminate discrepancies due to the inconsistent shape after the expansion. Finally, the average value has been used for the measurement. The same procedure was performed before heating to obtain the true unexpanded specimen volume values.

# 2.4 Preparation of the Adhesive Joint

The adhesive joint preparation process has been initiated by the manufacturing of glass fiber-reinforced polymer (GFRP) composite laminate for substrates. 4 layers of pre-impregnated glass fiber have been laid up on a transparent glass plate with a cross-ply configuration, in which the prepreg layers are aligned in 0° and 90° directions. Breather cloth was used to provide air path during the vacuum, and peel-ply was used to prevent the prepreg laminate from sticking to the glass plate. After this, the whole stack is covered by a plastic vacuum bag. Proper sealing was achieved by using tuck-tape around the edges of the vacuum bag. After obtaining a successful consolidation under vacuum, the prepreg composite laminate was placed in the curing oven for 2 hours at 120 °C under vacuum conditions. After curing, the oven was switched off, and the cured laminate was left in the oven for several hours until it cooled down to room temperature. This prevented the occurrence of micro-cracks in the laminate and possible shape deformations due to rapid cooling. The photo of the prepreg laminate inside the oven, ready for curing, is shown in Figure 27. This final thickness of the GFRP laminate is measured as 2.3 mm.

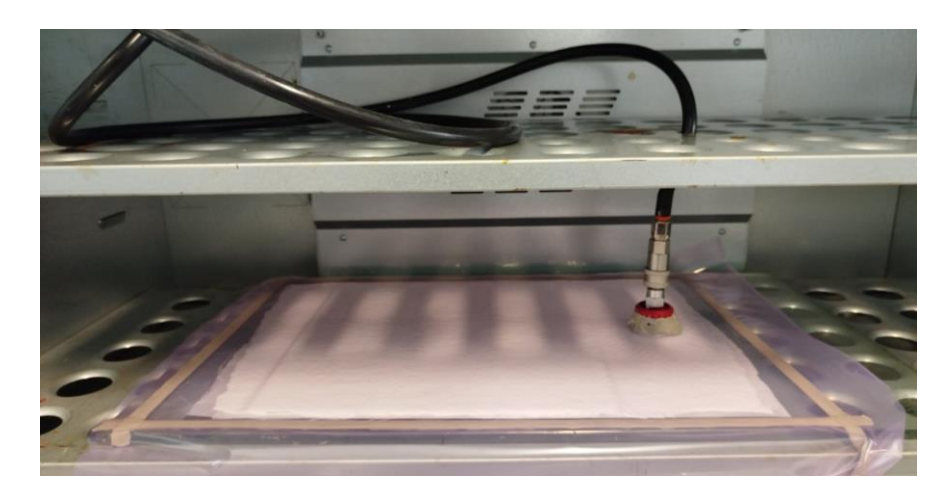


Figure 27. Prepreg Laminate Inside the Oven

After the curing process, the substrates were cut from the cured laminate by using WAZER waterjet cutting equipment with a length of 100 mm and a width of 19 mm. The image of the waterjet cutting machine is shown in Figure 28.



Figure 28. WAZER Waterjet Cutting Equipment [89]

After the GFRP substrate manufacturing procedure, surface treatment was performed as the next step before placing the carbon fiber layer in the overlap region. The surface treatment of the GFRP consists of grinding the overlap area with 1000-grit abrasive paper and then delicately cleaning it with acetone to enhance the ability of the GFRP surface to adhere to the CF layer. After surface treatment, a layer of carbon fiber prepreg with the same length as the overlap area is laid on the GFRP substrates, and the same prepreg vacuum-bagging procedure used previously is applied. The consolidated laminate was kept in the oven for 2 hours at 120 °C for curing. The image of the laminate before curing is shown in Figure 29.



Figure 29. Laminate Before Curing

As the final step for the substrate manufacturing process, the 0.5 mm thick CF layer and the 2.3mm thick GFRP substrate were cured again at 160 °C for 30 minutes. The thickness of the specimens after the curing is measured as 2.8 mm. The final view of the substrates is shown in Figure 30.

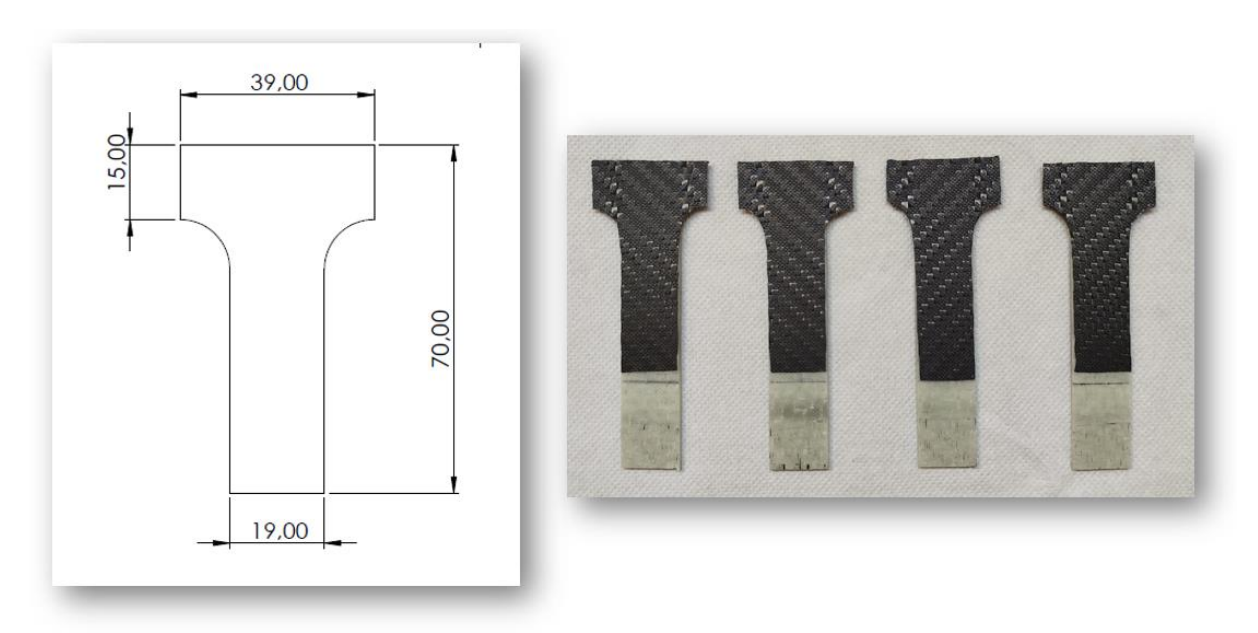


Figure 30. Single Lap Joint Substrates with Geometrical Dimensions

After manufacturing the substrate and the modified adhesive, the surface of the CF layer single-lap joint (SLJ) specimens was ground with 1000-grit abrasive paper and cleaned with acetone. Then, the substrates are delicately placed on the Teflon setup and fixed by using pins. The 0.3 mm adhesive thickness has been achieved

by placing 3D-printed plastic shims under the adherends. The setup used for SLJ specimen preparation is shown in Figure 31.

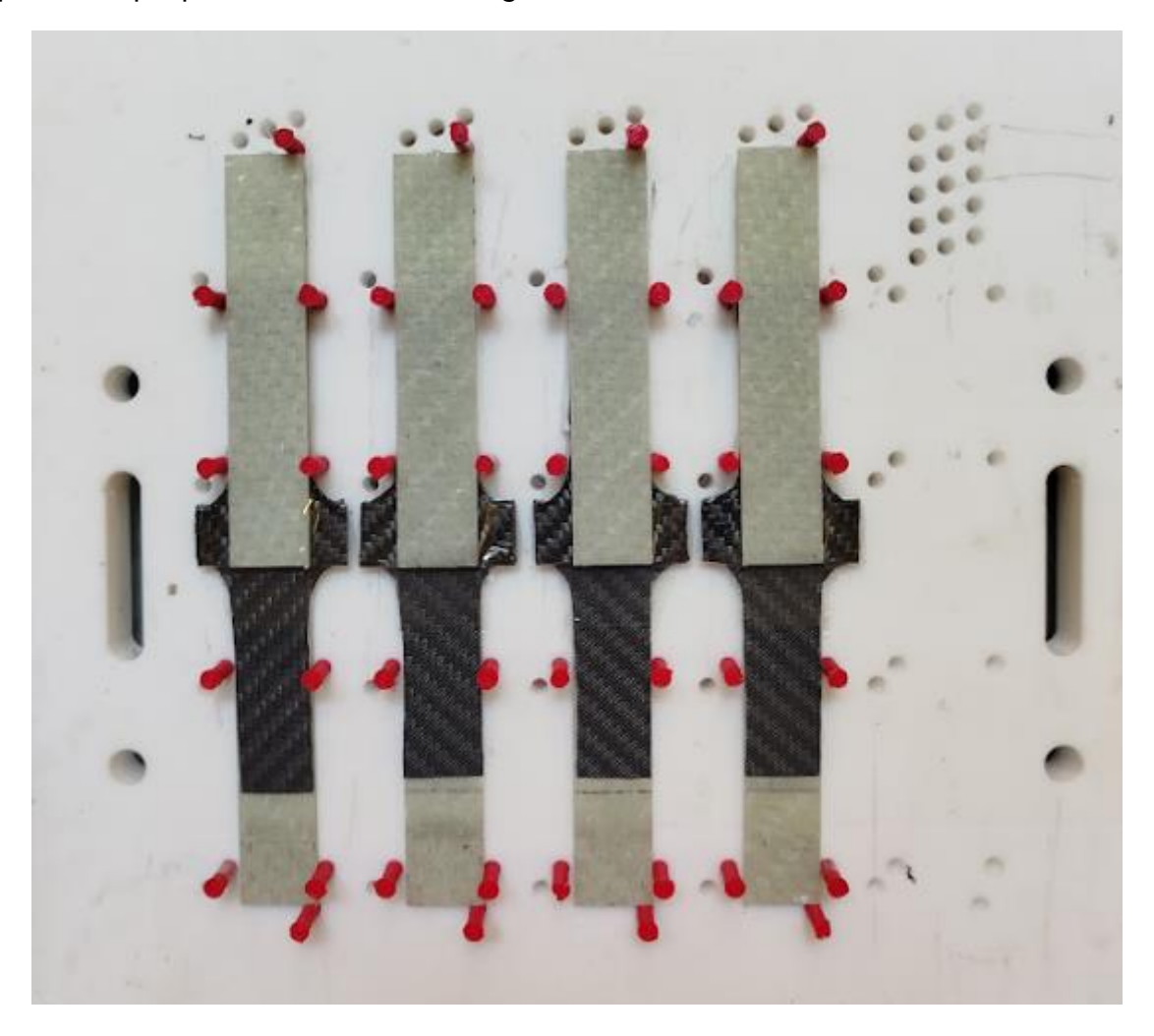


Figure 31. SLJ Specimen Preparation Setup

After applying the adhesive, the specimens were left to cure for 24 hours at room temperature. Upon curing, the tabs were attached to the end region of the substrates to prevent any misalignment during the tests. The dimensions of the SLJ specimens and a detailed view of the overlap region are shown in Figure 32.

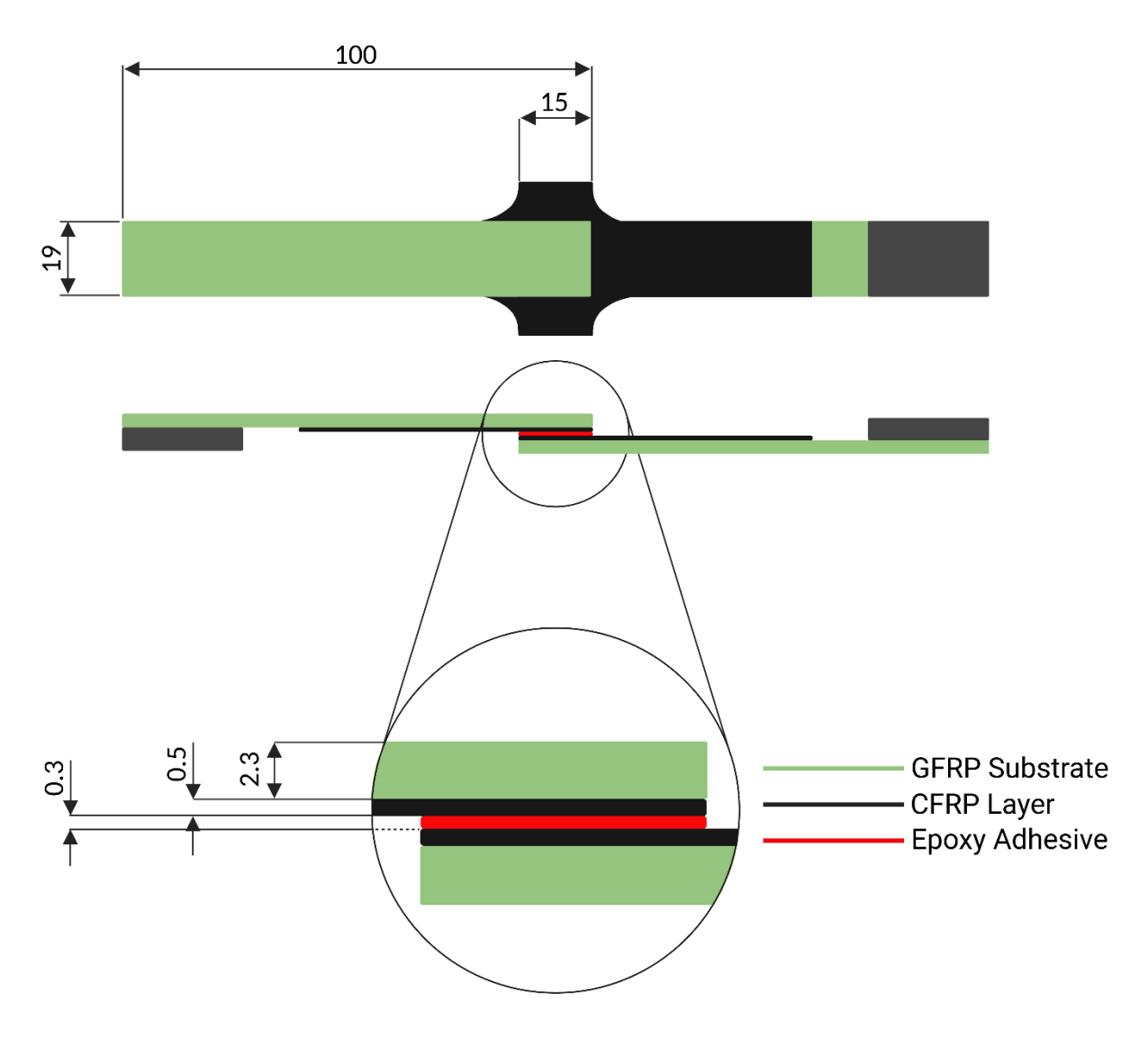


Figure 32. Dimensions of the SLJ Specimen

# 2.5 Mechanical Testing

For the single lap joint shear tests, ZwickRoell-050 universal testing machine with a 50 kN load cell has been used. The image of the ZwickRoell-050 that has been used in this study is shown in Figure 33 with the specimen attached to the grips.

Baseline, 5%, 10%, and 15% wt. TEP-modified epoxy adhesive specimens were tested, with 4 specimens for each percentage—2 unexpanded and 2 expanded. For the baseline, only 2 specimens were tested. The pre-load was set to 20 N, and the test speed was 1 mm/min. The testing machine's displacement sensor measured the displacement, and the load data was obtained from the load cell. The stress values are calculated by using the equation below.

$$Lap Shear Strength [MPa] = \frac{Force [N]}{Length [mm]x Width [mm]}$$
(1)



Figure 33. ZwickRoell-050 Universal Testing Machine with SLJ Specimen Attached

# 2.6 Heating Configuration

As a future study for this thesis, a reliable test setup is needed to evaluate the debonding behaviour of the modified joint at elevated temperatures. Figure 34 presents the ideal heating configuration for the future debonding tests. The test setup consists of a rod with a clamp for securely attaching the SLJ specimen, a heat source, and a free weight to exert the force needed for debonding. The heating-up technique is based on the Joule heating principle, which is defined as the conversion of electrical energy into heat energy. To apply this principle, the electrodes has to be clamped to an electrically conductive material. In this case, this material is one layer of carbon fiber placed on the substrates which is shown in Figure 32. During the test, firstly, the DC power supply turns on, and then the carbon fiber heats up via joule heating, and through the heat transfer from the carbon fiber layer, the modified adhesive reaches the desired temperature levels. At the final, the strength of the joint is expected to reduce significantly, thus the joint is expected to be separated with the help of the force that is applied by the attached free weight.

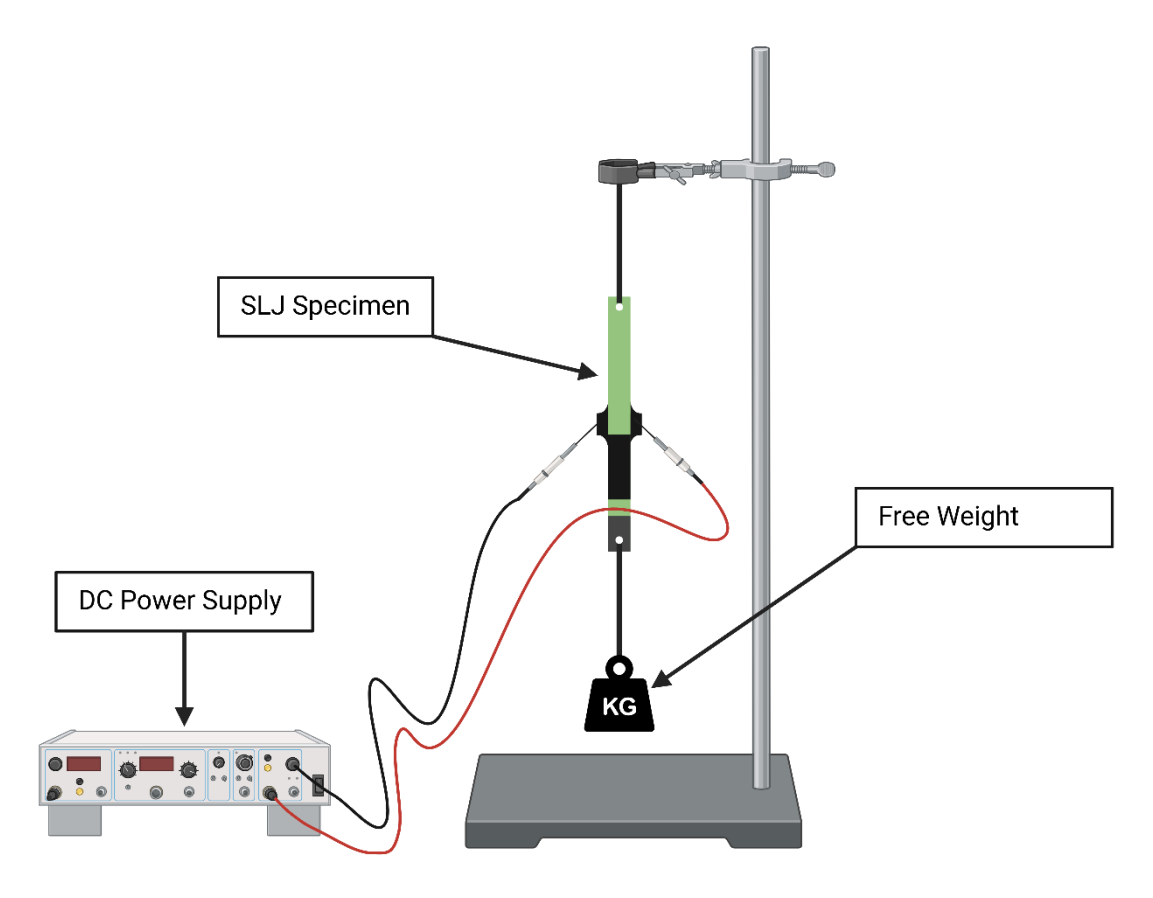


Figure 34. Joule Heating Configuration For the Debonding Tests

# 2.7 TGA Characterisation

Thermogravimetric analysis (TGA) of the epoxy adhesive has been done by using Mettler Toledo TGA/DSC 3+ equipment. TGA allows measuring the specimen's weight change under heating, cooling, or isothermal conditions over time. It provides information about when the adhesive starts to degrade, which is to be taken into account when reaching the maximum expansion temperature of the modified adhesive. The image of the equipment used in this analysis is shown in Figure 35.



Figure 35. Thermogravimetric Analysis Equipment

In this study, non-isothermal TGA analysis was conducted for the substrate material, which is a glass fiber reinforced polymer (GFRP), and for the two-component structural epoxy adhesive. The analysis environment was selected as air because it closely resembles the real-life conditions. During the analysis, the weight residue, the sample temperature, the reference temperature, the heat flow, and the time were recorded. For the GFRP, the maximum sample temperature was 850 °C with the heating rate of 10 °C/min. For the epoxy adhesive, the maximum sample temperature was 600 °C with the heating rate of 10 °C/min. In addition to the non-isothermal TGA, isothermal TGA has been conducted for only epoxy adhesive at a constant temperature of 160 °C for 1 hour.

# 2.8 FE-SEM Analysis

For the adhesive morphology characterization, TESCAN MIRA3 scanning electron microscopy (SEM) device has been used. The image of the device is shown in Figure 36.



Figure 36. TESCAN MIRA3 Scanning Electron Microscopy (FESEM) Device

The specimen preparation process consists of several steps including the cold mounting of the specimens inside an acryclic resin, polishing the surfaces and as the final step, platinum sputtering to make the specimen surfaces conductive. As the first step for the cold mounting, the mold and the specimen was prepared. Secondly, the PRESI KM–U acryclic powder resin and catalyst were mixed with given scoop ratios in a mixing cup. This step has been done slowly to prevent bubble generation. After pouring the acryclic resin into plastic molds and the resin started to cure. After reaching to enough hardness, the specimens were removed from the mold and polished with PRESI Mecatech 250 polishing equipment till the surface becomes smooth enough for SEM analysis. The image of the PRESI Mecatech 250 polishing device is shown in Figure 37.



Figure 37. PRESI Mecatech 250 Polishing Device [90]

As the final step, the cold mounted and polished specimens were platinum-sputtered with using physical vapor deposition. The image of the SEM analysis-ready TEPs modified epoxy adhesive specimen after sputtering is shown in Figure 38.

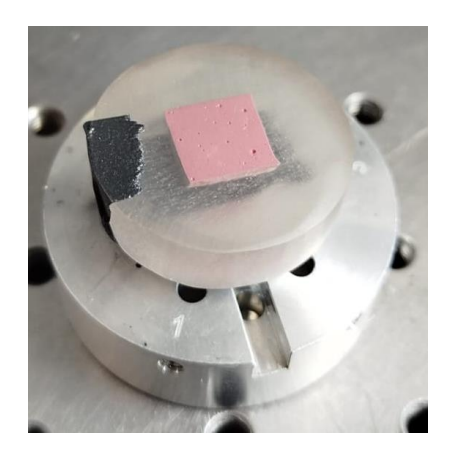


Figure 38. Cold-mounted FESEM Specimen After Sputtering

# 2.9 Optic Microscope Analysis

The Zeiss AxioVert A1 microscope has been used to observe the morphology of thermally expandable particles and their porosity. The image of the microscope used in this study is shown in Figure 39.



Figure 39. Zeiss AxioVert Al Microscope

# 3. Results and Discussion

### 3.1 Characterisation of Materials

### 3.1.1 TGA Results of the Modified Adhesive

Non-isothermal thermogravimetric analysis of GFRP has revealed that the material begins to degrade at approximately 220 °C. This is due to the degradation of the epoxy matrix. It is observed that the glass fiber did not degrade at 850°C. The weight loss is 1% at 160°C, which is the maximum temperature reached in this study. The non-isothermal TGA analysis result for the GFRP is shown in Figure 40.

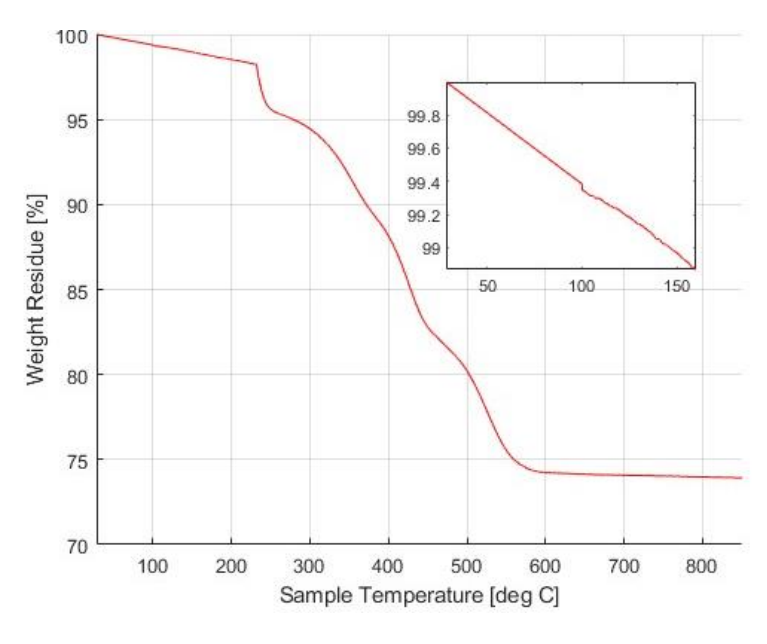


Figure 40. Non-isothermal TGA analysis result for the GFRP

Non-isothermal thermogravimetric analysis of Sikapower-1277 adhesive has revealed that the material begins to degrade at approximately 350 °C. At 160°C, the weight loss was recorded as 2%. The oxidation of the adhesive has started at 500°C as it affected the tendency of the reduction in weight residue. The non-isothermal TGA analysis results for the Sikapower-1277 are shown in Figures 41 and 42.

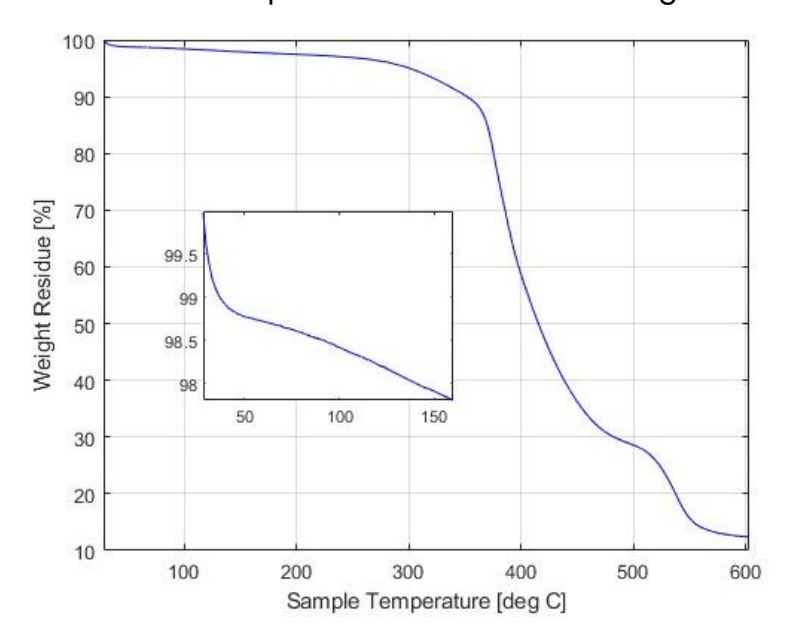


Figure 41. Non-isothermal TGA analysis result for the Sikapower-1277

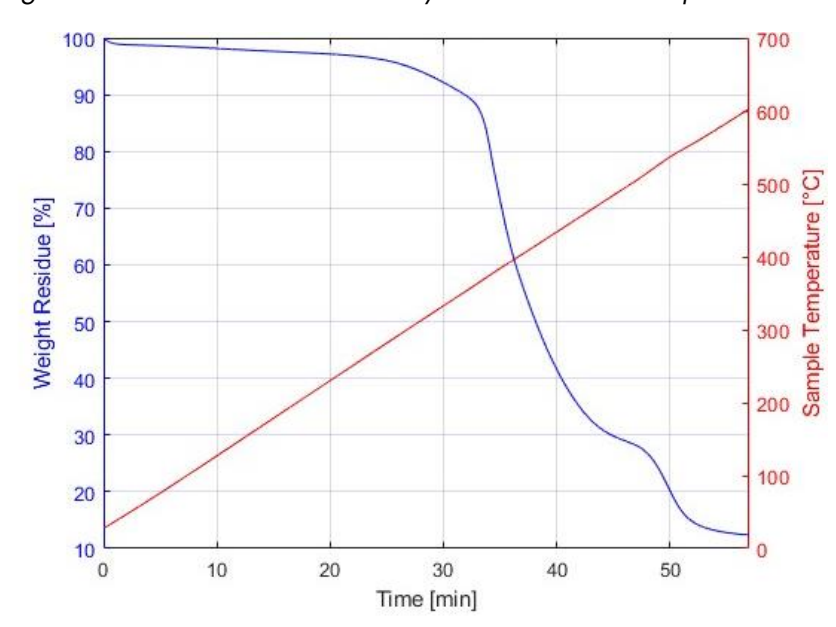


Figure 42. Non-isothermal TGA analysis result for the Sikapower-1277 with Time

After non-isothermal analysis, isothermal analysis was conducted to assess the adhesive's ability to resist the time period of expansion tests. The material loss was recorded as approximately % 3.5% after one hour, which is shown in Figure 43.

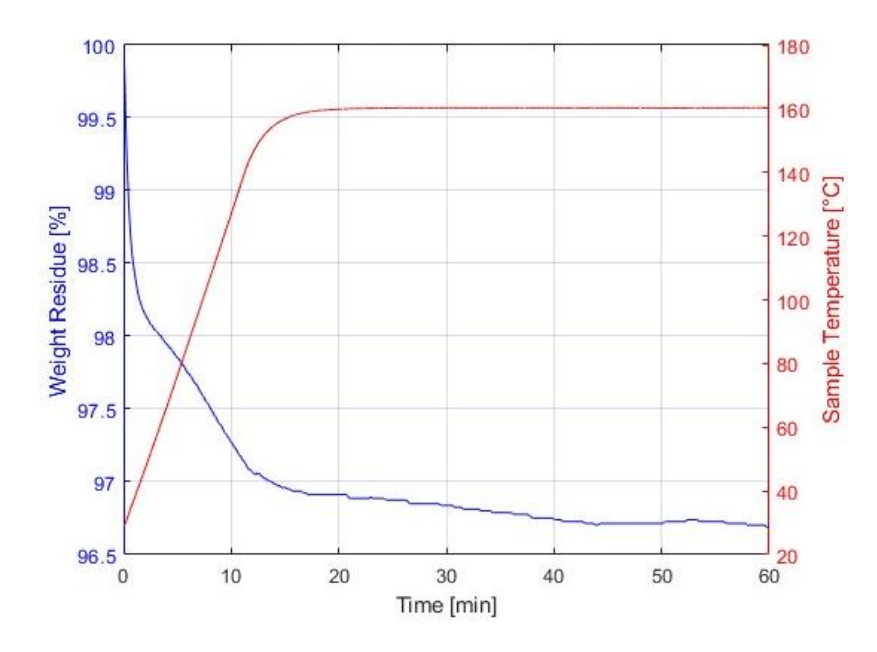


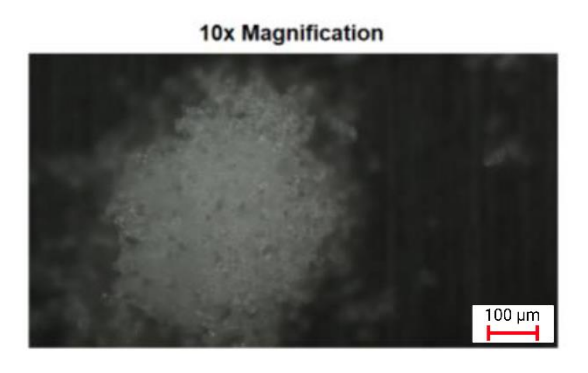
Figure 43. Isothermal TGA analysis result for the Sikapower-1277

# 3.1.2 Microscope Analysis of Particles and Adhesive Morphology

The diameter of the particles has been observed under an optical microscope to understand the expansion mechanism better. Firstly, the particles without an adhesive matrix were observed with different magnifications before and after activating the expansion with heat. The images are shown in Figures 44 and 45 with a clear view of the co-polymer shell. Then, these images are used to calculate the average diameter of expanded particles without the epoxy confinement, allowing for a later comparison of the effect of the adhesive matrix on expansion.

The diameter range of the unexpanded particles is specified in the technical datasheet of Expancel as  $16-24\,\mu m$ . After observation under the optical microscope, the average diameter was calculated as  $21.1\,\mu m$  with a standard deviation of 5.2 tabulated in Table 9.

# UNEXPANDED 100x Magnification 50x Magnification 20 μm 20 μm



50 µm

Figure 44. Unexpanded TEPs under optical microscope (no adhesive matrix)

On the other hand, the nominal diameter of the expanded particles is reported as 80  $\mu m$  in the technical datasheet. In this study, the average diameter of the expanded particles tested at 160°C without an adhesive matrix is reported as 58.2

μm, with a standard deviation of 11.3 tabulated in Table 9, which is significantly lower than the nominal value. The maximum diameter calculated was 80 μm, indicating that not all the particles are fully expanded.

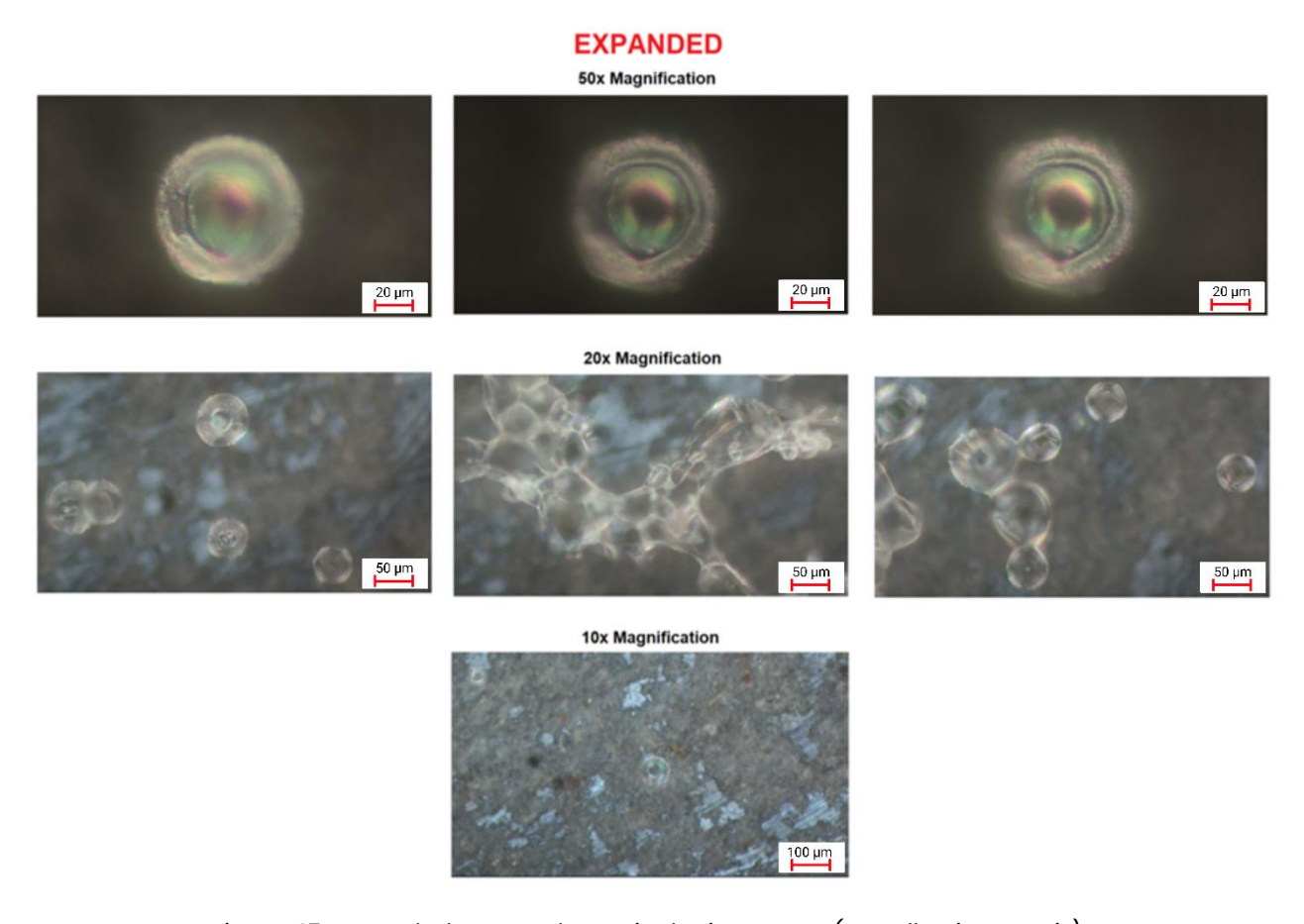


Figure 45. Expanded TEPs under optical microscope (no adhesive matrix)

The diameter values of the expanded TEPs without any adhesive confinement are compared with those of the TEPs inside the modified adhesive by taking average of the diameter of 30 different particles by using ImageJ software. The average particle diameter of the 5 wt.% TEPs modified adhesive calculated as 33.6  $\mu$ m expanded particles tested at 160°C without an adhesive matrix is reported as 58.2  $\mu$ m, with a standard deviation of 11.3. For the 10wt.% TEPs modified sample, the average value is calculated as 34.6  $\mu$ m with a standard deviation of 18.4. For the 15 wt.% TEPs modified sample, the average value is calculated as 36.2 with a standard deviation of 9.1, as given in Table 9.

It is concluded that the adhesive matrix limits the expansion of the TEPs. Additionally, a slight increase was seen in the average diameter values with increasing weight percentage of TEPS, which signifies that the higher the %wt., the easier it is to reach the maximum expansion diameter.

Table 9. Particle Diameter Calculation Results

Materials	Average [µm]	Std. Dev.	Min	Мах
Unexpanded (No adhesive)	21,1	5,2	13,8	38,0
Expanded (No adhesive)	58,2	11,3	46,7	80,2
5 wt.% TEPs / Expanded (mixed with adhesive)	33,6	12,4	15,1	69,0
10 wt.% TEPs/ Expanded (mixed with adhesive)	34,6	18,4	14,7	82,7
15 wt.% TEPs/ Expanded (mixed with adhesive)	36,2	9,1	19,4	70,6

The volumetric expansion coefficients of TEPs have been calculated by taking the ratio of volumes of the particles before and after the expansion occured based on the results summarized in Table 9. The volumetric expansion coefficients found as 4.04, 4.41, 5.05, and 20.99 for particles from 5 wt% TEP-modified adhesive, 10 wt% TEP-modified adhesive, 15 wt% TEP-modified adhesive, and particles without an adhesive matrix, respectively, as reported in Table 10 together with volumetric expansion rates. The tendency is increasing expansion rates by increasing the particle amount.

Table 10. Volumetric Expansion Coefficients and Volumetric Expansion Rates of TEPs

Materials	Vol. Expansion Coeff.	Vol. Expansion Rates
%5 wt. TEPs/ Expanded (mixed with adhesive)	4,04	304 %
%10 wt. TEPs/ Expanded (mixed with adhesive)	4,41	341 %
%15 wt. TEPs/ Expanded (mixed with adhesive)	5,05	405 %
Expanded (No adhesive matrix)	20,99	1999 %

To better understand the adhesive morphology and calculate the 2D-porosity created by the expandable particles, both heated and unheated TEP-modified adhesives have been observed using an optical microscope. The methodology for this analysis is shown in Figure 46. First, a clearly visible area with a low surface roughness in the adhesive matrix has been selected. Then, the image was captured

with the polarized light. The reason for this step was to increase the contrast to observe the spheres more clearly. After that, the Otsu's thresholding method is used to convert grayscale image to a black and white binary one. Finally, the amount of the black area, which represents the area occupied by particles in the adhesive matrix, has been calculated to achieve a porosity value and to visualize the histogram of particles through pore space segmentation.

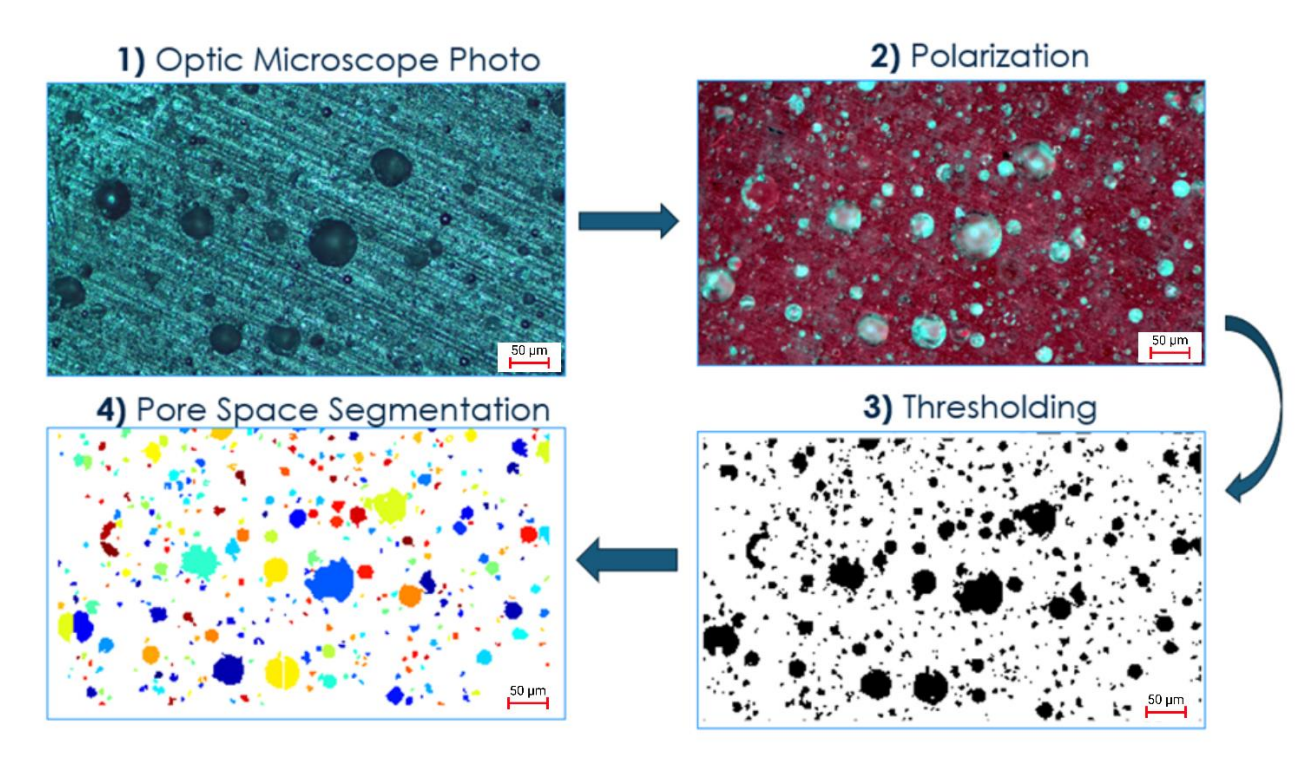


Figure 46. Optic Microscope Methodology for Adhesive Morphology

The microscope images of unheated specimens with different TEP wt.% are shown in Figure 47 It is worth noting that distinguishing the expandable spheres from air bubbles is not an easy task, as both have a similar refractive index that makes them look alike in images. Due to this problem, the 2D-porosity term mentioned in this study covers both TEPs and air bubbles that had entered the adhesive during mixing steps. Despite this similarity, there is a noticeable increase in the porosity for the unheated specimens, as shown in the histogram charts.

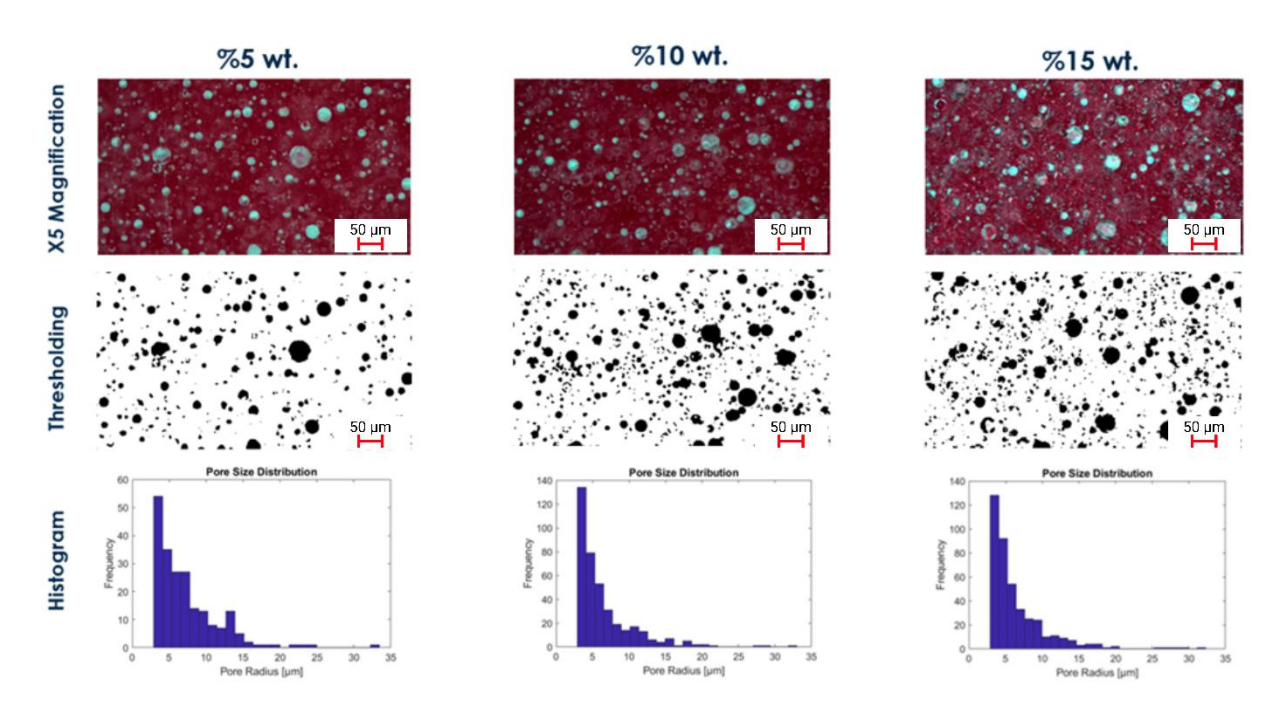


Figure 47. Microscope Images of Unheated Specimens with Varying TEP-wt.%

It is observed that the porosity significantly increases by heating the modified adhesive due to the expansion of the TEPs. It is clear that the higher the TEP wt.%, the more the porosity in the adhesive, as can be seen in Figure 48, with a comparison with the baseline reference adhesive sample with no modification.

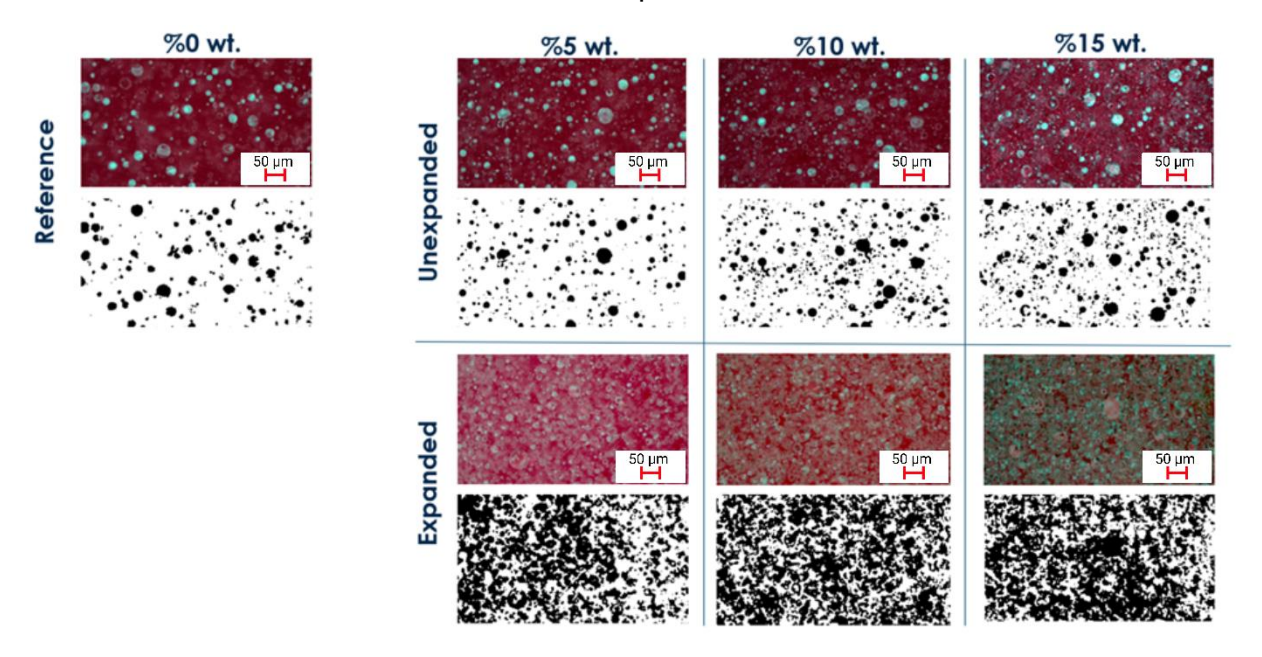


Figure 48. Microscope Images of Reference, Heated, and Unheated Specimens with Varying TEP-wt.%

The porosity was calculated by selecting three different regions in the adhesive and taking the average. The porosity values have been calculated as 10.6%, 13%, and 15% for unheated specimens with 5 wt.%, 10 wt.%, and 15 wt.% concentrations,

respectively. Whereas for the heated 5 wt.%, 10 wt.%, and 15 wt.% specimens, it reached up to 43.8%, 54.3% and 66%, respectively, as tabulated in Table 11.

Table 11. Average Porosity	Values for Unheated and Hea	ited Specimens with Varying TEP wt.%

Materials	#1	#2	#3	Average Porosity [%]	Std. Dev.
0 wt.% / Reference	8,8	10,4	10,3	9,8	0,8
5 wt.% / Unexpanded	9,0	13,4	9,4	10,6	2,0
10 wt.% / Unexpanded	9,6	14,6	14,9	13,0	2,4
15 wt.% / Unexpanded	13,9	15,7	15,4	15,0	0,8
5 wt.% / Expanded	48,0	51,3	32,1	43,8	8,4
10 wt.% / Expanded	57,6	47,7	57,7	54,3	4,7
15 wt.% / Expanded	77,3	61,7	59,1	66,0	8,0

It is concluded that the porosity increases significantly as the TEPs start gasification and expand in volume. The tendency for the increase is shown in Figure 49.

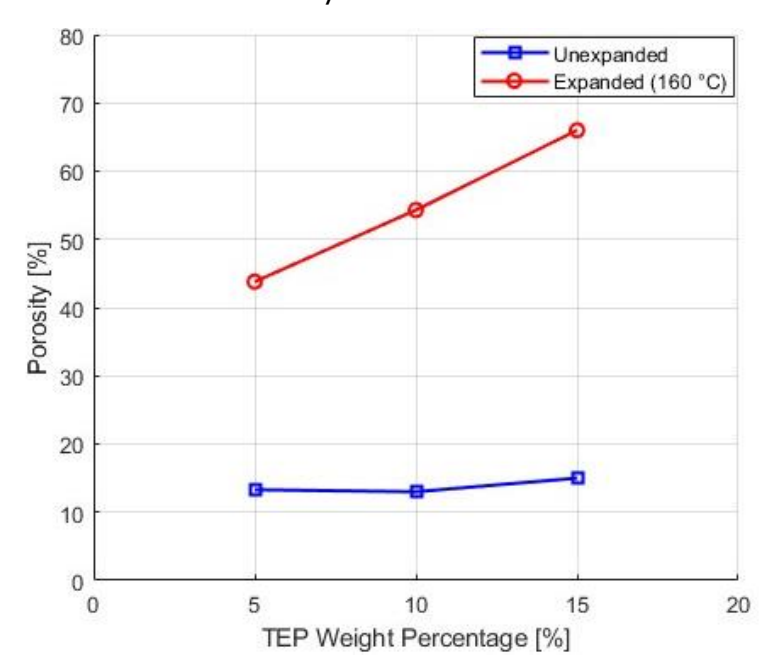


Figure 49. 2D-Porosity Analysis Results

The surfaces of the modified adhesive have also been observed using field-emission microscopy. It has been proven that the particle expansion under heat results in a cracked adhesive matrix, which is thought to contribute to the adhesive failure. The TEPs-induced crack and stopped crack propagation are shown in Figures 50 and 51.

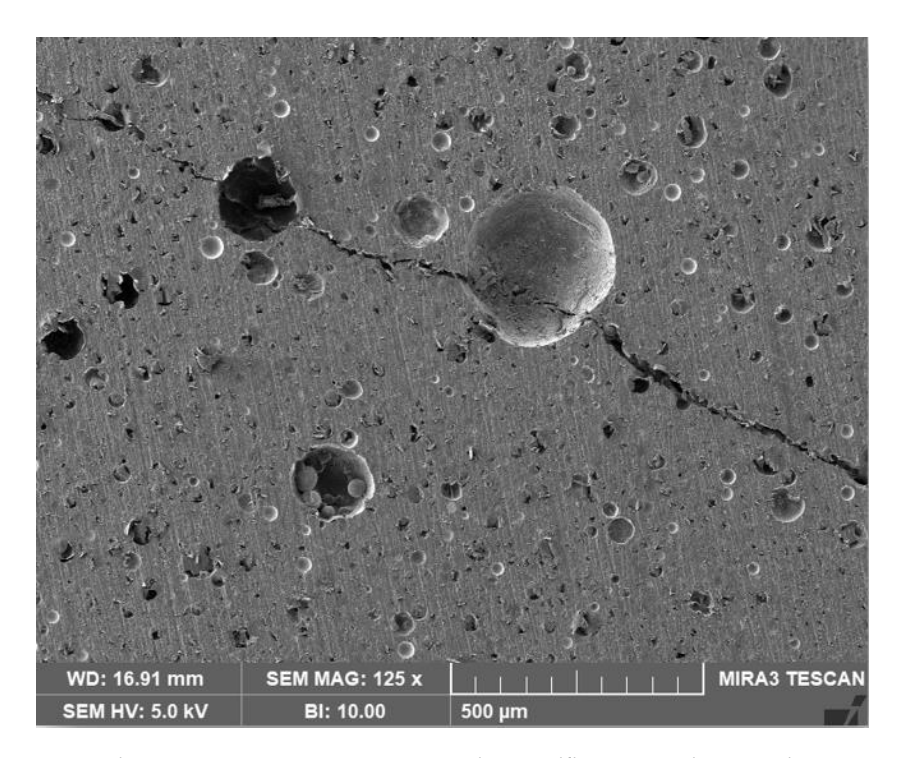


Figure 50. TEPs-Induced Crack in Modified Adhesive Matrix

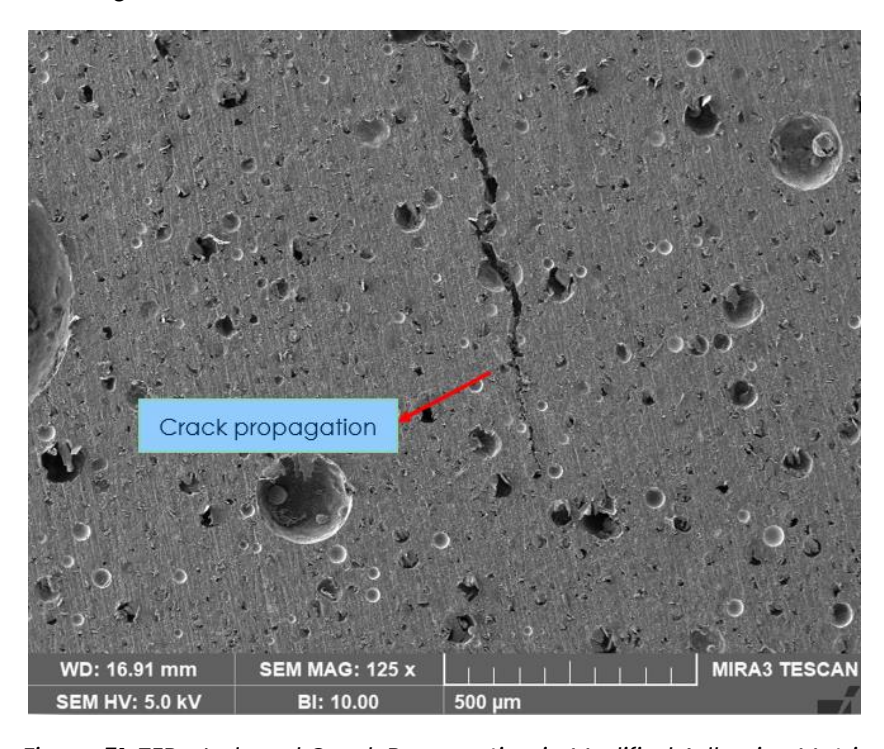


Figure 51. TEPs-Induced Crack Propagation in Modified Adhesive Matrix

# 3.1.3 Volume Expansion Coefficients

Volume expansion coefficient tests have been conducted at 160°C to see the effects of the expandable particles on the bulk expansion of the modified adhesive. The images of the heated and unheated cubic specimens with varying TEP wt.% are shown in Figure 52.

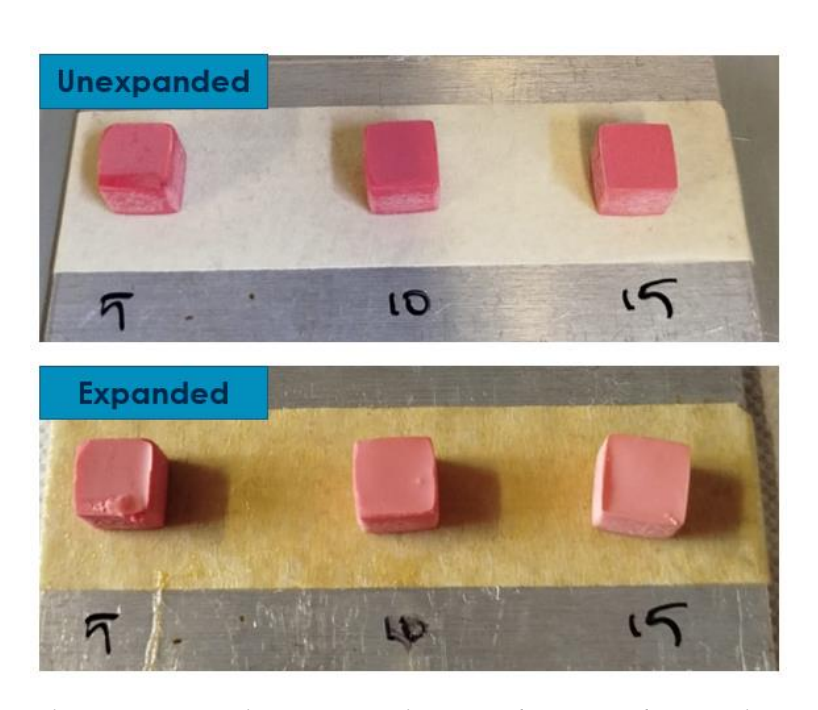


Figure 52. Expansion Test Specimens Before and After Heating

The tests have been conducted in two different time periods, i.e. 20 minutes and 1 hour to compare the duration of the heating on the expansion. For the 20 minutes of heating, the expansion coefficients have been calculated as 1.06, 1.13, and 1.32 for 5 wt.%, 10 wt.%, and 15 wt.% TEPs-modified epoxy adhesive, respectively. Volumetric expansion coefficient results of 20-minute heating with varying particle amount are shown in Figure 53.

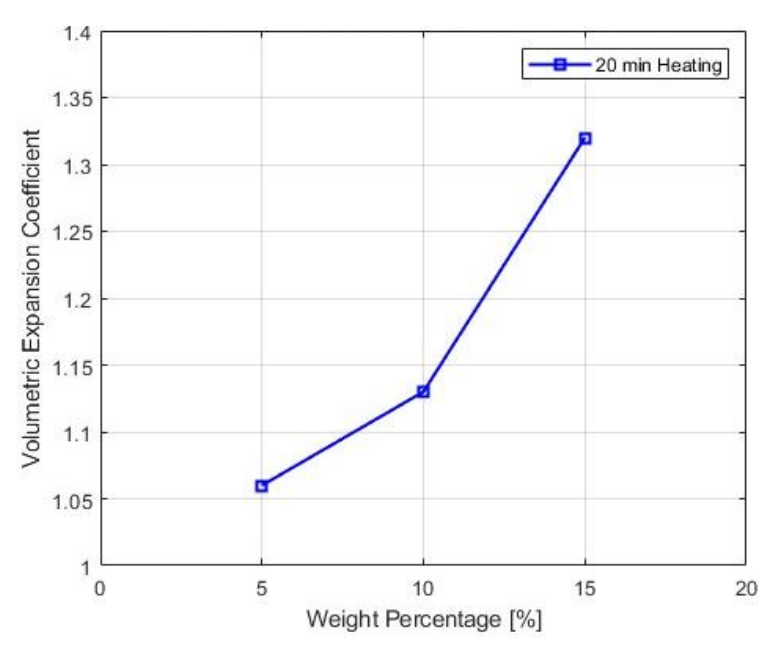


Figure 53. Volumetric Expansion Coefficient Results with Varying TEPs wt.% (20 Minutes of Heating)

For the 1-hour heating period, the expansion coefficients were calculated as 1.03, 1.13, and 1.27 for 5 wt.%, 10 wt.%, and 15 wt.% TEP-modified epoxy adhesives, respectively.

Volumetric expansion coefficient results of 1 hour heating with varying particle amounts are shown in Figure 54.

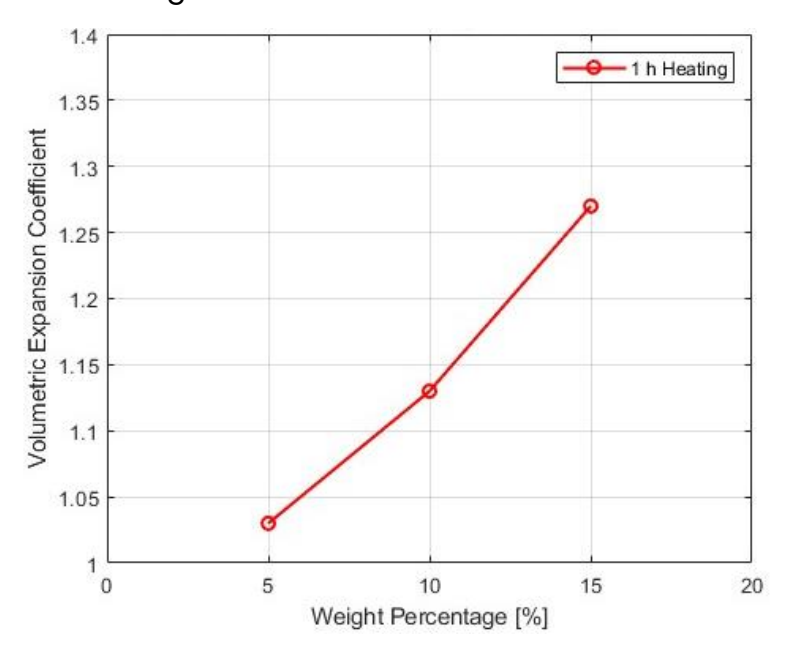


Figure 54. Volumetric Expansion Coefficient Results with Varying TEPs wt.% (1 Hour of Heating)

The durations of the heat applications have been compared. It has been seen that, when the adhesive was heated up for 1 hour, the expansion coefficient was slightly decreased by 5 wt.% The TEP-modified sample did not change for 10 wt.% TEP-modified sample. On the other hand, the expansion coefficient of the 1-hour heated 15 wt.% TEP-modified specimen was lower 3.8% than the 20 minutes of heating counterpart. This indicates that after 1 hour of heating, the specimen degrades. Possible reasons might be the degradation of the epoxy adhesive as it is observed at TGA analysis, and the deterioration of the co-polymer shell of the thermally expandable particles that results in overall volume decrease. The graph for the comparison of 20 minutes and 1 hourr heating is shown in Figure 55.

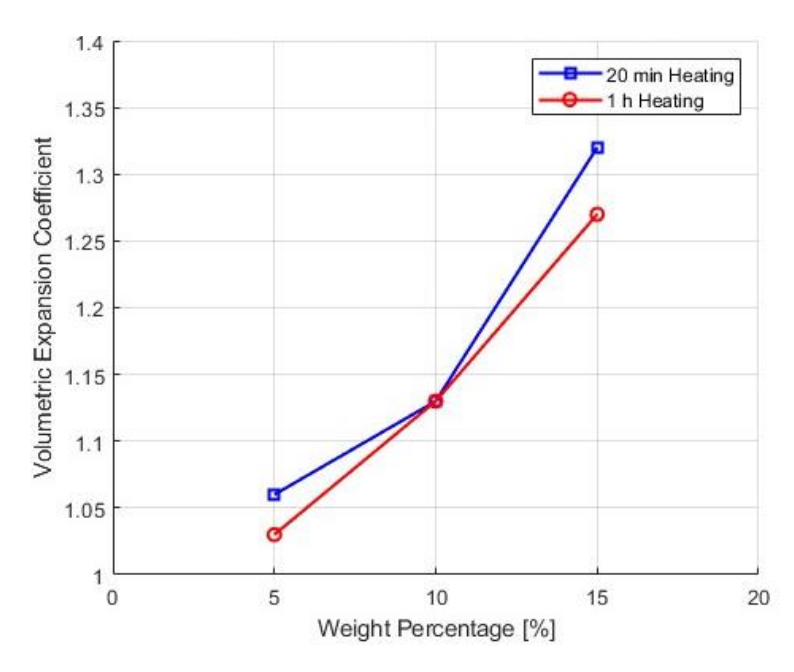


Figure 55. Volumetric Expansion Coefficient Results of 20 minutes and 1 Hour of Heating

All the results for the expansion coefficient tests have been tabulated in Table 12 together with the total time specimens were kept in the oven and other necessary information regarding the methodology.

Table 12. Volumetric Expansion Coefficient Test Results and Test Information

Particles	wt%	Expansion Temperature [°C]	Thermocouple	Expansion Coeff.	Specimen Dimension [mm]	Total Oven Time [min]	Mixing Method
043 DU 80	5	160 (max)	Yes	1,06	10x10x10	50	Mixer
043 DU 80	10	160 (max)	Yes	1,13	10x10x10	37	Mixer
043 DU 80	15	160 (max)	Yes	1,32	10x10x10	37	Mixer
043 DU 80	5	160 (max)	Yes	1,03	10x10x10	73	Mixer
043 DU 80	10	160 (max)	Yes	1,13	10x10x10	73	Mixer
043 DU 80	15	160 (max)	Yes	1,27	10x10x10	73	Mixer

#### 3.2 Mechanical Performance of Adhesive Joints

### 3.2.1 Lap Shear Strength of Joints with and without TEP

For the baseline specimens, the average maximum force was found to be 4239N with a standard deviation of 133. On the other hand, the average lap shear strength value was 14.9 MPa with a standard deviation of 0.5. The force-displacement & stress-displacement plots along with the fracture surfaces are shown in Figure 56

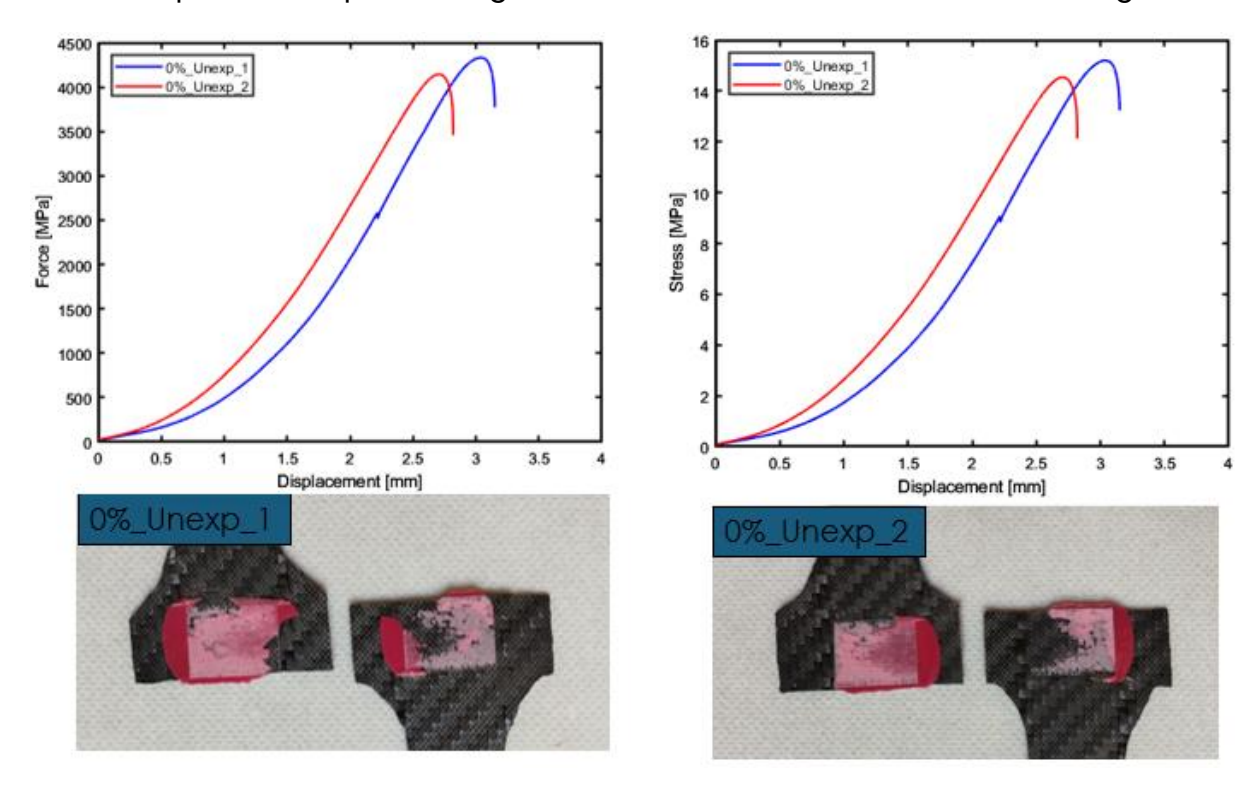


Figure 56. Baseline Adhesive - Single Lap Shear Test Results

For the unheated 5 wt.% TEP-modified epoxy adhesive specimens, the average maximum force was found to be 4416N with a standard deviation of 636. In addition, the average lap shear strength value was 15.5 MPa with a standard deviation of 2.2. The force-displacement & stress-displacement plots along with the fracture surfaces are shown in Figure 57.

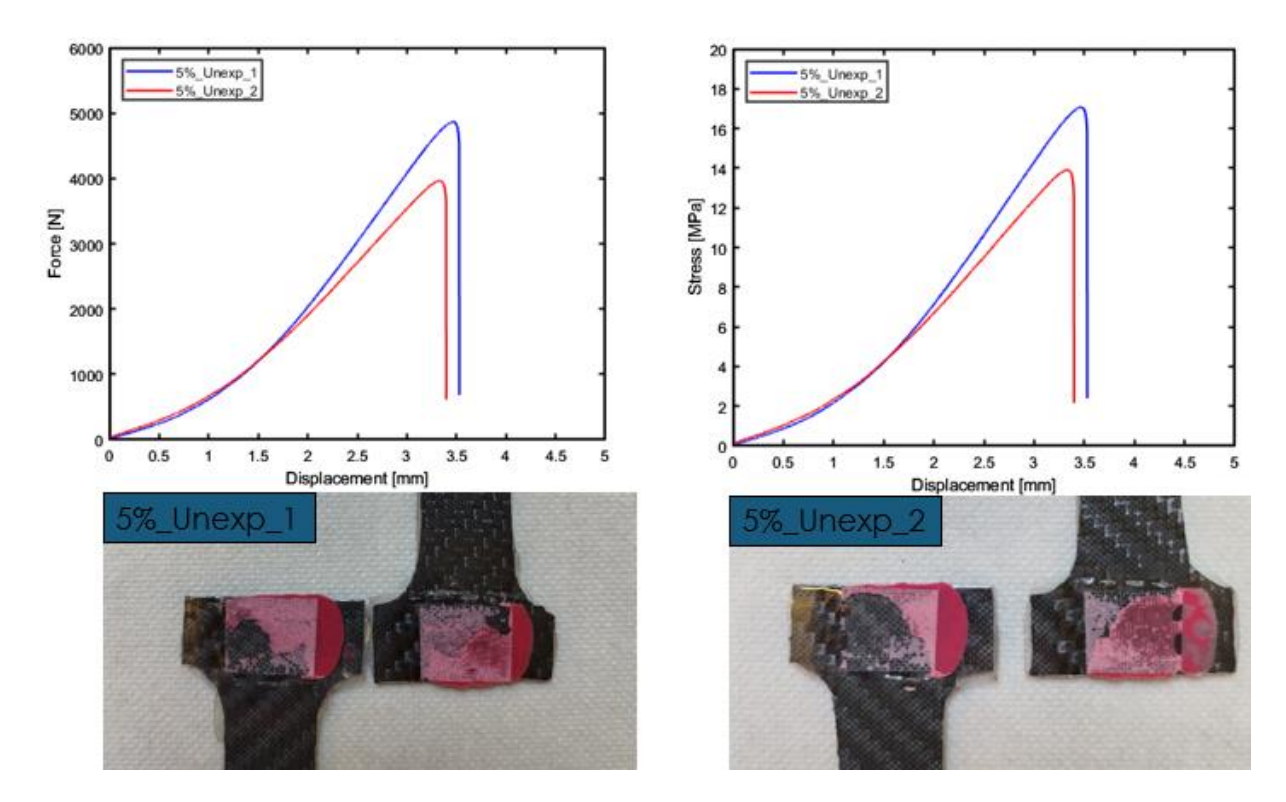


Figure 57. Unheated 5 wt.% TEP-modified Epoxy Adhesive - Single Lap Shear Test Results

For the heated 5 wt.% TEP-modified epoxy adhesive specimens, the average maximum force was found to be 4491N with a standard deviation of 985. Additionally, the average lap shear strength value was 15.8 MPa, with a standard deviation of 3.5. The force-displacement & stress-displacement plots along with the fracture surfaces are shown in Figure 58.

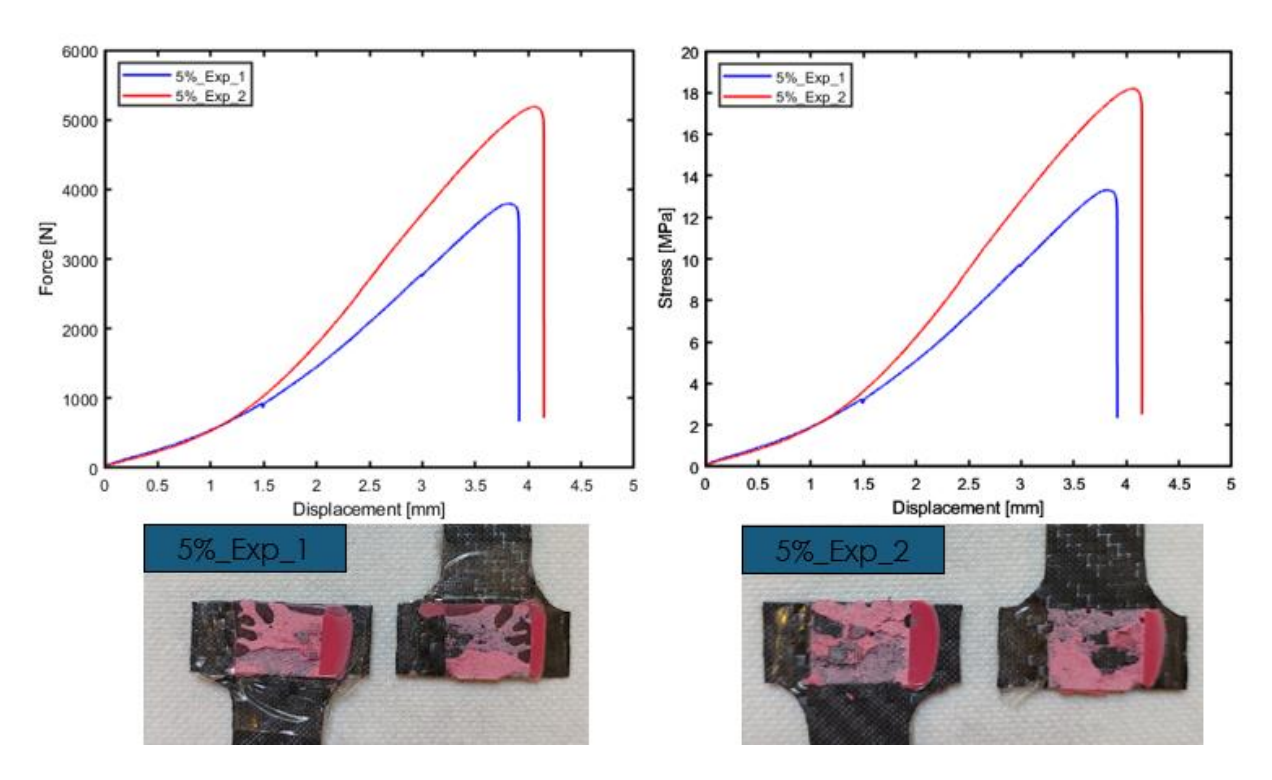


Figure 58. Heated 5 wt.% TEP-modified Epoxy Adhesive - Single Lap Shear Test Results

For the 5 wt.% TEP-modified specimens, it is concluded that even though there was a lack of adhesive in the overlap region of some heated(expanded) specimens, i.e. specimen 1, the strength of the heated joints increased 4.16% and 1.7% compared to the baseline and unheated(unexpanded) specimens, respectively. This might be attributed to the fact that the incorporation of a low amount of TEPs in the adhesive did not serve as stress concentration areas, but rather to make failure more cohesive, thereby increasing the strength slightly. The stress values of both heated and unheated specimens are shown in Figure 59.

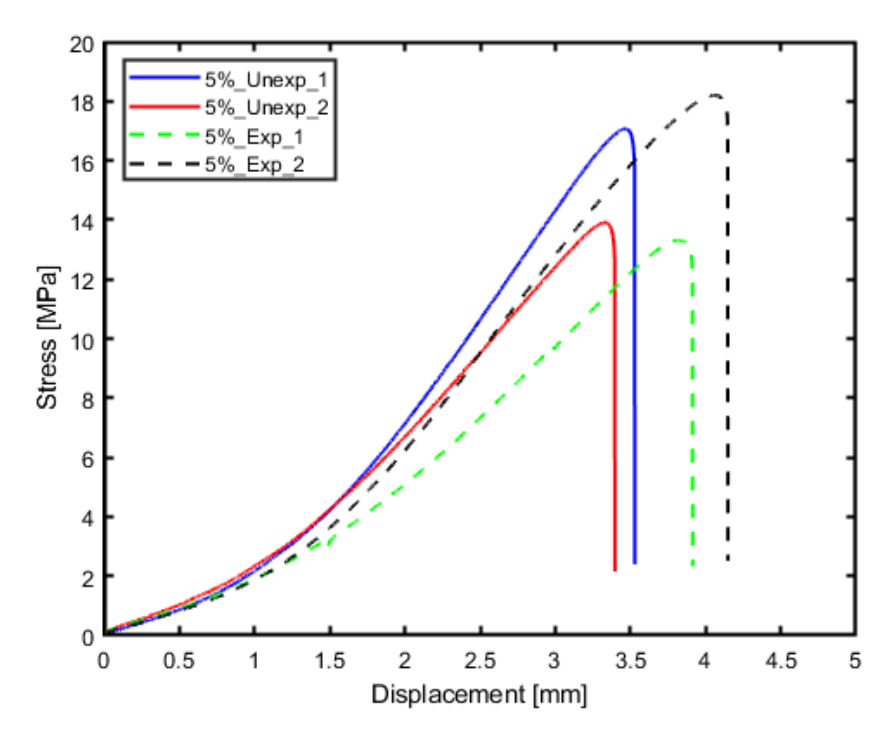


Figure 59. The Lap Shear Strength Plots of 5 wt.% TEP-Modified Specimens

For the unheated 10 wt.% TEP-modified epoxy adhesive specimens, the average maximum force was found to be 3784N with a standard deviation of 200. Additionally, the average lap shear strength value was 13.3 MPa, with a standard deviation of 0.7. The force-displacement & stress-displacement plots along with the fracture surfaces are shown in Figure 60.

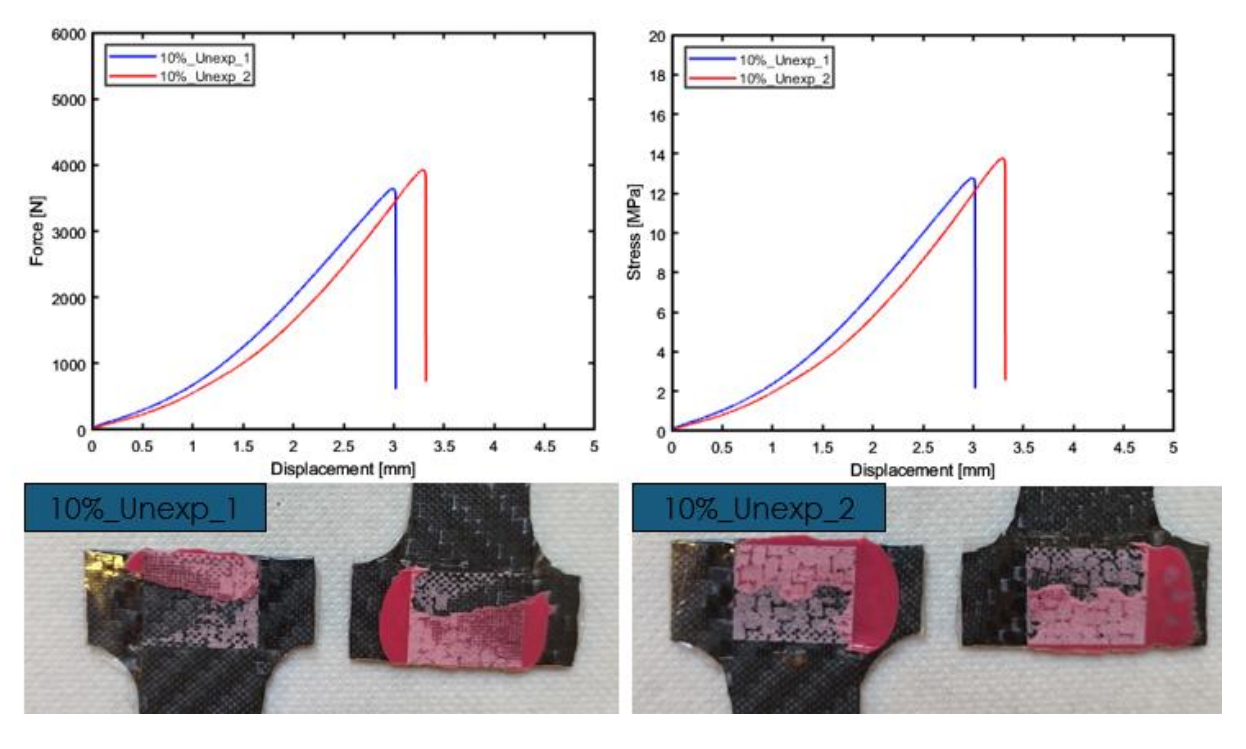


Figure 60. Unheated 10 wt.% TEP-modified Epoxy Adhesive - Single Lap Shear Test Results

For the heated 10 wt.% TEP-modified epoxy adhesive specimens, the average maximum force was found to be 3771 N with a standard deviation of 173. Additionally, the average lap shear strength value was 13.2 MPa, with a standard deviation of 0.6. The force-displacement & stress-displacement plots along with the fracture surfaces are shown in Figure 61.

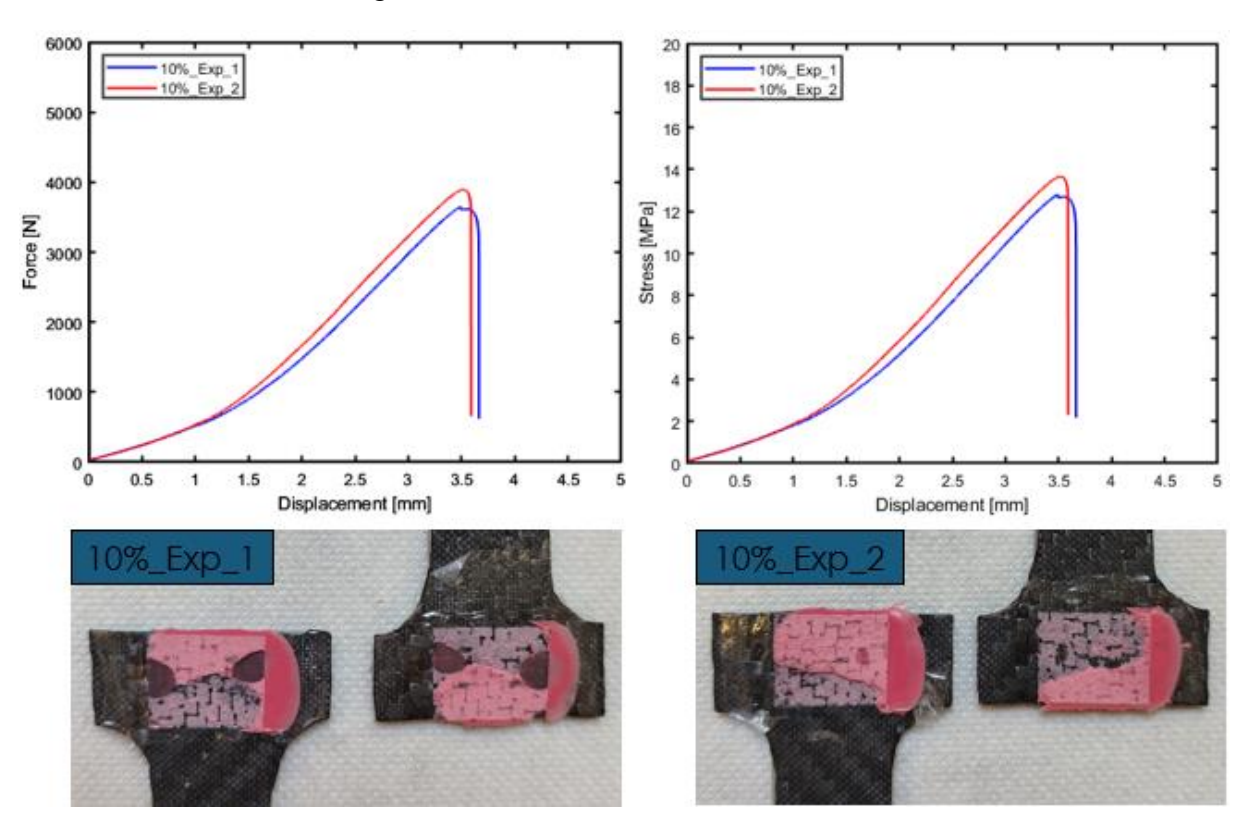


Figure 61. Heated 10 wt.% TEP-modified Epoxy Adhesive - Single Lap Shear Test Results

For the 10 wt.% TEP-modified adhesive specimens, it is noted that the stress has decreased by 10.7% and 11.1% for both heated and unheated specimens, respectively, compared to the baseline. Despite the lack of adhesion in some small areas on the overlap region, the failure mode of the heated specimens was more cohesive than that of the unheated specimens. The lap shear stress values of both heated and unheated specimens for 10 wt.% TEP modified specimens are shown in Figure 62.

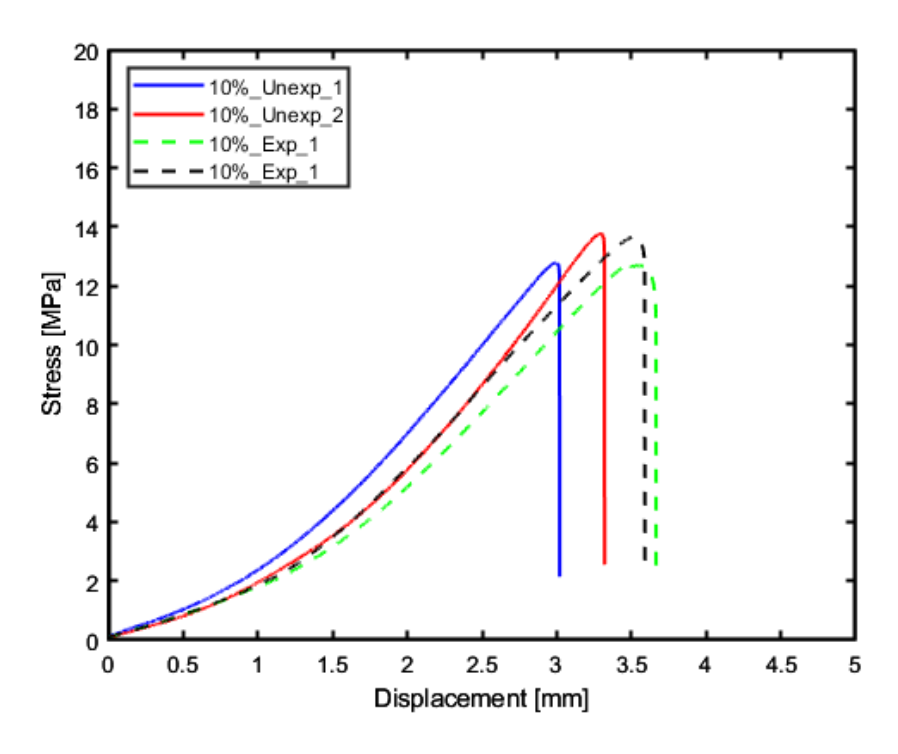


Figure 62. The Lap Shear Strength Plots of 10 wt.% TEP-Modified Specimens

For the unheated 15 wt.% TEP-modified epoxy adhesive specimens, the average maximum force was found to be 3409 N with a standard deviation of 308. Additionally, the average lap shear strength value was 12 MPa, with a standard deviation of 1.1. The force-displacement & stress-displacement plots along with the fracture surfaces are shown in Figure 63.

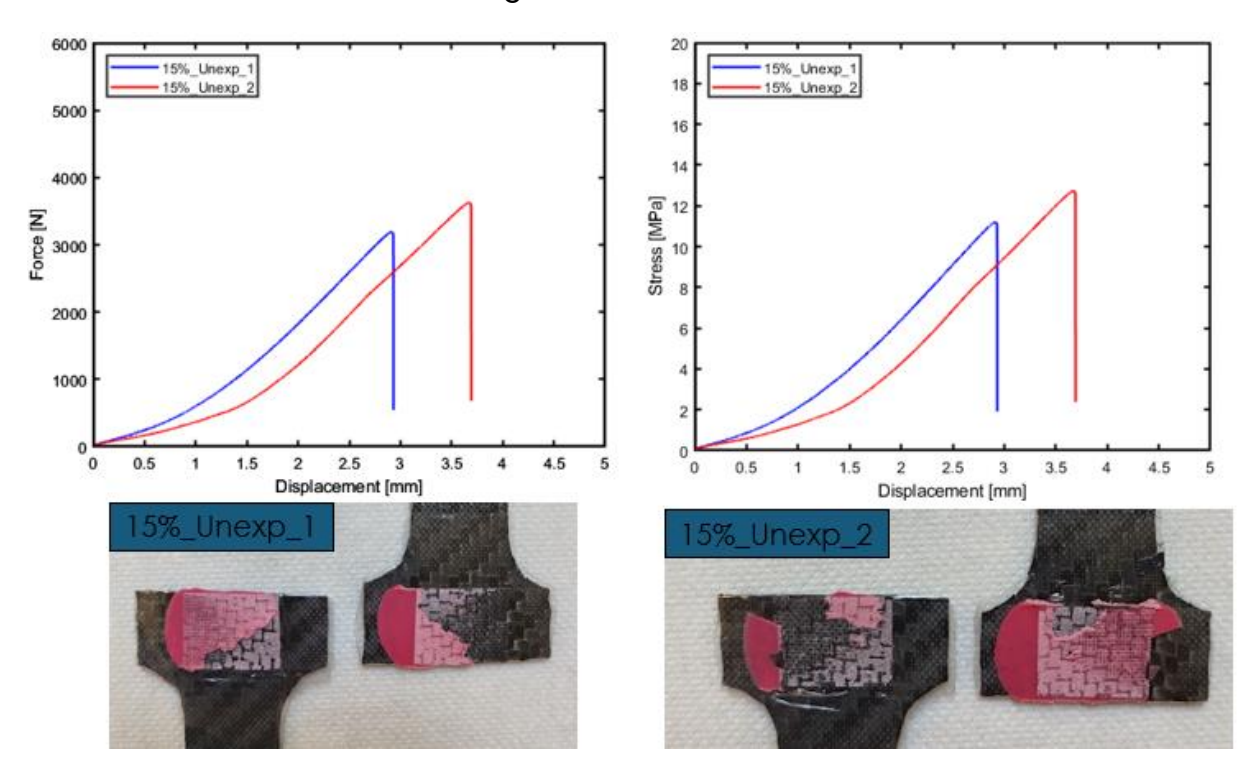


Figure 63. Unheated 15 wt.% TEP-modified Epoxy Adhesive - Single Lap Shear Test Results

For the heated 15 wt.% TEP-modified epoxy adhesive specimens, the average maximum force was found to be 2941 N with a standard deviation of 158. Additionally, the average lap shear strength value was 10.3 MPa, with a standard deviation of 0.6. The force-displacement & stress-displacement plots along with the fracture surfaces are shown in Figure 64.

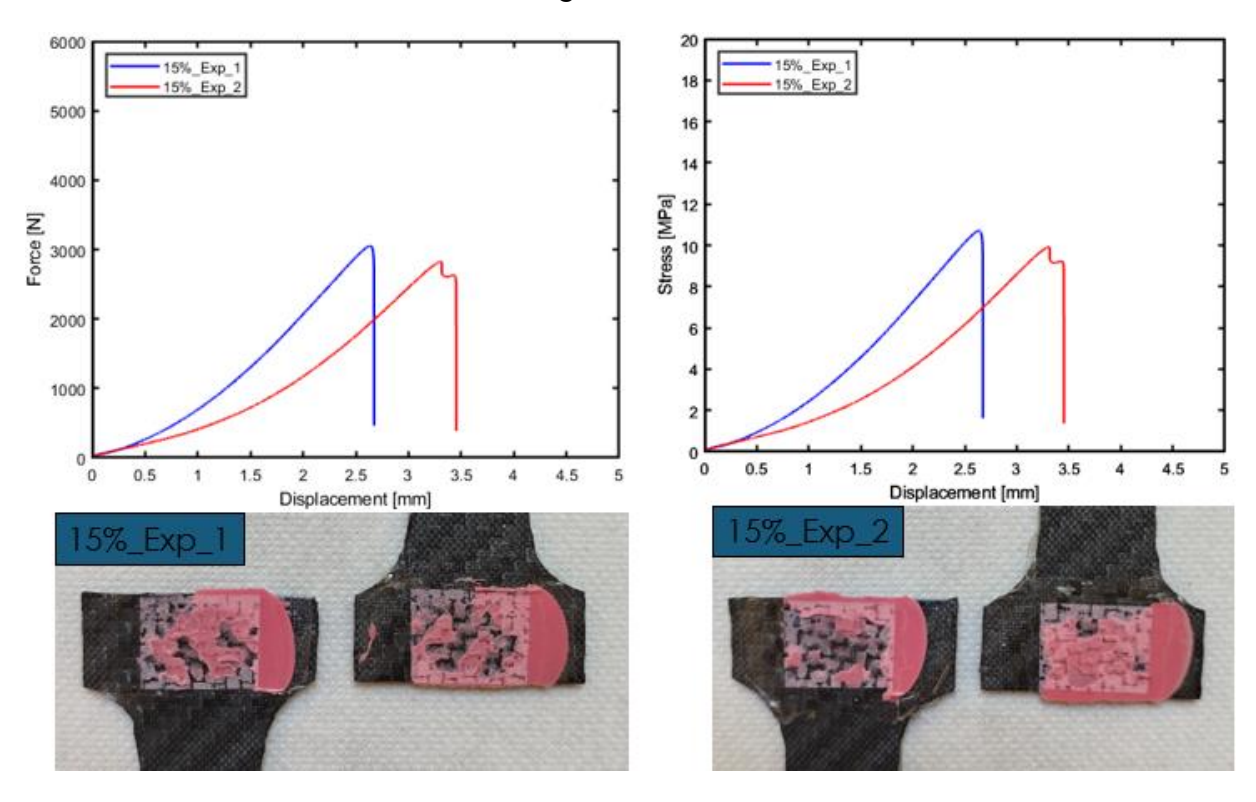


Figure 64. Heated 15 wt.% TEP-modified Epoxy Adhesive - Single Lap Shear Test Results

For the 15 wt.% TEP-modified adhesive specimens, it is noted that the stress has decreased by 30.6% and 19.6% for heated and unheated specimens, respectively, compared to the baseline adhesive specimens. The lap shear stress values of both heated and unheated specimens for 10 wt.% TEP modified specimens are shown in Figure 65.

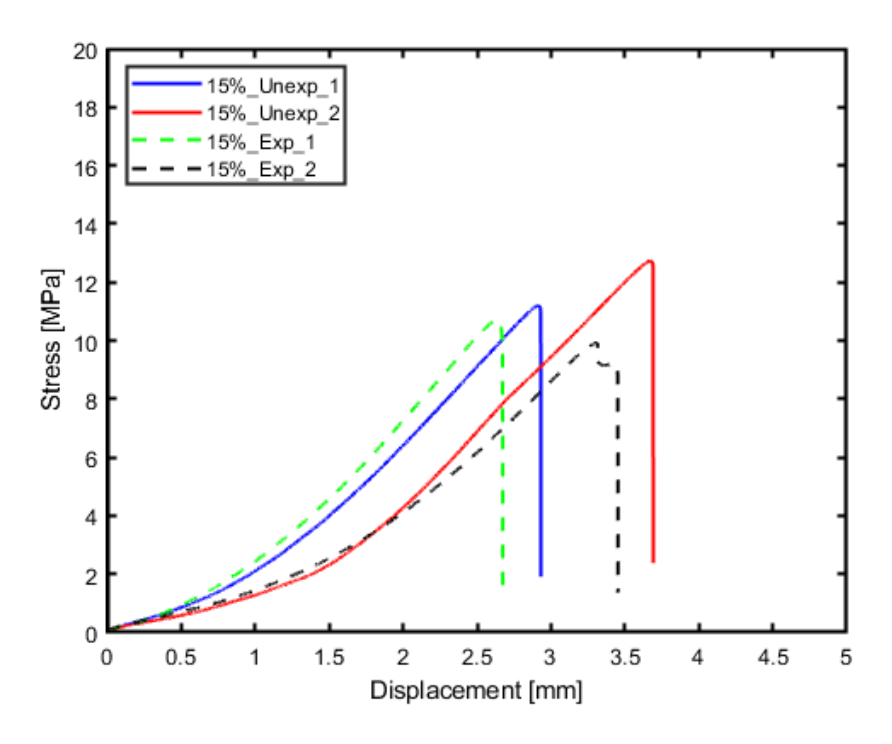


Figure 65. The Lap Shear Strength Plots of 15 wt.% TEP-Modified Specimens

The force-displacement & stress-displacement plots of the unheated specimens are shown in Figure 66. It is observed that there is a tendency for a reduction in the strength values except for the 5 wt.% TEP-modified samples.

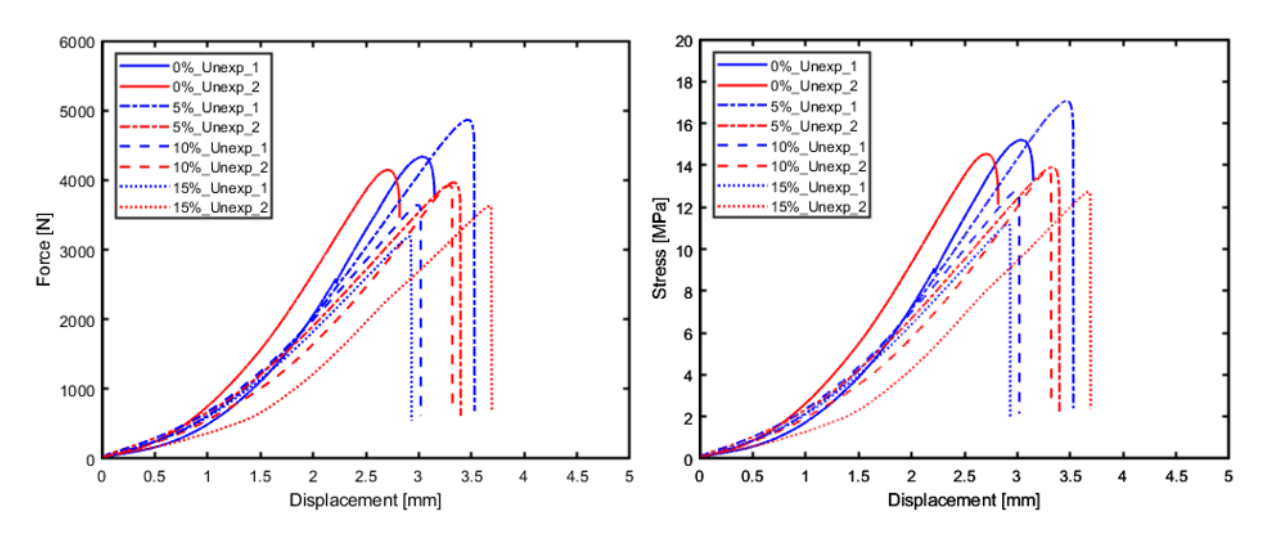


Figure 66. The Lap Shear Strength Plots of Unheated Specimens

The force-displacement & stress-displacement plots of the heated specimens are shown in Figure 67. It is observed that the lap-shear strength decreases more significantly for 15 wt.% samples compared to 5 wt.% and 10 wt.% samples, pointing

out that the strength reduces logarithmically with increasing TEP content in the adhesive.

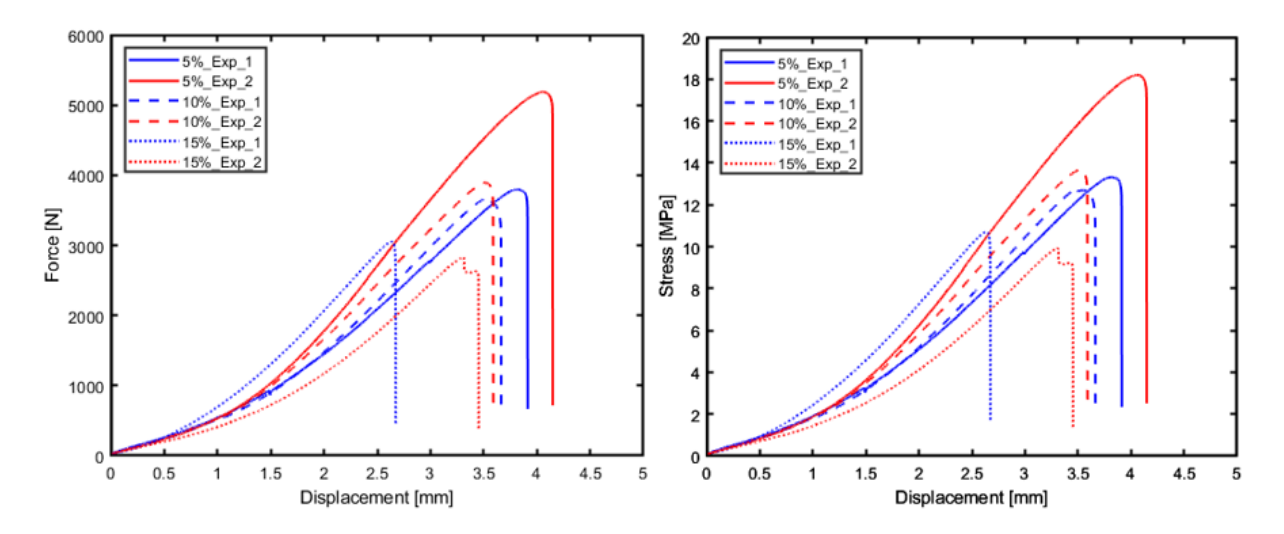


Figure 67. The Lap Shear Strength Plots of Heated Specimens

The force-displacement & stress-displacement master graphs for all the heated and unheated specimens, including the baseline samples, are given in Figures 68 and 69.

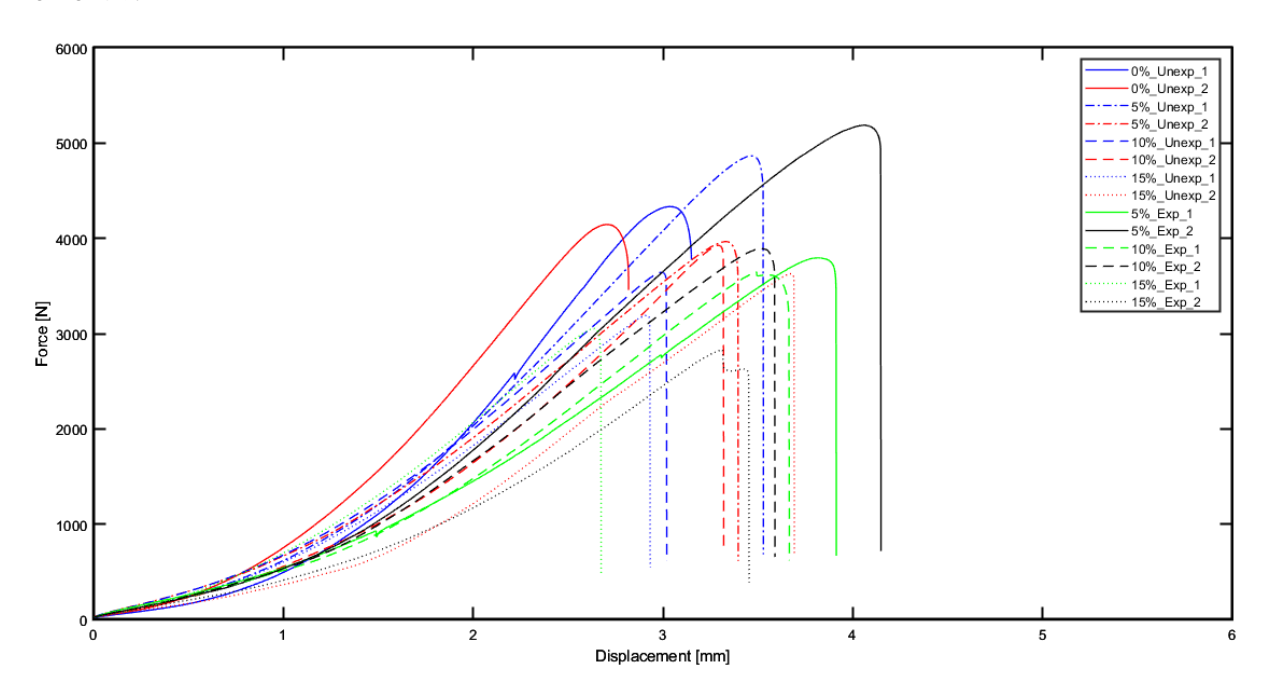


Figure 68. The Force-Displacement Master Graph

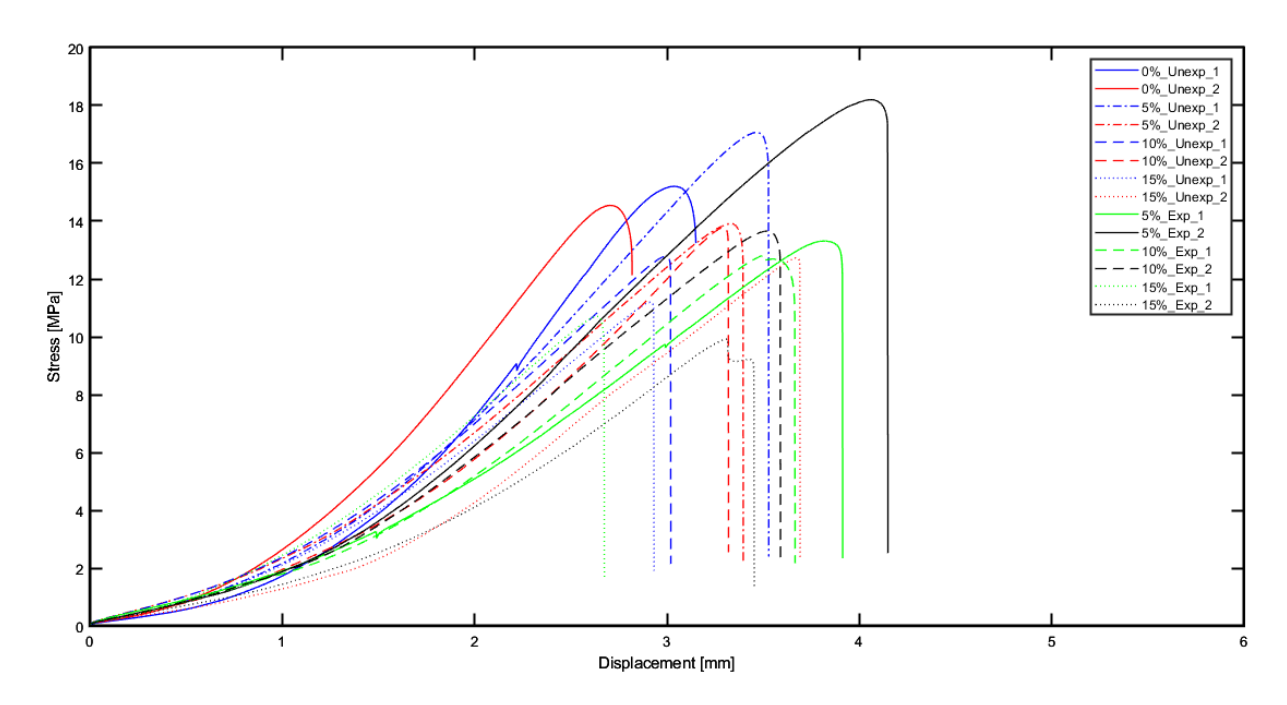


Figure 69. The Stress-Displacement Master Graph

The residual lap shear stress values after heating at 160 °C are shown in Figure 70. Compared to baseline lap shear stress(14.9 Mpa), the strength has increased for 5 wt.% samples for both heated and unheated scenarios. For the 10 wt.% samples, there is a slight decrease, and for the 15 wt.% samples, the strength significantly decreases, as mentioned before. In addition to the comparison with the baseline adhesive, the strength values before and after heating have been investigated for varying TEP weight percentage. For the 5 wt.% samples, it is found that the lap shear strength increased 1.7% after heating. For the 10 wt.% samples, it almost did not change, with a 0.3% decrease. For the 15 wt.% samples, it decreased by 13.7%.

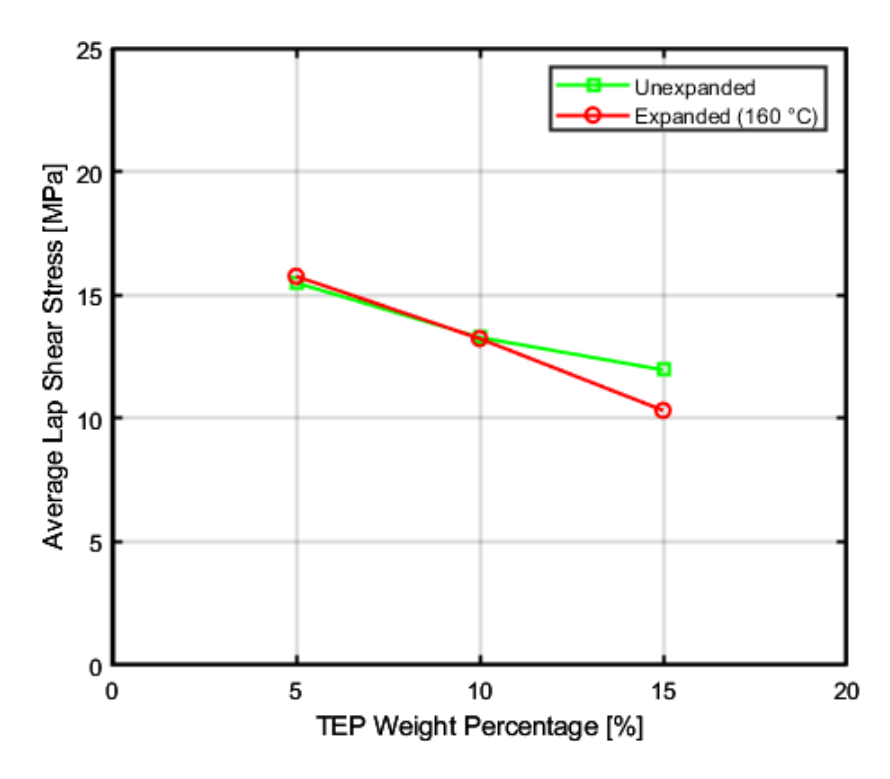


Figure 70. The residual lap shear stress values for varying TEP wt.%

The debonding effectiveness of each TEP-modified epoxy adhesive single lap joint sample has been calculated to quantitatively assess how well the joints maintain their lap shear strength after thermal exposure by using the formula below.

Debonding Effectiveness = 
$$\frac{\tau_{SLJ} - \tau'_{SLJ}}{\tau_{SLJ}}$$
 (2)

Where  $\tau_{SLJ}$  and  $\tau'_{SLJ}$  are the lap shear strengths at room temperature (not expanded or heated) and the residual lap shear strength after heating up to 160°C and cooling down to room temperature , respectively. For the 5 wt.%, 10 wt.%, and 15 wt.% TEP-modified adhesive samples, the debonding effectiveness was calculated as -1.71, 0.35, and 13.73, respectively. The results are tabulated in Table 13.

Table 13. The Deconding Effectiveness Results for Varying TEP wt.%

TEP wt.%	Average Shear Strength (Unexpanded)	Average Shear Strength (Expanded)	Debonding Effectiveness
5	15,5	15,8	-1,71
10	13,3	13,2	0,35
15	12,0	10,3	13,73

As seen in the Table 14, significant trends were observed in the mechanical behavior of the samples compared to the baseline reference sample (0%\_Unexp). As the amount of the TEPs increases, maximum average shear strength generally decreases; this decrease reaches 20–30%, particularly in samples with 15% wt. samples. Young's modulus values similarly decrease, indicating a loss of joint stiffness. Conversely, displacement at the fail moment tends to increase, suggesting a more ductile behavior. The decrease in stiffness and increase in the displacement values are particularly pronounced in the expanded samples.

Table 14. Comparison of Shear Strength, Stiffness, and Rupture Displacement with Varying TEP wt.%

Test	Average Shear [N/mm²]	Average Young's Modulus [MPa]	Displacement at Fail [mm]	Strength Change*	
0%_Unexp	14,9	1901	2,98	0,0%	
5%_Unexp	15,5	1685	3,46	+4,2%	
5%_Exp	15,8	1436	4,03	+5,9%	
10%_Unexp	13,3	1559	3,17	-10,7%	
10%_Exp	13,2	1409	3,63	-11,1%	
15%_Unexp	12,0	1359	3,31	-19,6%	
15%_Exp	10,3	1401	3,06	-30,6%	
*Compared to baseline adhesive (0%_Unexp)					

#### 3.2.2 Failure Modes and Adhesive Distribution

The adhesive distribution on the fracture surfaces has been investigated further by ImageJ software to determine the failure modes of the joints and to see how the incorporation of TEPs affects this.

For the baseline samples, it is observed that the adhesive failure area was 43.3% on average. For the unheated specimens, the adhesive failure area has increased with increased expandable particle amount in the epoxy matrix compared to the baseline, as shown in Figure 71.



Figure 71. Failure Mode Analysis of Unheated Specimens with Varying TEP wt.%

The remaining adhesive on the overlap regions of heated specimens has exhibited more cohesive behavior than the baseline samples. Compared to the heated samples, cohesive failure areas are increased significantly, as shown in Figure 72. In most cases, the fiber-tear failure mode was not observed.



Figure 72. Failure Mode Analysis of Heated Specimens with Varying TEP wt.%

The average cohesive failure area for the baseline sample was calculated as 56.7% and it has increased with increasing TEP amount for the heated joints. On average, this increase has been calculated as 17.4% for 5 wt.% TEP-modified samples, 23.5% for 10 wt.% TEP-modified samples, and 30.7% for 15 wt.% TEP-modified samples, indicating that bond strength becomes lower than the adhesive-substrate interface strength when the particles are expanded.

## 4. Conclusions and Future Work

This study investigates the thermal, morphological, and mechanical behavior of thermally expandable particle (TEP) modified structural epoxy adhesives for GFRP/GFRP bonding applications. Non-isothermal and isothermal TGA analyses have been conducted and they revealed that GFRP begins to degrade at approximately 220 °C due to epoxy matrix decomposition, while the Sikapower-1277 adhesive maintained stability up to 350 °C with minimal weight loss (≤3.5% at 160 °C). Microscope and porosity analyses showed that TEPs expand significantly upon heating, increasing the overall porosity of the adhesive, though the epoxy adhesive matrix restricted full expansion. The volumetric expansion and porosity both increased with higher TEP concentrations. Mechanical lap shear tests demonstrated that incorporating 5 wt.% TEP slightly increased the joint strength (+5.9%), whereas higher loadings (10−15 TEP wt.%) led to reduced lap shear strength (up to −30%), lower stiffness, and higher ductility. Failure mode analysis indicated a shift from adhesive to cohesive failure upon heating, confirming improved energy dissipation but weakened interface bonding at high TEP contents.

The main limitations of this work include extra porosity caused by air entrapped during hand mixing of the adhesive and hardener, and inadequate surface treatment of substrates, which makes the single lap joints prone to premature failures.

For future research, debonding tests using localized Joule or induction heating are recommended to debonding-on-command ability of the TEP-modified adhesive joints, along with investigating the effect of substrate surface treatment methods such as sandblasting, plasma, or chemical treatments to enhance adhesion between the adhesive and substrates.

#### **REFERENCES**

- [1] Gialos, A. A., Zeimpekis, V., Alexopoulos, N. D., Kashaev, N., Riekehr, S., & Karanika, A. (2018). Investigating the impact of sustainability in the production of aeronautical subscale components. Journal of Cleaner Production, 176, 785-799. <a href="https://doi.org/10.1016/j.jclepro.2017.12.151">https://doi.org/10.1016/j.jclepro.2017.12.151</a>
- [2]Goodenough, J., Fitzgerald, A., Bean, K., Hatcliffe, J., Slark, A., Hamerton, I., & Bond, I. (2023). Reversible adhesives and debondable joints for fibre-reinforced plastics: Characteristics, capabilities, and opportunities. Materials Chemistry and Physics, 299, 127464. <a href="https://doi.org/10.1016/j.matchemphys.2023.127464">https://doi.org/10.1016/j.matchemphys.2023.127464</a>
- [3] Scheiner, M., Dickens, T. J., & Okoli, O. (2016). Progress towards self-healing polymers for composite structural applications. Polymer, 83, 260-282. https://doi.org/10.1016/j.polymer.2015.11.008
- [4] Extreme Measures: At 107 Meters, The World's Largest Wind Turbine Blade Is Longer Than A Football Field. Here's What It Looks Like | GE News. (n.d.). Retrieved 16 September 2025, from <a href="https://www.ge.com/news/reports/extreme-measures107-meters-worlds-largest-wind-turbine-blade-longer-football-field-heres-looks">https://www.ge.com/news/reports/extreme-measures107-meters-worlds-largest-wind-turbine-blade-longer-football-field-heres-looks</a> like?fbclid=IwAR287OZvQQILRIDf5LP1cHbK0SADbvPRHwEuRyXRdkK54idojcSmVZaJSq
- [5] Habenicht, G. (2008). Applied Adhesive Bonding: A Practical Guide for Flawless Results. Wiley. <a href="https://books.google.com.tr/books?id=Vu\_GvO7jUToC">https://books.google.com.tr/books?id=Vu\_GvO7jUToC</a>
- [6] Greb, C., Lenz, C., Lengersdorf, M., & Gries, T. (2017). Fabrics for reinforcement of engineering composites. Engineering of High-Performance Textiles, 489-512. https://doi.org/10.1016/B978-0-08-101273-4.00019-6
- [7] Khan, F., Hossain, N., Mim, J. J., Rahman, S. M., Iqbal, M. J., Billah, M., & Chowdhury, M. A. (2025). Advances of composite materials in automobile applications A review. Journal of Engineering Research, 13(2), 1001-1023. https://doi.org/10.1016/j.jer.2024.02.017
- [8] Praveenkumar, B., & Darius Gnanaraj, S. (2020). Case Studies on the Applications of Phenolic Resin-Based Composite Materials for Developing Eco-Friendly Brake Pads. Journal of The Institution of Engineers (India): Series D, 101(2), 327–334. https://doi.org/10.1007/s40033-020-00231-4
- [9] Maleque, M. A., Afdzaluddin, A., Ria Jaafar, T., & Halim, Z. (2012). New natural fibre reinforced aluminium composite for automotive brake pad. International Journal of Mechanical and Materials Engineering (IJMME), 7(2), 166–170.
- [10] Idusuyi, N., Babajide, I., Ajayi, O. K., & Olugasa, T. T. (2013). A Computational Study on the Use of an Aluminium Metal Matrix Composite and Aramid as

- Alternative Brake Disc and Brake Pad Material. Journal of Engineering, 2014(1), 494697. https://doi.org/10.1155/2014/494697
- [11] Kong, C., Lee, H., & Park, H. (2016). Design and manufacturing of automobile hood using natural composite structure. Composites Part B: Engineering, 91, 18–26. https://doi.org/10.1016/j.compositesb.2015.12.033
- [12] Kwak, D., Jeong, J., Cheon, J., & Im, Y. (1997). Optimal design of composite hood with reinforcing ribs through stiffness analysis. Composite Structures, 38(1-4), 351-359. https://doi.org/10.1016/S0263-8223(97)00070-6
- [13] Kim, D., Jung, K., Kim, D., Park, S., Kim, D., Lim, J., Nam, B., & Kim, H. (2017). Improving pedestrian safety via the optimization of composite hood structures for automobiles based on the equivalent static load method. Composite Structures, 176, 780-789. https://doi.org/10.1016/j.compstruct.2017.06.016
- [14] Prucz, J. C., Shoukry, S. N., William, G. W., & Shoukry, M. S. (2013). LIGHTWEIGHT COMPOSITE MATERIALS FOR HEAVY DUTY VEHICLES.
- [15] Sanjay, M., Arpitha, G., & Yogesha, B. (2014). Study on Mechanical Properties of Natural Glass Fibre Reinforced Polymer Hybrid Composites: A Review. Materials Today: Proceedings, 2(4-5), 2959-2967. https://doi.org/10.1016/j.matpr.2015.07.264
- [16] Veeraswamy, K., & VenkataSudheerBabu, V. (2016). DESIGN AND ANALYSIS OF A COMPOSITE BEAM FOR SIDE IMPACT PROTECTION OF A CAR DOOR. 03(02).
- [17] Chauhan, V., Kärki, T., & Varis, J. (2022). Review of natural fiber-reinforced engineering plastic composites, their applications in the transportation sector and processing techniques. Journal of Thermoplastic Composite Materials. <a href="https://doi.org/10.1177/0892705719889095">https://doi.org/10.1177/0892705719889095</a>
- [18] Lyu, M.-Y., & Choi, T. G. (2015). Research trends in polymer materials for use in lightweight vehicles. *International Journal of Precision Engineering and Manufacturing*, 16(1), 213–220. https://doi.org/10.1007/s12541-015-0029-x
- [19] Huang, Y., Xiao, X., Kang, H., Lv, J., Zeng, R., & Shen, J. (2022). Thermal management of polymer electrolyte membrane fuel cells: A critical review of heat transfer mechanisms, cooling approaches, and advanced cooling techniques analysis. *Energy Conversion and Management*, 254, 115221. <a href="https://doi.org/10.1016/j.enconman.2022.115221">https://doi.org/10.1016/j.enconman.2022.115221</a>
- [20] Sherwani, S., Sapuan, S., Leman, Z., Zainuddin, E., & Ilyas, R. (2020). Application of polymer composite materials in motorcycles: A comprehensive review. *Biocomposite and Synthetic Composites for Automotive Applications*, 401-426. https://doi.org/10.1016/B978-0-12-820559-4.00015-8
- [21] Are composite materials, which are being widely used in newer aircraft, better at handling bird strikes? Aviation Stack Exchange. (n.d.). Retrieved 16 September

- 2025, from <a href="https://aviation.stackexchange.com/questions/22148/are-composite-materials-which-are-being-widely-used-in-newer-aircraft-better-a">https://aviation.stackexchange.com/questions/22148/are-composite-materials-which-are-being-widely-used-in-newer-aircraft-better-a</a>
- [22] Gebrehiwet, L., Abate, E., Negussie, Y., Teklehaymanot, T., & Abeselom, E. (2023). Application Of Composite Materials In Aerospace & Automotive Industry:Review. https://doi.org/10.35629/5252-0503697723
- [23] Nixon, W. (1987). Preliminary Structural Design of Composite Main Rotor Blades for Minimum Weight.
- [24] Campbell, F. Introduction to Composite Materials and Processes: Unique Materials that Require Unique Processes. *Manufacturing Processes for Advanced Composites*. https://doi.org/10.1016/B978-185617415-2/50002-2
- [25] Otani, L. Elastic Moduli characterization of composites using the Impulse Excitation Technique. <a href="https://doi.org/10.13140/RG.2.1.1551.2481">https://doi.org/10.13140/RG.2.1.1551.2481</a>
- [26] Al-Furjan, M., Shan, L., Shen, X., Zarei, M., Hajmohammad, M., & Kolahchi, R. (2022). A review on fabrication techniques and tensile properties of glass, carbon, and Kevlar fiber reinforced rolymer composites. *Journal of Materials Research and Technology*, 19, 2930–2959. https://doi.org/10.1016/j.jmrt.2022.06.008
- [27] Gangu Naidu, C., V.V. Ramana, C., Srinivasa Rao, Y., Vara Prasada Rao, K., Vasudha, D., Anusha, G., & B. Rajeshbabu, K. (2023). A Concise Review on Carbon Fiber-Reinforced Polymer (CFRP) and Their Mechanical Significance Including Industrial Applications. IntechOpen. doi: 10.5772/intechopen.109339
- [28] Rajak, D. K., Wagh, P. H., & Linul, E. (2021). Manufacturing Technologies of Carbon/Glass Fiber-Reinforced Polymer Composites and Their Properties: A Review. *Polymers*, *13*(21), 3721. <a href="https://doi.org/10.3390/polym13213721">https://doi.org/10.3390/polym13213721</a>
- [29] Denchev, Z., & Dencheva, N. (2012). *Manufacturing and Properties of Aramid Reinforced Composites* (pp. 251–280). <a href="https://doi.org/10.1007/978-1-56990-525-8">https://doi.org/10.1007/978-1-56990-525-8</a>
- [30] Khan, L., & Mehmood, A. (2015). Cost-effective composites manufacturing processes for automotive applications. *Lightweight Composite Structures in Transport*, 93-119. <a href="https://doi.org/10.1016/B978-1-78242-325-6.00005-0">https://doi.org/10.1016/B978-1-78242-325-6.00005-0</a>
- [31] Halley, P. (2011). Rheology of thermosets: The use of chemorheology to characterise and model thermoset flow behaviour. *Thermosets*, 92-117. https://doi.org/10.1533/9780857097637.1.92
- [32] Campbell, F. Commercial Composite Processes: These Commercial Processes Produce Far More Parts than the High-performance Processes. *Manufacturing Processes for Advanced Composites*. <a href="https://doi.org/10.1016/B978-185617415-2/50012-5">https://doi.org/10.1016/B978-185617415-2/50012-5</a>

- [33] Mallick, P. (2009). Thermoset–matrix composites for lightweight automotive structures. *Materials, Design and Manufacturing for Lightweight Vehicles*, 208-231. https://doi.org/10.1533/9781845697822.1.208
- [34] Summerscales, J. (2012). Resin Infusion Under Flexible Tooling (RIFT). In Wiley Encyclopedia of Composites (pp. 1–11). John Wiley & Sons, Ltd. <a href="https://doi.org/10.1002/9781118097298.weoc216">https://doi.org/10.1002/9781118097298.weoc216</a>
- [35] Hindersmann, A. (2019). Confusion about infusion: An overview of infusion processes. *Composites Part A: Applied Science and Manufacturing*, 126, 105583. <a href="https://doi.org/10.1016/j.compositesa.2019.105583">https://doi.org/10.1016/j.compositesa.2019.105583</a>
- [36] Vacuum Assisted Resin Transfer Molding | The Gund Company. (n.d.).
  Retrieved 16 September 2025, from
  <a href="https://thegundcompany.com/capabilities/materials-manufacturing/vartm/">https://thegundcompany.com/capabilities/materials-manufacturing/vartm/</a>
- [37] Sarfraz, M. S., Hong, H., & Kim, S. S. (2021). Recent developments in the manufacturing technologies of composite components and their cost-effectiveness in the automotive industry: A review study. *Composite Structures*, 266, 113864. https://doi.org/10.1016/j.compstruct.2021.113864
- [38] Azlin, M., Sapuan, S., Zainudin, E., Zuhri, M., & Ilyas, R. (2019). Natural Polylactic Acid-Based Fiber Composites: A Review. *Advanced Processing, Properties, and Applications of Starch and Other Bio-Based Polymers*, 21–34. <a href="https://doi.org/10.1016/B978-0-12-819661-8.00003-2">https://doi.org/10.1016/B978-0-12-819661-8.00003-2</a>
- [39] Sarfraz, M. S., Hong, H., & Kim, S. S. (2021). Recent developments in the manufacturing technologies of composite components and their cost-effectiveness in the automotive industry: A review study. *Composite Structures*, 266, 113864. https://doi.org/10.1016/j.compstruct.2021.113864
- [40] Campbell, F. Introduction to Composite Materials and Processes: Unique Materials that Require Unique Processes. *Manufacturing Processes for Advanced Composites*. <a href="https://doi.org/10.1016/B978-185617415-2/50002-2">https://doi.org/10.1016/B978-185617415-2/50002-2</a>
- [41] Minsch, N., Herrmann, F., Gereke, T., Nocke, A., & Cherif, C. (2016). Analysis of Filament Winding Processes and Potential Equipment Technologies. *Procedia CIRP*, 66, 125-130. <a href="https://doi.org/10.1016/j.procir.2017.03.284">https://doi.org/10.1016/j.procir.2017.03.284</a>
- [42] Groover, M. P. (2010). Fundamentals of Modern Manufacturing: Materials, Processes, and Systems. John Wiley & Sons.
- [43] Banea, M. D. (2008). Adhesively bonded joints in composite materials: An overview. *Proceedings of the Institution of Mechanical Engineers, Part L: Journal of Materials: Design and Applications*. <a href="https://doi.org/10.1243/14644207JMDA219">https://doi.org/10.1243/14644207JMDA219</a>

- [44] American Welding Society (AWS). Adhesive bonding. In WHB Welding Handbook 9.3-Welding Processes, Part 2; American Welding Society (AWS): Miami, FL, USA, 2007; Volume 3, pp. 334–341.
- [45] Jeevi, G., Nayak, S. K., & Abdul Kader, M. (2019). Review on adhesive joints and their application in hybrid composite structures. *Journal of Adhesion Science and Technology*, 33(14), 1497–1520. https://doi.org/10.1080/01694243.2018.1543528
- [46] Lang, T., & Mallick, P. (1999). The effect of recessing on the stresses in adhesively bonded single-lap joints. *International Journal of Adhesion and Adhesives*, 19(4), 257-271. https://doi.org/10.1016/s0143-7496(98)00069-4
- [47] Belingardi, G., Goglio, L., & Tarditi, A. (2001). Investigating the effect of spew and chamfer size on the stresses in metal/plastics adhesive joints. *International Journal of Adhesion and Adhesives*, 22(4), 273-282. <a href="https://doi.org/10.1016/S0143-7496(02)00004-0">https://doi.org/10.1016/S0143-7496(02)00004-0</a>
- [48] Fitton, M., & Broughton, J. (2005). Variable modulus adhesives: An approach to optimised joint performance. *International Journal of Adhesion and Adhesives*, 25(4), 329-336. https://doi.org/10.1016/j.ijadhadh.2004.08.002
- [49] Ganesh, V. K., & Choo, T. S. (2002). Modulus Graded Composite Adherends for Single-Lap Bonded Joints. *Journal of Composite Materials*. https://doi.org/10.1177/0021998302036014172
- [50] Maggiore, S., Banea, M. D., Stagnaro, P., & Luciano, G. (2020). A Review of Structural Adhesive Joints in Hybrid Joining Processes. *Polymers*, *13*(22), 3961. https://doi.org/10.3390/polym13223961
- [51] Eshtayeh, M. M., Hrairi, M., & Mohiuddin, A. K. M. (2016). Clinching process for joining dissimilar materials: State of the art. *The International Journal of Advanced Manufacturing Technology*, 82(1), 179–195. <a href="https://doi.org/10.1007/s00170-015-7363-0">https://doi.org/10.1007/s00170-015-7363-0</a>
- [52] Pirondi, A., & Moroni, F. (2011). Science of Clinch–Adhesive Joints. In L. F. M. da Silva, A. Pirondi, & A. Öchsner (Eds), *Hybrid Adhesive Joints* (pp. 109–147). Springer. <a href="https://doi.org/10.1007/8611\_2010\_36">https://doi.org/10.1007/8611\_2010\_36</a>
- [53] Mulcahy, K. R., Kilpatrick, A. F. R., Harper, G. D. J., Walton, A., & Abbott, A. P. (2022). Debondable adhesives and their use in recycling. *Green Chem.*, 24(1), 36–61. <a href="https://doi.org/10.1039/DIGC03306A">https://doi.org/10.1039/DIGC03306A</a>
- [54] Hohl, D. K., & Weder, C. (2019). (De)bonding on Demand with Optically Switchable Adhesives. *Advanced Optical Materials*, 7(16), 1900230. https://doi.org/10.1002/adom.201900230
- [55] Ciardiello, R., Belingardi, G., Litterio, F., & Brunella, V. (2021). Effect of iron oxide and graphene particles on joint strength and dismounting characteristics of a

- thermoplastic adhesive. *International Journal of Adhesion and Adhesives*, 107, 102850. https://doi.org/10.1016/j.ijadhadh.2021.102850
- [56] Haydon, D. (2002). ElectRelease electrically disbonding epoxy adhesive. Assembly Automation, 22(4), 326–329. https://doi.org/10.1108/01445150210446175
- [57] Leijonmarck, S., Cornell, A., Danielsson, C., Åkermark, T., Brandner, B. D., & Lindbergh, G. (2011). Electrolytically assisted debonding of adhesives: An experimental investigation. *International Journal of Adhesion and Adhesives*, 32, 39-45. <a href="https://doi.org/10.1016/j.ijadhadh.2011.09.003">https://doi.org/10.1016/j.ijadhadh.2011.09.003</a>
- [58] Tachi, H., & Suyama, K. (2017). Development of Pressure-Sensitive Adhesives Degradable on Ultrasonic Irradiation. *Journal of Photopolymer Science and Technology*, 30(2), 253–257. https://doi.org/10.2494/photopolymer.30.253
- [59] McCurdy, R., Hutchinson, A., & Winfield, P. (2013). The mechanical performance of adhesive joints containing active disbonding agents. *International Journal of Adhesion and Adhesives*, 46, 100-113. https://doi.org/10.1016/j.ijadhadh.2013.06.001
- [60] Lim, J. S. K., Gan, C. L., & Hu, X. M. (2019). Unraveling the Mechanistic Origins of Epoxy Degradation in Acids. *ACS Omega*, 4(6), 10799–10808. https://doi.org/10.1021/acsomega.9b00859
- [61] Yang, P., Zhou, Q., Yuan, X., Van Kasteren, J. M., & Wang, Y. (2012). Highly efficient solvolysis of epoxy resin using poly(ethylene glycol)/NaOH systems. *Polymer Degradation and Stability*, 97(7), 1101-1106. https://doi.org/10.1016/j.polymdegradstab.2012.04.007
- [62] Mallick, P.K. (2007). Fiber-Reinforced Composites: Materials, Manufacturing, and Design, Third Edition (3rd ed.). CRC Press. <a href="https://doi.org/10.1201/9781420005981">https://doi.org/10.1201/9781420005981</a>
- [63] Hwang, H.-Y. (2020). Debondable adhesives using shape memory fibers. Functional Composites and Structures, 2(1), 015003. https://doi.org/10.1088/2631-6331/ab74fb
- [64] D. S. J. Morehouse and R. J. Tetreault, Expansible thermoplastic polymer particles containing volatile fluid foaming agent and method of foaming the same, US Patent 3.615,972 assigned to Dow Chemical Co, (1971).
- [65] Banea, M.D. (2019). Debonding on Demand of Adhesively Bonded Joints: A Critical Review. *Reviews of Adhesion and Adhesives*.
- [66] Expancel® thermoplastic microspheres—Nouryon. (n.d.). Retrieved 17 September 2025, from <a href="https://www.nouryon.com/products/expancel-microspheres">https://www.nouryon.com/products/expancel-microspheres</a>

- [67] Nishiyama, Y., Uto, N., Sato, C., & Sakurai, H. (2002). Dismantlement behavior and strength of dismantlable adhesive including thermally expansive particles. *International Journal of Adhesion and Adhesives*, *23*(5), 377-382. <a href="https://doi.org/10.1016/S0143-7496(03)00067-8">https://doi.org/10.1016/S0143-7496(03)00067-8</a>
- [68] Gadhave, R. and Gadhave, C. (2022) Application of Thermally Expandable Microspheres in Adhesives: Review. *Open Journal of Polymer Chemistry*, **12**, 80-92. doi: 10.4236/ojpchem.2022.122005.
- [69] Lu, Y., Broughton, J., & Winfield, P. (2014). A review of innovations in disbonding techniques for repair and recycling of automotive vehicles. *International Journal of Adhesion and Adhesives*, 50, 119-127. https://doi.org/10.1016/j.ijadhadh.2014.01.021
- [70] Banea, M. D., da Silva, L. F. M., Carbas, R. J. C., & Campilho, R. D. S. G. (2015). Structural Adhesives Modified with Thermally Expandable Particles. *The Journal of Adhesion*, 91(10–11), 823–840. https://doi.org/10.1080/00218464.2014.985785
- [71] Lu, Y., Broughton, J., & Winfield, P. (2016). Surface modification of thermally expandable microspheres for enhanced performance of disbondable adhesive. *International Journal of Adhesion and Adhesives*, 66, 33-40. <a href="https://doi.org/10.1016/j.ijadhadh.2015.12.007">https://doi.org/10.1016/j.ijadhadh.2015.12.007</a>
- [72] Wanghofer, F., Wolfberger, A., Oreski, G., Neumaier, L., & Schlögl, S. (2023). Investigation of expandable fillers for reversible adhesive bonding in photovoltaic modules. *International Journal of Adhesion and Adhesives*, *126*, 103454. https://doi.org/10.1016/j.ijadhadh.2023.103454
- [73] Piazza, G., Burczyk, M., Gerini-Romagnoli, M., Belingardi, G., & Nassar, S. A. (2022). Effect of thermally expandable particle additives on the mechanical and reversibility performance of adhesive joints. *Journal of Advanced Joining Processes*, 5, 100088. <a href="https://doi.org/10.1016/j.jajp.2021.100088">https://doi.org/10.1016/j.jajp.2021.100088</a>
- [74] Caglar, H., Sridhar, I., Sharma, M., & Chian, K. S. (2022). Debonding of bonded composite joints with TEP modified epoxy adhesives. *The Journal of Adhesion*, 99(10), 1626–1649. https://doi.org/10.1080/00218464.2022.2152333
- [75] Banea, M., Da Silva, L., Carbas, R., & Campilho, R. (2014). Mechanical and thermal characterization of a structural polyurethane adhesive modified with thermally expandable particles. *International Journal of Adhesion and Adhesives*, 54, 191-199. https://doi.org/10.1016/j.ijadhadh.2014.06.008
- [76] Banea, M. D., da Silva, L. F. M., Carbas, R. J. C., & de Barros, S. (2016). Debonding on command of multi-material adhesive joints. *The Journal of Adhesion*, 93(10), 756–770. https://doi.org/10.1080/00218464.2016.1199963
- [77] Abenojar, J., López de Armentia, S., del Real, J.-C., & Martínez, M.-A. (2024). Influence of the Magnetization of Thermally Expandable Particles on the Thermal

- and Debonding Properties of Bonding Joints. *Inorganics*, 12(5), 129. https://doi.org/10.3390/inorganics12050129
- [78] Duque, A. L. H., Patterson, B. M., Kuettner, L. A., Robillard, S. R., Mang, J. T., & Perry, W. L. (2020). Novel PBX formulations containing thermally-expandable microspheres for on-demand control of explosive behavior. *AIP Conference Proceedings*, 2272(1), 100006. <a href="https://doi.org/10.1063/12.0000787">https://doi.org/10.1063/12.0000787</a>
- [79] Uratani, Y., Sekiguchi, Y., & Sato, C. (2017). Expansion characteristics of thermally expandable microcapsules for dismantlable adhesive under hydrostatic pressure or in resin. *The Journal of Adhesion*, *93*(10), 771–790. https://doi.org/10.1080/00218464.2017.1306442
- [80] Kim, D., Chung, I., & Kim, G. (2012). Dismantlement studies of dismantlable polyurethane adhesive by controlling thermal property. *Journal of Adhesion Science and Technology*, 26(23), 2571–2589. https://doi.org/10.1080/01694243.2012.690213
- [81] Cingil, H. E., Balmer, J. A., Armes, S. P., & Bain, P. S. (2010). Conducting polymer-coated thermally expandable microspheres. *Polymer Chemistry*, 1(8), 1323–1331. https://doi.org/10.1039/C0PY00108B
- [82] Banea, M., Da Silva, L., & Carbas, R. (2015). Debonding on command of adhesive joints for the automotive industry. *International Journal of Adhesion and Adhesives*, 59, 14-20. <a href="https://doi.org/10.1016/j.ijadhadh.2015.01.014">https://doi.org/10.1016/j.ijadhadh.2015.01.014</a>
- [83] Banea, M. D., Da Silva, L. F. M., Carbas, R. J. C., Cavalcanti, D. K. K., & De Souza, L. F. G. (2019). The effect of environment and fatigue loading on the behaviour of TEPs-modified adhesives. *The Journal of Adhesion*, 96(1–4), 423–436. https://doi.org/10.1080/00218464.2019.1680546
- [84] Bonaldo, J., Banea, M. D., Carbas, R. J. C., Da Silva, L. F. M., & De Barros, S. (2018). Functionally graded adhesive joints by using thermally expandable particles. *The Journal of Adhesion*, 95(11), 995–1014. https://doi.org/10.1080/00218464.2018.1456338
- [85] Banea, M., Silva, L. F. M., Campilho, R., & Sato, C. (2014). Smart Adhesive Joints: An Overview of Recent Developments. *Journal of Adhesion*, 90. https://doi.org/10.1080/00218464.2013.785916
- [86] SikaPower®-1277 | Specialty Vehicles. (n.d.). Retrieved 17 September 2025, from <a href="https://industry.sika.com/en/home/transportation/specialty-vehicles/sikapower-1277.html">https://industry.sika.com/en/home/transportation/specialty-vehicles/sikapower-1277.html</a>
- [87] ARE-250 CE / THINKY's mixers and defoamers. (n.d.). Retrieved 17 September 2025, from <a href="https://www.thinkymixer.com/en-gl/products/are-250-ce/">https://www.thinkymixer.com/en-gl/products/are-250-ce/</a>

- [88] *Products-Pro—Fiberforce*. (n.d.). Retrieved 17 September 2025, from <a href="https://www.fiberforce.it/products-pro/">https://www.fiberforce.it/products-pro/</a>
- [89] WAZER Waterjet Cutters for Any Shop. (n.d.). Retrieved 17 September 2025, from
- https://wazer.com/?\_gl=1\*1f3ygb4\*\_gcl\_au\*MTUzNDU3NDM1OS4xNzQ5NTY1NTgw
- [90] MECATECH 250 SPC Presi. (n.d.). Retrieved 17 September 2025, from <a href="https://www.presi.com/en/product/mecatech-250-spc/">https://www.presi.com/en/product/mecatech-250-spc/</a>
- [91] XC130 280g 2/2 Twill Glass Fibre Reinforced Prepreg—Easy Composites. (n.d.). Retrieved 10 October 2025, from https://www.easycomposites.co.uk/XC130-280g-2x2-twill-prepreg-carbon-fibre
- [92] XC110 416g 2x2 Twill 6k Prepreg Carbon Fibre 1.25m—Easy Composites. (n.d.). Retrieved 10 October 2025, from <a href="https://www.easycomposites.co.uk/xc110-416g-22-twill-6k-prepreg-carbon-fibre">https://www.easycomposites.co.uk/xc110-416g-22-twill-6k-prepreg-carbon-fibre</a>
- [93] Banea, M. D. Debonding on Demand of Adhesively Bonded Joints. 33-50. https://doi.org/10.1002/9781119749882.ch2